

"
MOSSBAUER SPECTROSCOPY OF FE-N AND FE-C SOLID SOLUTIONS

BY

NICHOLAS JOHN DECRISTOFARO

S. B., S. M. Massachusetts Institute of Technology

1973

Submitted in partial fulfillment of the requirements

for the degree of


DOCTOR OF PHILOSOPHY

at the

Massachusetts Institute of Technology

February, 1976

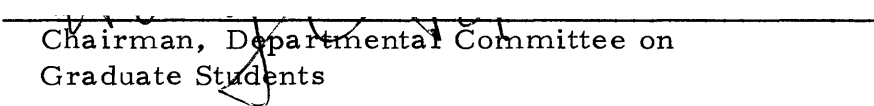
Signature of Author


Department of Materials/Science and
Engineering, January 14, 1976

Certified by


Thesis Supervisor

Accepted by


Chairman, Departmental Committee on
Graduate Students



"⁵⁷MOSSBAUER SPECTROSCOPY OF FE-N AND FE-C SOLID SOLUTIONS

BY

NICHOLAS JOHN DECRISTOFARO

Submitted to the Department of Materials Science and Engineering on January 14, 1976, in partial fulfillment of the requirements for the degree of Doctor of Philosophy.

ABSTRACT

Mössbauer Fe⁵⁷ spectroscopy allows comparison of Fe-N and Fe-C interstitial solid solutions. The spectrum of Fe-N retained austenite indicates that nitrogen atoms are randomly distributed in octahedral interstitial sites, with this configuration being inherited, upon transformation, by the virgin martensite. These results are in contrast to Fe-C data. Carbon atoms in retained austenite tend to be far apart on their octahedral sites, and this non-random distribution is inherited by the virgin martensite. Virgin nitrogen martensite ages at room temperature by local ordering of nitrogen atoms. In that process, three new iron atom environments develop, characteristic of the α' -Fe₁₆N₂ structure. However, the excessive width of the peaks indicates that the perfect order of the Fe₁₆N₂ precipitate is not achieved, except after very long times. Further aging at 100°C leads to the complete decomposition of the virgin martensite to the discrete phases α -iron and Fe₁₆N₂.

The rate of clustering of carbon atoms into regions of ordered Fe₄C has been studied by Mössbauer spectroscopy. The activation energy associated with this process is 89,525 ± 12,000 joules per mole.

In Fe-N alloys, the hexagonal-close-packed phase can be completely retained metastably at room temperature by rapid quenching from 700°C, with nitrogen contents ranging from about 17 to 27 at.% N; (between the latter composition and 33 at.% N, the hexagonal phase

is stable at room temperature). The phase is ferromagnetic; the Curie temperature is a sharp function of nitrogen content, with the maximum Curie point (about 300°C) occurring at 24 at. % N. The Curie point is below room temperature in the hexagonal phase for nitrogen contents of less than 17 or greater than 31.8 at. % N. For alloys of the Fe₃N composition quenched from various temperatures, ⁵⁷Mössbauer spectroscopy indicates that the hexagonal phase undergoes ordering of nitrogen atoms on interstitial sites.

⁵⁷Mössbauer spectra were taken at room temperature and below room temperature of an iron - 2.4 wt. % nitrogen sample containing various amounts of martensite and austenite. The intensities of the martensite spectra increased with decreasing temperatures as expected from the normal thermal variation of the recoilless fraction. Conversely, the intensities of the austenite spectra are smaller below room temperature corresponding to a decrease in the recoilless fraction. This is associated with a lessening of lattice resistance to excitations caused by transference of the gamma-ray momentum and is thought to be related to the instability of the austenite phase.

Thesis Supervisor: Professor Roy Kaplow

Title: Professor of Materials Science

TABLE OF CONTENTS

<u>Chapter No.</u>		<u>Page No.</u>
	ABSTRACT	2
	TABLE OF CONTENTS	4
	LIST OF FIGURES	7
	LIST OF TABLES	11
	ACKNOWLEDGEMENTS	12
I.	INTRODUCTION	13
I.1	Introduction to Mössbauer Spectroscopy	13
I.2	Literature Review	25
I.2.1	Mössbauer Spectroscopy of Iron-Carbon Alloys	25
I.2.2	Mössbauer Spectroscopy of Iron-Nitrogen Alloys	29
I.3	Historical Context of the Plan for Work	35
I.3.1	Outline of Work	35
I.3.2	Advances in Mössbauer Spectroscopy	38
II.	INTERSTITIAL ATOM CONFIGURATIONS IN STABLE AND METASTABLE FE-N AND FE-C SOLID SOLUTIONS	45
II.1	Introduction	45
II.2	Experimental Procedure	47
II.3	Experimental Results	54
II.3.1	Iron-Carbon Alloys	57
II.3.1.1	Carbon-Austenite	57
II.3.1.2	Virgin Carbon-Martensite	61
II.3.1.3	Aging of Martensite	67

<u>Chapter No.</u>		<u>Page No.</u>
	II.3.2 Iron-Nitrogen Alloys	67
	II.3.2.1 Nitrogen-Austenite	67
	II.3.2.2 Virgin Nitrogen- Martensite	68
	II.3.2.3 Aging of Nitrogen- Martensite	77
	II.4 Austenite Configurational Models and Thermodynamic Data	85
	II.5 Crystallographic Symmetries in Carbide and Nitride Structures	91
	II.6 Summary	93
III.	THE KINETICS OF CARBON CLUSTERING IN MARTENSITE	99
	III.1 Introduction	99
	III.2 Experimental Procedure	101
	III.3 Experimental Results	102
	III.4 Discussion	111
	III.5 Summary	118
IV.	" MOSSBAUER SPECTROSCOPY OF HEXAGONAL IRON-NITROGEN ALLOYS	122
	IV.1 Introduction	122
	IV.2 Experimental Procedure	127
	IV.2.1 Sample Preparation	127
	IV.2.2 Mossbauer Spectroscopy	128
	IV.3 Experimental Results	130
	IV.4 Discussion	153
	IV.4.1 Hyperfine Magnetic Field	153
	IV.4.2 Ordering in Fe ₃ N	158
	IV.5 Conclusions	163
V.	LOSS OF LATTICE RIGIDITY IN AUSTENITE	167
	V.1 Introduction	167

<u>Chapter No.</u>		<u>Page No.</u>
	V.2 Experimental Procedure	169
	V.3 Experimental Results	174
	V.4 Discussion	179
	V.5 Summary	186
VI.	SUMMARY	190
VII.	SUGGESTIONS FOR FURTHER WORK	192
	APPENDIX A: Alloy Preparation	195
	APPENDIX B: The Mössbauer Spectrometer	199
	APPENDIX C: Error Analysis	205
	APPENDIX D: Computer Programs	220
	APPENDIX E: Loss of Lattice Rigidity in Iron-Nitrogen Austenite: N. DeCristofaro and R. Kaplow, Scripta Met., 1975, vol. 9, p. 781.	227
	APPENDIX F: Iron-Manganese-Nitrogen Alloys	234

LIST OF FIGURES

<u>Figure No.</u>		<u>Page No.</u>
I. 1	Hyperfine Interactions	20
I. 2	Decay Scheme of Co^{57}	23
I. 3	Fe_{16}N_2 Structure	33
II. 1a	Austenite Structure	49
1b	Martensite Structure	50
II. 2	^{57}Fe Mossbauer Spectrum of Fe - 1.86 wt. % C Austenite (points)	58
2a	compared to "separated" model of carbon atoms (line)	59
2b	compared to "random" model of carbon atoms (line)	60
II. 3a	^{57}Fe Mossbauer Spectrum of Fe - 1.86 wt. % C Virgin Martensite	63
3b, c	Comparison of Virgin Martensite Spectrum (points) to "separated" model of carbon atoms (line)	64, 65
II. 4	^{57}Fe Mossbauer Spectrum of Fe - 2.34 wt. % N Austenite (points)	69
4a	compared to "separated" model of nitrogen atoms (line)	70
4b	compared to "random" model of nitrogen atoms (line)	71
II. 5a	^{57}Fe Mossbauer Spectrum of Fe - 2.83 wt. % N Virgin Martensite	73
5b, c	Comparison of Virgin Martensite Spectrum (points) to "random" model of nitrogen atoms (line)	74, 75
II. 6	^{57}Fe Mossbauer Spectrum of Fe - 2.34 wt. % N Martensite Aged 24 Hours at 100°C. Indicated is the spectrum of $\alpha\text{-Fe}_{16}\text{N}_2$	79

<u>Figure No.</u>		<u>Page No.</u>
II. 7	Mössbauer Spectrum of Fe - 2.83 wt. % N Martensite	82
II. 8	Difference Spectrum for Aging Fe - 2.83 wt. % N Martensite at Room Tempera- ture (from Figures II. 5 and II. 7), indicating the formation of Fe ₁₆ N ₂ Spectrum.	84
III. 1a	Mössbauer Spectrum of Iron - 1.86 wt. % Carbon Virgin Martensite Plus Austenite, Measured at -193°K.	104
1b	Mössbauer Spectrum of Martensite Aged at 323°K for 25 Hours, Measured at -193°K	106
1c	Difference Spectrum of Martensite: Changes Occurring during 25 Hours of Aging at 323°K, Measured at -193°K. Indicated are the spectra from the two iron atom sites in Fe ₄ C and the spectrum for the "pure iron" in the carbon-depleted regions.	108
III. 2	Isothermal Transformation Curves for the Clustering of Carbon Atoms in Martensite based on Mössbauer Measurements: fraction transformed, f, vs. time, t.	110
III. 3	Isothermal Transformation Curves for the Clustering of Carbon Atoms in Martensite: f vs. ln t.	113
III. 4	Isothermal Transformation Curves for the Clustering of Carbon Atoms in Martensite: ln (-ln (1-f)) vs. ln t.	116
III. 5	A Possible Carbon Concentration Profile of the Aged Martensite, indicating Regions still Possessing the Virgin Structure, Carbon-depleted Regions, and Fe ₄ C Regions.	120

<u>Figure No.</u>		<u>Page No.</u>
IV. 1	Hexagonal-Close-Packed Structure	124
IV. 2	^{57}Fe Mossbauer Spectra of ϵ -Nitride	132
2a	23.8 at. % N	133
2b	21.6 at. % N	134
2c	18.2 at. % N	135
2d	17.7 at. % N	136
2e	17.1 at. % N	137
IV. 3	^{57}Fe Mossbauer Spectra of ϵ -Nitride Measured at -193°C :	138
3a	21.6 at. % N	139
3b	18.2 at. % N	140
3c	17.1 at. % N	141
IV. 4	^{57}Fe Mossbauer Spectrum of ϵ -Nitride (17.1 at. % N) at Room Temperature following Quenching to -193°C .	145
IV. 5	^{57}Fe Mossbauer Spectrum of Fe_3N ϵ -Nitride:	147
5a	Quenched from 640°C	148
5b	Quenched from 625°C	149
5c	Quenched from 610°C	150
5d	Quenched from 580°C	151
5e	Quenched from 550°C	152
IV. 6	Hyperfine Magnetic Fields of Fe_{II} as a Function of Nitrogen Content	156
IV. 7	Curie Temperature of ϵ -Nitride as a Function of Nitrogen Content	160
IV. 8	Fe_3N Structure from Hendricks and Kosting. ³	162
V. 1	The Temperature Dependence of the Recoilless Fraction, as Calculated by the Debye Theory and Measured by Experiment	173

<u>Figure No.</u>		<u>Page No.</u>
V.2	The Mössbauer Spectrum of Fe - 2.4 wt. % N Martensite and Austenite	176
A.1	The Nitriding Apparatus	198
B.1	The Mössbauer Spectrometer	201
C.1	Comparison Between Model and Experimental Data for Five Values of F_o near 0.495.	209
F.1	The Mössbauer Spectrum of Fe - 12.2 wt. % Mn-3.9 wt. % N Austenite	236
F.2	The Mössbauer Spectrum of Fe - 12.2 at. % Mn-3.9 wt. % N Austenite after Tempering for Six Hours at 220°C	238

LIST OF TABLES

<u>Table No.</u>		<u>Page No.</u>
I.1	Physical Parameters of Fe ⁵⁷	24
II.1	Mössbauer Parameters of Iron Atom Environments	53
II.2	Fraction of Iron Atoms in Austenite having No Interstitial Atom Neighbors	88
IV.1	Hyperfine Magnetic Fields of Fe _{II} in ϵ -Nitride	154
V.1	The Relative Recoilless Fractions and Mean-Square Amplitudes of Displacement for Austenite and Martensite as Estimated from Theory and Measured by Experiment	178
V.2	Estimated Values of f_s and E_s^* , based on $f_s = 1.0$ at 295°K	184
V.3	Estimated Values of f_s and E_s^* , based on $f_s = 1.0$ at 320°K	185
C.1	Slopes, Intercepts and Variances	217

ACKNOWLEDGEMENTS

In undertaking a project of the scope and magnitude of a doctoral thesis, one becomes indebted to many people both within and without his department.

First, the author would like to thank his parents, whose love and support have played an indispensable role throughout his entire educational process.

The author is greatly indebted to his thesis advisor, Professor Roy Kaplow, for the daily guidance, encouragement and patience he has provided over the last four years.

Special thanks are extended to Professor Morris Cohen, whose continued interest and constructive contributions to this thesis have been invaluable.

Discussions with the thesis review committee, including Professors J. Elliott and W. S. Owen were also very helpful. Their sincere interest in this work is appreciated.

Discussions with Professors Elliott and J. Chipman, and with Dr. L. Kaufman, concerning the thermodynamics of austenite, were greatly appreciated as they played an important role in the development of many ideas.

The assistance and friendship of his fellow students, especially Steve Hansen and Carl Russo, were most welcome.

The author wishes to thank the Office of Naval Research, who supported this project.

Finally, much of the credit for this thesis deserves to be shared with the author's wife Sandy, whose assistance in conquering life's hassels, including the preparation of this manuscript, cannot be underestimated.

I. INTRODUCTION

I.1 Introduction to Mössbauer Spectroscopy

In 1961, Rudolph L. Mössbauer was awarded the Nobel Prize in physics for the discovery and interpretation of the recoil-free emission and resonant absorption of nuclear gamma-rays in Ir.¹⁹¹ From the time of Mössbauer's first experiments in the late 1950's,¹ this phenomenon, which now bears his name, has been observed in some forty-five different isotopes. The most heavily investigated of these has been Fe,⁵⁷ as that isotope exhibits the effect most readily and because of the scientific and commercial importance of iron-based alloys.

The theory behind the Mössbauer effect and its applications to iron-based systems has been the topic of a number of books and reviews.^{2, 3, 4, 5} This introduction will be fashioned predominantly after the thesis review of Gielen⁶ and Choo.⁷

Gamma-rays originate from nuclear transitions between an excited state, E_e , and a ground state, E_g . A recoil momentum is associated with such a process, and if the atom were free to move, a corresponding recoil energy, R , would be transferred to the emitting nucleus as kinetic energy of the atom. In a solid, however, R is much smaller than the energy binding the atom to its lattice site and only of the same order as the quantized energy required to excite the phonons.

The linear momentum is, therefore, transferred to the lattice as a whole but energy can only be dissipated in or gained from phonons or other lattice excitations. There is a finite probability, f , that an individual nuclear transition will occur without such an exchange of energy. Thus, a fraction of the transitions occur in a "recoil-free" fashion, and gamma-rays can be emitted (or absorbed) at the precise energy of the nuclear level.

This recoil-free fraction, f , is temperature dependent. For a nucleus embedded in a perfectly rigid solid, f will be unity. For a Debye solid, it is dependent on the free atom recoil energy, R , the Debye temperature, θ_D , and the temperature, T . As in the case of X-ray "Bragg" diffraction maxima:

$$f = e^{-2w} \quad (\text{I. 1})$$

where

$$2w = \frac{3R}{k\theta_D} \left\{ \frac{1}{4} + \left(\frac{T}{\theta_D} \right)^2 \int_0^{\theta_D/T} \frac{x dx}{e^x - 1} \right\} \quad (\text{I. 2})$$

A more general expression for vibrational excitations is referred to as the Lamb-Mössbauer factor:⁸

$$f = e^{(-4\pi^2 \bar{x}^2 / \lambda^2)} \quad (\text{I. 3})$$

where λ is the wavelength of the gamma-ray, and \bar{x}^2 is the component of the mean square vibrational amplitude of the nucleus in the direction

of gamma-ray propagation.

The nuclear level itself exhibits an intrinsic energy distribution of Lorentzian shape.

$$I(E) = \frac{2}{\pi\Gamma} \frac{\Gamma^2/4}{(E-E_o)^2 + \Gamma^2/4} \quad (I.4)$$

where $E_o = E_e - E_g$. Although this distribution is very sharp compared to the magnitude of R , the theoretical shape and breadth are important parameters, since the latter is comparable to experimental resolution. Γ is the natural width of the gamma-ray dictated by the lifetime of the excited state of the nucleus, τ , according to the uncertainty principle:

$$\tau\Gamma \geq \frac{h}{2\pi}$$

where h is Planck's constant. For Fe^{57} , Γ is equal to 4.67×10^{-9} ev, corresponding to a τ of 9.97×10^{-8} seconds.^{9, 10}

The thermal motion of atoms in solids will produce a temperature shift of the center of gravity of the energy distribution of gamma-rays by the amount ΔE (the second order Doppler shift).¹¹

$$\Delta E = -E_o \frac{\bar{v}^2}{2c^2} \quad (I.5)$$

where \bar{v}^2 is the mean square velocity of the atoms and c is the speed of light.

In order for the Mössbauer effect to be observed, nuclei of the same species must be present in both a source and absorber of the gamma-rays. If the emitting and absorbing nuclei are in the same electronic environment and if the source and absorber are at the same temperature, the recoil-free emitted gamma-rays will have exactly the energy needed for them to be resonantly absorbed. When the nuclei have different electronic surroundings, the different hyperfine interactions between the nuclei and the environments would cause the energy required for absorption to differ from that of the emitted photons, and resonance is either weakened or destroyed. However, resonance can be restored by superimposing the proper external Doppler shift on either the emitter or absorber to compensate for the difference.

In a typical Mössbauer experiment, the gamma-ray source is moved with respect to the absorber at a velocity, v . The energy of the emitted gamma-rays are shifted by the Doppler effect by an amount:

$$\Delta E = \frac{v}{c} E_0 \quad (\text{I.6})$$

The intensity of the gamma-ray beam transmitted through the absorber is measured as a function of the source velocity. When resonance absorption occurs at a positive velocity, the energy separation between the excited and ground states of the absorber is greater than that of the emitter.

Three types of hyperfine interactions cause perturbations of the energy levels of the nucleus: the isomer shift, the electric quadrupole interaction, and the magnetic dipole interaction.

The isomer shift is a result of the electrostatic interaction between the nucleus and the s-electrons, which have a finite probability of being at the nucleus, causing perturbations of the ground and excited states and changing their separation in energy. Thus, if the electronic charge density at the nuclei in the source is different from that in the absorber, the energy separation of the ground and excited states will generally also differ by an amount δ . Resonant absorption will then occur at a Doppler velocity corresponding to this energy difference.

The electric quadrupole interaction is created by an electric field gradient at the nucleus. This splits the excited state of Fe^{57} into two substates and resonant absorption will occur at two velocities corresponding to the energy difference between the ground state and each of the excited substates.

The magnetic dipole interaction is due to an effective magnetic field acting on the nucleus that splits the excited and ground states of the nucleus into four and two substates respectively. The magnitude of the splitting is proportional to the strength of the effective field. Although this gives rise to eight possible energy differences between ground and excited states, the selection rule for nuclear

magnetic transitions ($\Delta m = 0$ or ± 1) allows only six. When the source comprises only a single "line" (i.e., all Fe^{57} environments in the source have neither electronic quadrupole nor magnetic interactions), resonance in a ferromagnetic absorber will occur at six different velocities, resulting in a six-peak spectrum. In a randomly oriented polycrystalline absorber, the relative intensities of the six peaks in order of increasing energy, or velocity, will be 3:2:1:1:2:3 for Fe^{57} ¹².

The effects of these hyperfine interactions on the nuclear states are illustrated in Figure I. 1. When the three types of hyperfine interactions are combined with Fe^{57} nuclei, a six-peak magnetic-hyperfine-like Mössbauer spectrum is still obtained, but with altered peak positions. The energies of the transitions, represented in terms of Doppler velocities, and in order of increasing velocities, are:⁷

$$v_1 = \delta - \frac{c\mu}{E_0} (0.5g_{gr} - 1.5g_{ex})H + \epsilon \quad (\text{I.7})$$

$$v_2 = \delta - \frac{c\mu}{E_0} (0.5g_{gr} - 0.5g_{ex})H - \epsilon$$

$$v_3 = \delta - \frac{c\mu}{E_0} (0.5g_{gr} + 0.5g_{ex})H - \epsilon$$

$$v_4 = \delta + \frac{c\mu}{E_0} (0.5g_{gr} + 0.5g_{ex})H - \epsilon$$

$$v_5 = \delta + \frac{c\mu}{E_0} (0.5g_{gr} - 0.5g_{ex})H - \epsilon$$

$$v_6 = \delta + \frac{c\mu}{E_0} (0.5g_{gr} - 1.5g_{ex})H + \epsilon$$

Figure I.1

Hyperfine Interactions

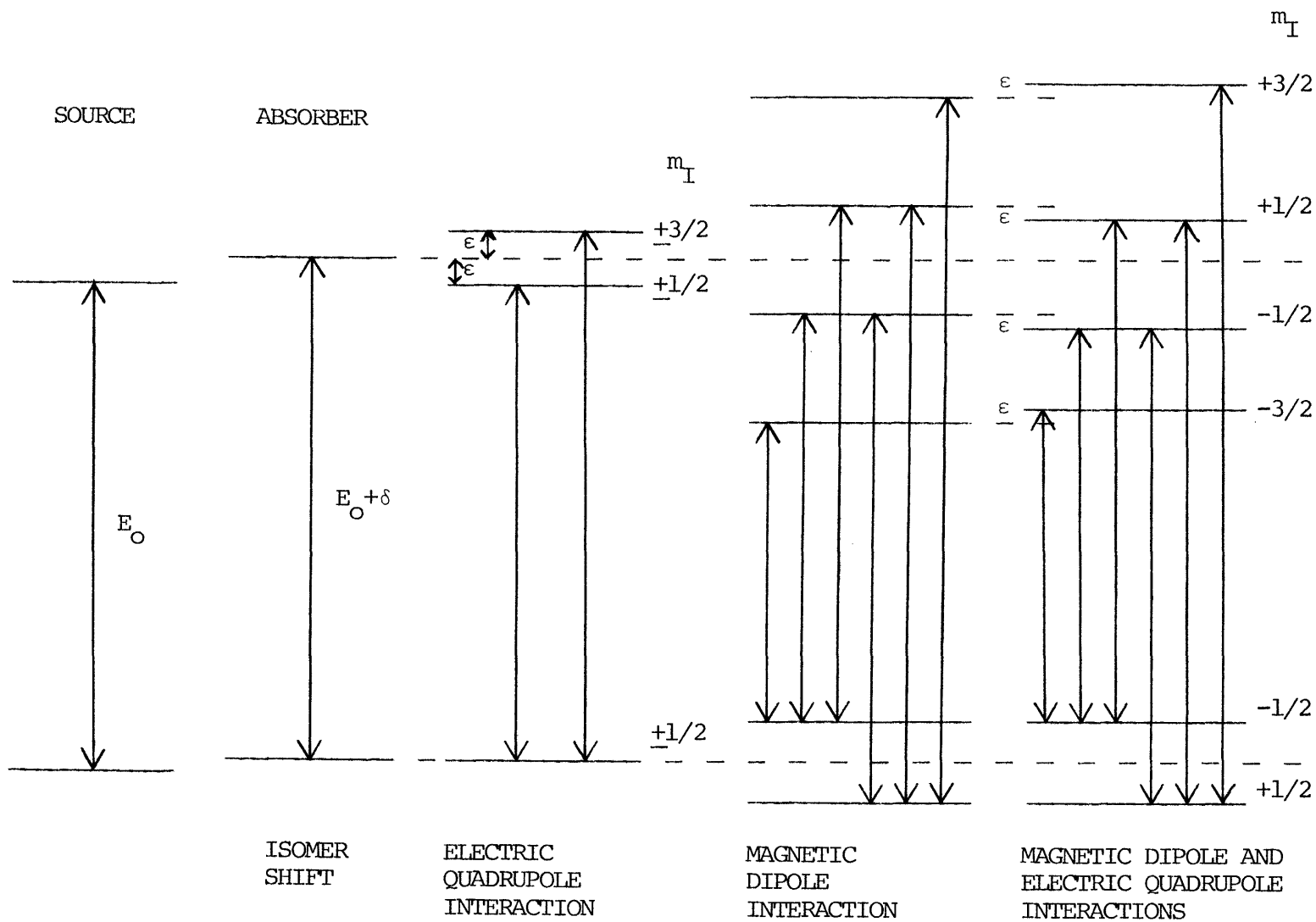


FIGURE I.1 HYPERFINE INTERACTIONS

where δ is the isomer shift (in mm/sec), ϵ is the quadrupole splitting (in mm/sec), H is the effective magnetic field (in KOe), μ is the nuclear Bohr magneton, and g_{gr} and g_{ex} the gyromagnetic ratios of the ground and excited states respectively. Equivalently, the hyperfine parameters may be defined and measured in terms of Doppler velocities. For Fe^{57} ,

$$\delta = 1/4 (V_1 + V_2 + V_5 + V_6) \quad (I.8)$$

$$\epsilon = 1/4((V_6 - V_5) - (V_2 - V_1))$$

$$H = 30.96 (V_6 - V_1) \text{ (in KOe)}^{12}$$

Application of Mössbauer spectroscopy to the study of iron alloys is facilitated by a convenient source of gamma-rays, radioactive Co^{57*} which decays by electron capture to Fe^{57} in the excited state. The half-life of this process is 270 days. The transition of Fe^{57} from the excited to ground states occurs either directly, with the emission of 137 Kev gamma-ray, or indirectly through an intermediate 14.37 Kev state, as shown in Figure I.2. This relatively low energy yields a large recoil-free fraction, f , and is therefore, the gamma-ray used in the Mössbauer spectroscopy of iron. The radioactive Co^{57} atoms are diffused into a non-magnetic host metal (copper in this experiment) to fabricate a source.

Figure I.2 Decay Scheme of Co^{57}

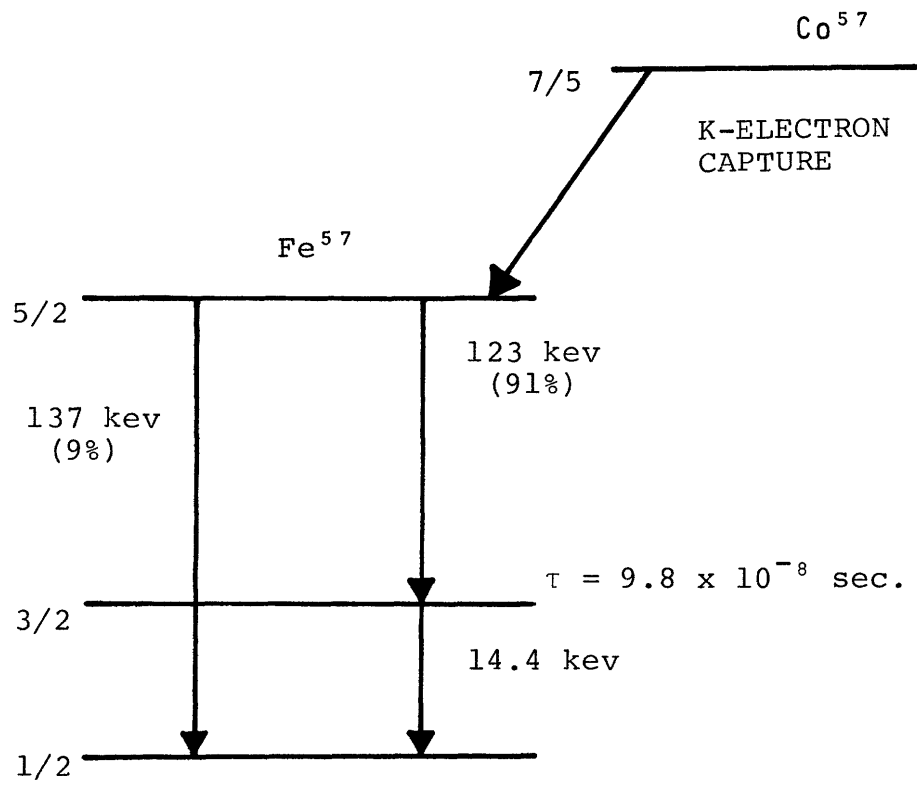


TABLE I. 1
Physical Parameters of Fe⁵⁷
 (ref. 5)

Gamma-ray energy	E_0	14.37 Kev
Half-life of excited state	τ	9.77×10^{-8} sec.
Natural width	Γ	4.6697×10^{-9} ev or 0.09714 mm./sec.
Minimum observable width	2Γ	0.19427 mm./sec.
Nuclear spin:		
ground state		1/2
excited state		3/2
Gyromagnetic ratio:		
ground state	g_{gr}	0.1806
excited state	g_{ex}	-0.102
Recoil energy	R	1.9567×10^{-3} ev
Natural abundance		2.17%

Although the Fe^{57} isotope is present at a natural abundance of only 2.17%,⁵ the large recoil-free fraction associated with this nucleus permits a useful resonant effect even in unenriched absorbers. The physical parameters associated with the Mössbauer effect in Fe^{57} are given in Table I. 1.

I. 2 Literature Review

I. 2. 1 Mössbauer Spectroscopy of Iron-Carbon Alloys

The identification of the various carbide structures known to form either during the equilibrium cooling of austenite or by precipitation from metastable martensite and retained austenite is essential to the understanding of the Mössbauer spectroscopy of iron-carbon alloys. Cementite (Fe_3C), the most stable and well-defined of these carbides, has been the subject of extensive Mössbauer studies since Shinjo et al¹³ first reported its Mössbauer spectrum. Although two crystallographically distinct iron atoms sites exist in the cementite structure,¹⁴ the Mössbauer pattern shows only a single ferromagnetic spectrum. By studying the Mössbauer pattern of cementite as a function of temperature, Ron¹⁵ observed that above the Curie Point (215°C),¹⁶ only an asymmetric quadrupole split doublet existed. This spectrum was later interpreted as being due to two superimposed doublets, revealing the two iron environments.¹⁷ Choo and Kaplow demonstrated a magnetic hyperfine difference between these sites in the Mössbauer spectrum

of Fe_3B which is isostructural to Fe_3C .¹⁸ Bernas et al¹⁹ were the first to report the ^{57}Fe Mössbauer spectrum of Fe_5C_2 (the χ -carbide) which was chemically synthesized from iron oxide. Three ferromagnetic spectra were observed for the three different iron atom sites in the χ structure. Subsequently, Ino and co-workers²⁰ detected the precipitation of χ -carbide during the tempering of iron-carbon martensite as low as 220°C , and its gradual transformation to cementite at higher temperatures. Ino also reported the detection of ϵ -carbide after a one hour anneal of the martensite at 140°C . Because of the small quantities of ϵ -carbide present, these authors were only able to approximate the hyperfine field, reported as being 265 KOe. The difficulty in the detection of minute quantities of ϵ -carbide is emphasized by Genin and Flinn's²¹ inability to fully resolve the ^{57}Fe Mössbauer spectrum of iron-carbon martensite tempered at 120°C . Choo and Kaplow²² were able to ascertain the presence of a carbide phase characterized by a hyperfine magnetic field of 240 KOe after aging a martensitic sample at 80°C only by taking the difference between normalized ^{57}Fe Mössbauer spectra taken before and after aging. This same spectra also was observed in austenitic samples tempered at 160°C ²³ and has been attributed to ϵ -carbide. Samples containing large volume fractions (approximately 35%) of a hexagonal-close-packed carbide have been

produced by the oxygen reduction of Fe_3O_4 by CO and H_2 gas mixtures.²⁴ Although this carbide was presumed to be ϵ -carbide, its Mössbauer spectrum revealed that it contained three distinct iron atom sites, which remains unexplainable in terms of either the traditional hexagonal $\text{Fe}_{2.4}\text{C}$ ²⁵ or more recent orthorhombic Fe_2C ²⁶ structures proposed for ϵ -carbide precipitated from martensite. However, the site having the largest hyperfine magnetic field, reported as 237 KOe, compares well with that detected by Kaplow.

Ron and co-workers^{15,27} studied the ϵ -, χ -, and cementite carbides extracted from tempered alloy steels containing silicon, manganese and carbon. Although silicon stabilizes ϵ -carbide to higher temperatures,²⁸ thus facilitating its study, the carbides formed in this steel were found to contain considerable amounts of both silicon and manganese substituting for iron. As a result, the hyperfine parameters reported for the carbides differ slightly from the other works reviewed.

Face-centered-cubic austenite has also been the subject of numerous Mössbauer studies.^{21,22,29,30,31} All investigators agree that the paramagnetic, three-peak spectrum, characteristic of austenite, is composed of quadrupole split doublet, due to the iron atoms which are the nearest neighbors of interstitial carbon atoms,

and a single peak due to all other iron atoms.

Similarly, the Mössbauer spectrum of martensite has been extensively examined. However, because of the complexity of the body-centered-tetragonal structure, its inherent ferromagnetism, and the ability of carbon atoms to redistribute themselves even at room temperature, it has remained a topic of debate. Some of the earliest studies of martensite were actually on the room temperature aged structure.^{32, 33} Genin and Flinn²¹ were the first to detect the changes which occur in the Mössbauer spectrum when martensite is allowed to age at room temperature. Their interpretation of the spectrum of virgin martensite is formulated in terms of iron atoms which neighbor an isolated carbon atom and those which neighbor a cluster of carbon atoms. They do not, however, differentiate between the two iron atoms which form the "dipole distortion" due to the presence of a carbon atom in the octahedral interstitial position (the first near neighbor of a carbon atom) and the four other iron atoms which surround an occupied interstitial site in a plane perpendicular to the c-axis of the bct martensite (the second near neighbors).

Lesoille and Gielen³¹ also attempted a quantitative interpretation of the Mössbauer spectrum of virgin martensite. However,

their analysis was based on the assumption that carbon atoms in virgin martensite occupy tetrahedral interstitial positions, which is now thought to be an incorrect model.^{34, 35}

A more recent study by Choo and Kaplow²² involved a detailed analysis of the changes occurring in the ^{57}Fe Mössbauer spectrum of virgin martensite during room temperature aging, which yielded a model for the structural changes which occur and a consistent interpretation of the spectrum of virgin martensite. Three ferromagnetic spectra were observed for virgin martensite, from iron atoms which were the first-, second-, and third-near-neighbors of a carbon interstitial. These spectra decreased in intensity upon aging at room temperature, and three new ferromagnetic spectra appeared. One of these was virtually identical to the spectrum of α -iron and was thereby related to the iron atoms which had lost all carbon neighbors in the aging process. The two other spectra were attributed to the formation of regions of ordered Fe_4C . The relative rates at which these spectra either appeared or disappeared were consistent with the proposed structural models for the alloy.

I.2.2 ^{57}Fe Mössbauer Spectroscopy of Iron-Nitrogen Alloys

^{57}Fe Mössbauer investigation of the iron-nitrogen system began with the identification of the spectrum of Fe_4N by Shirane.³⁶ The

crystal structure of this ferromagnetic nitride is a face-centered-cubic arrangement of iron atoms with a nitrogen at the body-centered position.³⁷ The hyperfine fields are 345 KOe for the corner and 215 KOe for the face-centered iron atoms. Nozik³⁸ claimed that the face-centered iron in Fe_4N actually consisted of two distinct species with opposite quadrupole splittings and different isomer shifts. This effect is explained to be a result of the interaction of the p-like orbitals of the nitrogen with the internal magnetic field.

Gielen and Kaplow²⁹ and later Yamaoka, Mekata and Takaki³⁹ both studied iron-nitrogen austenite. They observed a spectrum similar to that of iron-carbon austenite in that it consisted of a quadrupole split doublet due to the six iron atoms which are the nearest neighbors of each nitrogen atom, and a single peak due to the remaining iron atoms. The major differences are: (a) the quadrupole splitting for the neighbors of the nitrogen is less than that for the carbon (approximately 0.3 as compared to 0.6 mm/sec respectively), and (b) in the iron-nitrogen austenite, the doublet has a large positive isomer shift as compared to the single peak. Gielen attributes this behavior to bonding differences: carbon atoms contribute electrons to the iron 4s band, which will not greatly affect the isomer shift,

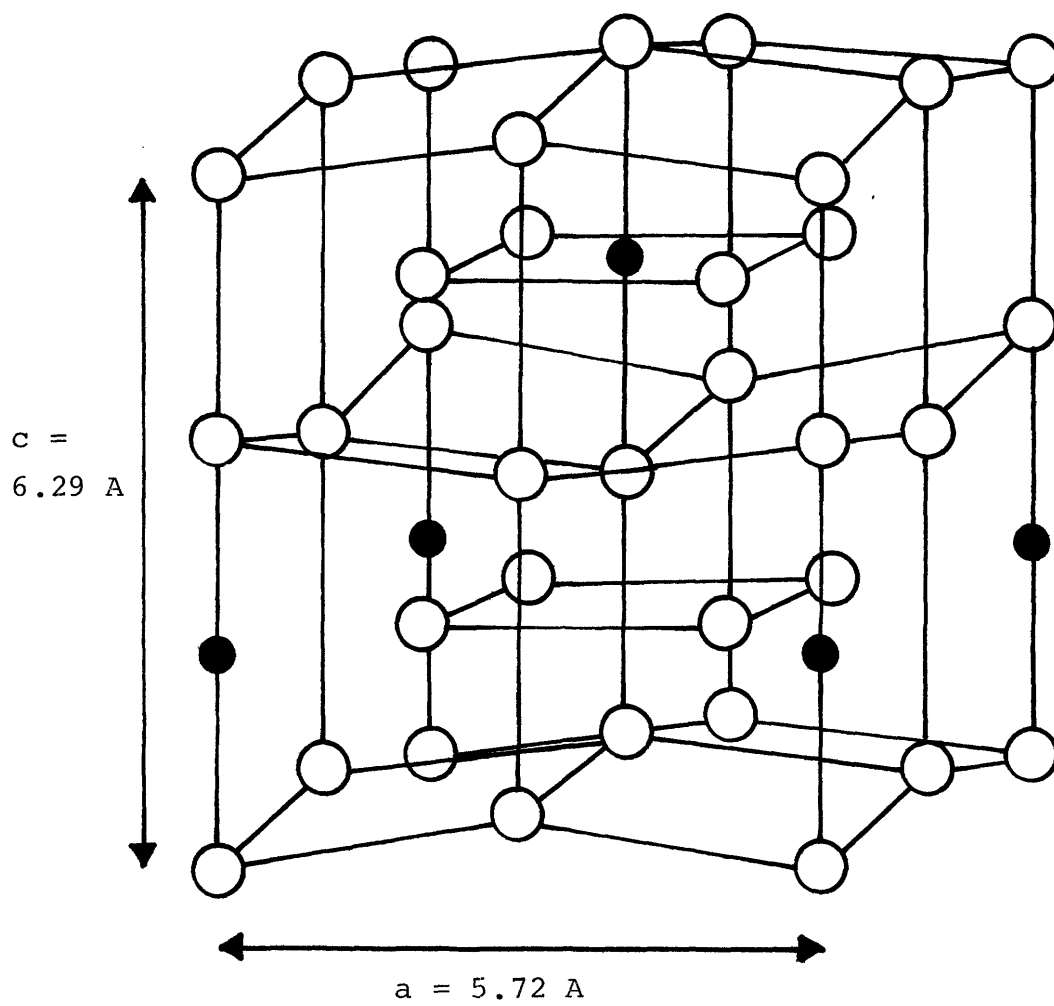
while the presence of nitrogen leaves iron in a $3d^8$ state, reflecting a covalent bond as in Fe_4N .³⁶

The understanding of the ^{57}Fe Mössbauer spectra of iron-nitrogen martensite and of the low temperature nitride $\alpha''-Fe_{16}N_2$ has remained confused. Since Gielen's²⁹ preliminary work, only two other studies have been made. Genin and Foct⁴⁰ measured the Mössbauer spectra of martensite freshly quenched, i. e., virgin, and martensite aged at $50^\circ C$. However, Genin interpreted these spectra in the same manner as he interpreted iron-carbon martensites,²¹ described previously. Thus, the spectrum of $Fe_{16}N_2$ was described as being composed of two ferromagnetic spectra whereas crystallographically, the structure has three different iron sites as described in Figure I.3.⁴¹ (Genin did not differentiate between the first- and second-near-neighbors of the nitrogen interstitial, thus making two of the three $Fe_{16}N_2$ sites equivalent.)

Ino and co-workers⁴² clearly demonstrated that the ^{57}Fe Mössbauer spectrum of $Fe_{16}N_2$ consisted of three ferromagnetic spectra, reflecting the three iron atom environments in the structure, but were unable to determine their relative intensities. Thus, they could not conclusively correlate the observed spectra to the crystallographic

Figure I.3

Fe_{16}N_2 Structure



○ IRON ATOM

● NITROGEN ATOM

sites in the Fe_{16}N_2 structure.

The remainder of the Mössbauer research on the iron-nitrogen system focuses on the hexagonal-close-packed (ϵ) iron phase. Although this structure is described as existing over a wide range of temperatures and compositions,^{43,44} it becomes increasingly difficult to retain the hcp phase as the nitrogen content is decreased below 27 at.%, which represents the phase boundary at room temperature. Thus, most investigations of the ϵ -nitride have been limited to the upper range of nitrogen composition.

Bridelle⁴⁵ has shown the Curie temperature of the ϵ phase to be a sharp function of nitrogen content, ranging from a maximum of about 300°C at 25 at.% nitrogen (Fe_3N) to well below room temperature at 30 at.%. This behavior has been verified by many Mössbauer experiments. The Mössbauer spectrum of an iron-32.0 at.% nitrogen alloy, when measured at room temperature, is a paramagnetic doublet with isomer shift of 0.40 mm./sec. and a quadrupole splitting of 0.25 mm./sec.⁴⁶ (The Curie temperature of this alloy is approximately -190°C.) An alloy of 23.8 at.% nitrogen (Curie temperature of approximately 300°C) when measured at room temperature, shows two ferromagnetic spectra, attributed to iron

atoms which have two nitrogen neighbors ($H = 238 \text{ KOe}$), and iron atoms with one nitrogen neighbor ($H = 298 \text{ KOe}$).⁴⁷ The magnetic moments of these iron atoms were calculated as $1.9 \mu_B$ and $2.4 \mu_B$ respectively. The ferromagnetic spectrum for an iron atom with three nitrogen neighbors ($H = 150 \pm 50 \text{ KOe}$) was reported in a Mössbauer study of a series of hcp alloys ranging from 28.6 to 33.0 at. % nitrogen. The Mössbauer spectra illustrated the decrease in the Curie temperature accompanying an increase in the nitrogen content. For alloys with a Curie temperature below room temperature, the magnetic transformation was demonstrated by the measurement of ferromagnetic spectra at liquid nitrogen or liquid helium temperature.⁴⁸

I.3 Historical Context of the Plan of Work

I.3.1 Outline of Work

The original purpose of the present work was the comparison of the nature and stability of iron-carbon and iron-nitrogen metastable solid solutions, primarily through the study of their Mössbauer spectra (Chapter II). The foundation of the investigation was the identification of the components of the Mössbauer spectra of each phase, considered in terms of structural models of the atomic arrangements. Whereas many of the pertinent spectra had already been resolved in this context, those associated with iron-nitrogen

martensite, i. e., the virgin structure, the room temperature aged structure and the Fe_{16}N_2 precipitate, remained confused. At the same time, the spectral identification of specific iron-carbon atomic environments deserved further confirmation. The basic problem involved with these identifications has been the resolution of overlapping ferromagnetic spectra of phases containing numerous iron-atom environments and/or environments present in only small amounts. The difference spectrum technique of directly comparing spectra measured at different stages of aging, developed by Choo and Kaplow in this laboratory, was again required to unravel the complex spectra involved.

The quantitative measurement of the components of each Mössbauer spectrum necessitated the refinement of mathematical fitting procedures to adequately represent the experimental peak shape. These must incorporate physically meaningful parameters describing both instrumental broadening and the intrinsic broadening observed in martensitic spectra, in addition to the basic theoretical model of gamma-ray emission and absorption.

The success encountered in the quantitative measurement of spectra, together with information available in Choo's thesis, encouraged an attempt to obtain additional kinetic data and to measure

the rate of carbon atom rearrangement in martensite at low temperature (Chapter III). Mössbauer measurements provide a direct method of calculating the fraction of virgin martensite transformed. This contrasts with electrical resistivity methods, which are based on conjectures regarding the magnitude of the many individual effects contributing to the overall resistivity changes in a sample.

In the process of preparation of iron-nitrogen alloys by rapid-quenching from the nitriding atmosphere, it became apparent that the hexagonal-close-packed phase could be retained at room temperature with nitrogen contents as low as 17.1 at.%. This represents a much wider range of composition, for the hexagonal phase, than previously reported. As this phase exhibits interesting magnetic properties at high nitrogen contents, a Mössbauer investigation of the lower range was deemed appropriate (Chapter IV).

The sensitivity of the Mössbauer effect to lattice excitations, coupled with recent interest in the association of lattice instabilities with structural transformations, directed the final portion of this project toward the investigation of the stability of iron-nitrogen austenite as a function of temperature (Chapter V).

Obtaining accurate results has been facilitated by advances in technology and analysis of Mössbauer spectroscopy. Therefore, it

was deemed reasonable to attempt the projects outlined above, each of which require relatively high precision.

I. 3. 2 Advances in Mössbauer Spectroscopy

The most important aspect in the evolution of Mössbauer spectroscopy has been the rapid development of the spectrometer itself. Recent advances have provided solutions to two problems which had seriously limited the use of the Mössbauer effect as a modern scientific tool: the speed of data acquisition and the calibration of the Doppler velocity scale.

The modern constant acceleration spectrometer incorporates an automated, electromechanical drive unit coupled with a multichannel analyzer which permits continuous measurement and storage of an entire spectrum. The Doppler velocity waveform may be adjusted so that the full multichannel analyzer memory may be utilized for the accumulation of a single spectrum, thereby increasing the point-to-point resolution.

When direct, channel to channel comparisons are made of two Mössbauer spectra, as in the difference spectrum technique, the calibration of the Doppler velocity scale becomes a critical issue. Use of a "standard" calibration absorber, such as α -iron, produces a

six-peak ¹¹¹Mössbauer spectrum, providing only six reference points from which the entire spectrum (usually 512 channels) must be calibrated. The addition of a laser interferometer to the spectrometer provides means for velocity calculation at periodic intervals through the spectrum. For a 512 channel multichannel analyzer, 32 channels (or more, if desired) may be utilized for velocity measurements. This abundance of information makes accurate interpolation possible for the velocity calibration of individual channels.

Thus, laser interferometry as a means of velocity calibration not only minimizes the horizontal error in the point-by-point representation of an individual spectrum, but also provides a means of representing any two spectra on the same velocity scale, point-to-point, so that they may be directly compared.

References

1. R. Mössbauer: Kernresonanz fluoreszenz von Gammastrahlung in Ir¹⁹¹, Z. Physik, 1958, vol. 151, 1. 124.
2. H. Frauenfelder: The Mössbauer Effect, W. A. Benjamin, Inc., New York, 1962.
3. G. Wertheim: Mössbauer Effect, Academic Press, Inc., New York, 1964.
4. V. I. Goldanskii and R. H. Herber: Chemical Applications of Mössbauer Spectroscopy, Academic Press, Inc., New York, 1968.
5. A. Muir, K. Ando and H. Coogan: Mössbauer Effect Data Index 1958-1965, Interscience, New York, 1966.
6. J. M. Gielen: Mössbauer Effect in Iron-Carbon and Iron-Nitrogen Solid Solutions, Ph.D. Thesis, M.I.T., 1965.
7. W. K. Choo: Mössbauer Effect Studies of Splat Quenched Iron Carbon and Iron Boron Alloys, Ph.D. Thesis, M.I.T., 1971.
8. J. Boyle, D. Bunbry, C. Edwards, and H. Hall: The Mössbauer Effect in Tin from 120°K to the Melting Point, Proc. Phys. Soc. (London), 1966, vol. 89, p. 187.
9. O. C. Kistner and A. W. Sunyar: Excited States of Fe⁵⁷ Populated in Co⁵⁷ Decay, Phys. Rev., 1965, vol. 139, p. 295B.
10. M. Eckhause, R. J. Harris, W. B. Schuler and R. E. Welsh: A measurement of the Lifetime of the 14.4 Kev Level of ⁵⁷Fe, Proc. Phys. Soc. (London), 1966, vol. 89, p. 187.
11. R. V. Pound and G. A. Rebka: Variation with Temperature of the Energy of Recoil-Free Gamma Rays from Solids, Phys. Rev. Letters, 1960, vol. 4, p. 274.

12. R. S. Preston, S. S. Hanna and J. Heberle: Mössbauer Effect in Metallic Iron, *Phys. Rev.*, 1962, vol. 128, p. 2207.
13. T. Shinjo, F. Itoh, H. Takaki, Y. Nakamura and N. Skikazono: Mössbauer Effect in Fe_2B , FeB , and Fe_3C , *J. Phys. Soc. Japan*, 1964, vol. 19, p. 1252.
14. H. Lipson and N. J. Petch: The Crystal Structure of Cementite, Fe_3C , *J. Iron Steel Inst.*, 1940, vol. 142, p. 95.
15. M. Ron, H. Schechter and S. Niedzwiedz: Precipitation of Iron Carbides in Tempered Martensite, *J. App. Phys.*, 1968, vol. 39, p. 265.
16. W. Hume-Rothery: The Structure of Alloys of Iron, 1965, Pergamon Press, Ltd., London.
17. M. Ron and Z. Mathalone: Hyperfine Interactions of ^{57}Fe in Fe_3C , *Phys. Rev. B*, 1971, vol. 4, p. 774.
18. W. K. Choo and R. Kaplow (private communication)
19. H. Bernas, L. A. Campbell and R. Fruchart: Electronic Exchange and the Mössbauer Effect in Iron Based Interstitial Compounds, *Phys. Chem. Sol.*, 1968, vol. 28, p. 17.
20. H. Ino, T. Moriya, F. E. Fugita, Y. Maeda, Y. Ono, and Y. Inokuti: A Study of the Mössbauer Effect During the Tempering of Iron-Carbon Martensite, *J. Phys. Soc. Japan*, 1968, vol. 25, p. 88.
21. J. M. Gielen and P. Flinn: Mössbauer Effect Study of the Clustering of Carbon Atoms during the Room Temperature Aging of Iron-Carbon Martensite, *Trans. A.I.M.E.*, 1968, vol. 242, p. 1419.
22. W. K. Choo and R. Kaplow: Mössbauer Measurements on the Aging of Iron-Carbon Martensite, *Acta Meta.*, 1973, vol. 21, p. 725.
23. N. DeCristofaro: The Aging of Martensite and Austenite, S.M. Thesis, M.I.T., 1973.

24. R. A. Arents, Yu V. Maksimov, I.P. Suzdalev, V.K. Imshennik, and Yu. F. Krupyanskiy: Mössbauer Study of the Local Magnetic Structure of Iron ϵ -Carbide and the Intermediate Carbides which arise during $\epsilon \rightarrow \gamma \rightarrow \theta$ Transformations, Phys. Metal. and Metallog., 1973, vol. 36, p. 46.
25. C. S. Roberts, B. L. Averbach, and M. Cohen: The Mechanism and Kinetics of the First Stage of Tempering, Trans. Am. Soc. Met., 1953, vol. 45, p. 576.
26. Y. Hirotsu and S. Nagakura: Crystal Structure and Morphology of the Carbide Precipitated from Martensitic High Carbon Steel During the First Stage of Tempering, Acta Met., 1972, vol. 20, p. 645.
27. Z. Mathalone, M. Ron, J. Pipman and S. Niedzwiedz: Mössbauer Characteristics of ϵ, χ & θ Iron Carbides, J. App. Phys., 1971, vol. 42, p. 687.
28. S. Murphy and J. A. Whiteman: The Precipitation of ϵ -Carbide in Twinned Martensite, Met. Trans., 1970, vol. 1, p. 843.
29. P. M. Gielen and R. Kaplow: Mössbauer Effect in Iron-Carbon and Iron-Nitrogen Alloys, Acta Met., 1967, vol. 15, p. 49.
30. B. Christ and P. Giles: On the Detection of Retained Austenite in High-Carbon Steels by Fe^{57} Mössbauer Spectroscopy, Trans. A.I.M.E., 1968, vol. 242, p. 1915.
31. M. Lesoille and P. M. Gielen: Mössbauer Spectroscopy Study of Iron-Carbon Austenite and Virgin Martensite, Met. Trans., 1972, vol. 3, p. 2681.
32. H. Ino, T. Moriya, E. Fugita and Y. Maeda: Mössbauer Effect in Iron-Carbon Martensite Structure, J. Phys. Soc. Japan, 1968, vol. 24, p. 60.
33. M. Ron and A. Kidron, H. Schechter and S. Niedzwiedz: Structure of Martensite, J. App. Phys., 1967, vol. 38, p. 590.

34. M. Cohen: The Strengthening of Steel, Trans. A.I.M.E., 1962, vol. 224, p. 638.
35. G. V. Kurdjumov and A. G. Kachaturyan: Nature of Axial Ratio Anomalies of the Martensite Lattice and Mechanism of Diffusionless $\gamma \rightarrow \alpha$ Transformation, Acta Met. 1975, vol. 23, p. 1077.
36. G. Shirane, W. J. Takei and S. L. Ruby: Mössbauer Study of Hyperfine Fields and Isomer Shifts in Fe_4N and $(\text{Fe}, \text{Ni})_4\text{N}$, Phys. Rev., 1962, vol. 126, p. 49.
37. K. H. Jack: The Iron-Nitrogen System: The Structures of Fe_4N and Fe_2N , Proc. Roy. Soc. (London), 1948, vol. A195, p. 34.
38. A. J. Nozik, J. C. Wood, and G. Haacke: High Resolution Mössbauer Spectrum of Fe_4N , Sol. St. Comm., 1969, vol. 7, p. 1677.
39. Y. Yamaoka, M. Mekata and H. Takaki: Mössbauer Effect Study of Face-Centered Cubic Fe Nitrides, J. Phys. Soc. Japan, 1973, vol. 35, p. 63.
40. J. M. Genin and J. Foct: Mössbauer Spectroscopy of Disordered and Ordered Iron-Nitrogen Solid Solutions, Phys. Stat. Sol. (a), 1973, vol. 17, p. 395.
41. K. H. Jack: The Occurrence and the Crystal Structure of α' -Iron Nitride, Proc. Roy. Soc. (London), 1951, vol. A208, p. 216.
42. T. Moriya, Y. Sumitomo, H. Ino, F. E. Fugita, and Y. Maeda: Mössbauer Effect in Iron-Nitrogen Alloys and Compounds, J. Phys. Soc. Japan, 1973, vol. 35, p. 1378.
43. V. G. Paranjpe, M. Cohen, M. B. Bever and C. Floe: The Iron Nitrogen System, Trans. A.I.M.E., 1950, vol. 188, p. 261.
44. K. H. Jack: The Iron-Nitrogen System: The Crystal Structures of ϵ -Phase Iron Nitrides, Acta Cryst., 1952, vol. 5, p. 404.

45. R. Bridelle: Sur Les Nitrures et Carbonitrures de Fer,
Ann. Chim. (Paris), 1955, ser. 12, vol. 10, p. 824.
46. M. Chabanel, C. Janot and J. Motte: Etude par effet Mössbauer
des nitrures de fer ϵ et ξ au voisinage de la
composition Fe_2N , C. R. Acad. Sc. Paris (B),
1968, vo. 266, p. 419.
47. K. H. Eickel and W. Pitsch: Magnetic Properties of the
Hexagonal Iron Nitride ϵ - $\text{Fe}_{3.2}\text{N}$, Phys. Stat. Sol.,
1970, vol. 39, p. 121.
48. M. Mekata, H. Yoshimura and H. Takaki: Magnetic Study on
Hexagonal Nitrides of 3d Transition Metals, J. Phys.
Soc. Japan, 1972, vol. 33, p. 62.

II. INTERSTITIAL ATOM CONFIGURATIONS IN STABLE AND METASTABLE FE-N AND FE-C SOLID SOLUTIONS

ABSTRACT

Mössbauer Fe⁵⁷ spectroscopy allows comparison of Fe-N and Fe-C interstitial solid solutions. The spectrum of Fe-N retained austenite indicates that nitrogen atoms are randomly distributed in octahedral interstitial sites, with this configuration being inherited, upon transformation, by the virgin martensite. These results are in contrast to Fe-C data. Carbon atoms in retained austenite tend to be far apart on their octahedral sites, and this nonrandom distribution is inherited by the virgin martensite. Virgin nitrogen martensite ages at room temperature by local ordering of nitrogen atoms. In that process, three new iron atom environments develop, characteristic of the α'' -Fe₁₆N₂ structure. However, the excessive width of the peaks indicates that the perfect order of the Fe₁₆N₂ precipitate is not achieved, except after very long times. Further aging at 100°C leads to the complete decomposition of the virgin martensite to the discrete phases α -iron and Fe₁₆N₂.

II.1 Introduction

Interstitial alloys of iron have been studied for many years because of their versatility and remarkable mechanical properties. During centuries of investigation, virtually every available experimental tool has been used - ranging from hardness testing to electron microscopy. This report relates to a study by Mössbauer spectroscopy¹, which appears to be one of the most powerful means for understanding behavior of interstitial atoms in iron.

The first comprehensive Mössbauer study of both iron-carbon and iron-nitrogen solid solutions was done by Gielen and Kaplow² in 1967. Subsequent experiments have focused on iron-carbon martensite, and have explored tempering effects³ as low as room temperature.⁴ Choo and Kaplow's⁵ detailed analysis of the changes occurring in the Mössbauer spectrum of virgin martensite during room temperature aging have yielded a model for the structural modifications which occur, and also provide a consistent interpretation of the spectrum of virgin martensite. Recently, Lesoille and Gielen⁶ have attempted quantitative interpretation of the Mössbauer spectra of iron-carbon austenite and virgin martensite. However, their analysis was based on the assumption that carbon atoms in virgin martensite occupy tetrahedral interstitial positions, which is now thought to be an incorrect model.^{7,8}

Similar, but less numerous, reports have been published on the iron-nitrogen system,^{9,10,11} but these do not provide an adequate picture of the structure and tempering processes associated with iron-nitrogen austenite and martensite.

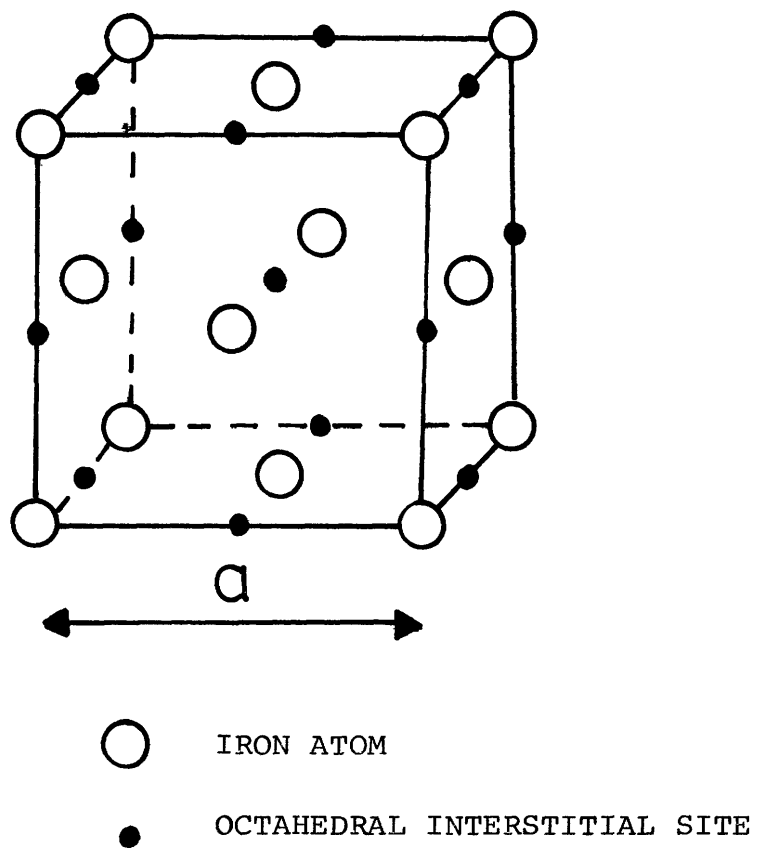
Interpretation of the Mössbauer patterns of interstitial alloys of iron requires consideration of the basic atomic arrangements involved. For example, carbon and nitrogen atoms in face-centered-

cubic austenite occupy the octahedral interstitial sites as shown in Figure (II. 1a). The six nearest neighbor iron atoms which surround the site form a regular octahedron and are symmetrically displaced when the site is filled. In body-centered-tetragonal martensite, carbon and nitrogen atoms occupy the set of octahedral interstitial sites inherited from the austenite by the Bain transformation. These octahedra are not regular, but shortened in one direction (Figure II. 1b). When occupied, the two iron atoms which are the first-near neighbors of the interstitial site are severely displaced, along the four-fold symmetry axis, producing "dipole distortions". The four second-near neighbor and eight third-near neighbor iron atoms of the site are also displaced, but to a lesser extent.

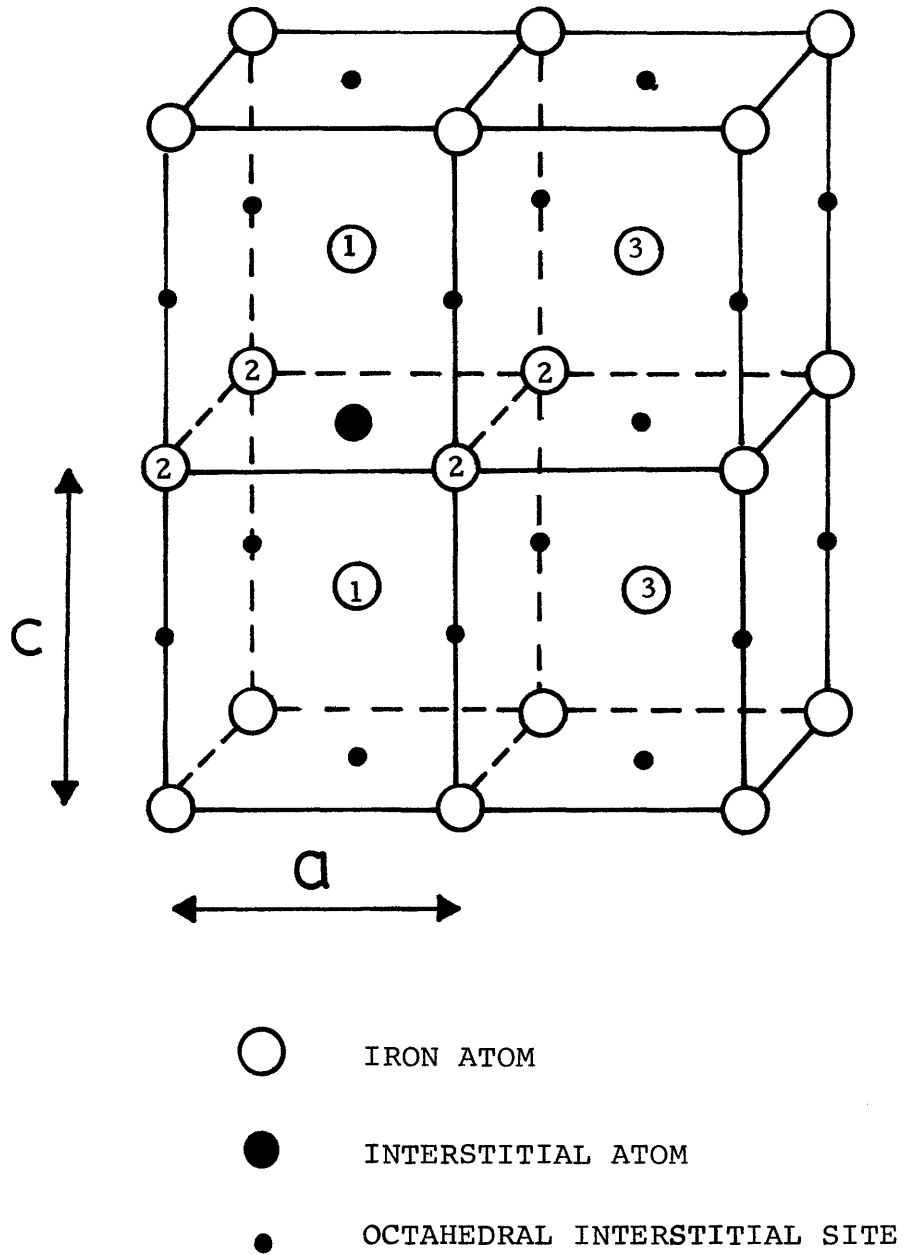
II. 2 Experimental Procedure

To facilitate the study of retained austenite, virgin martensite and the structural rearrangements which martensite experiences at room temperature, alloys with M_s temperatures close to or below room temperature were needed. Iron 1.86 wt. % carbon⁵ and iron-nitrogen alloys of greater than 2.34 wt. % nitrogen¹² satisfy this criterion. Virtually fully austenitic flakes (0.0005 inches in thickness) of the iron-carbon alloy were obtained by splat quenching from the melt onto a cooled copper substrate.⁵ Iron-nitrogen samples

Figure II.1 a Austenite Structure
b Martensite Structure



II.1 a



were produced by nitriding a pure iron (99.9%) foil, 0.001 inches thick, in flowing mixtures of ammonia and hydrogen at temperatures between 650°C and 700°C . The furnace was vertical, and rapid quenching rates were produced by dropping the samples from the nitriding atmosphere into a brine bath. In this manner, fully austenitic foils were produced with nitrogen contents ranging from 2.34 to 2.83 wt.%. For a more complete description of sample preparation, refer to Appendix A. Phases present in all samples were checked by X-ray diffraction and M^{II} össbauer spectroscopy. Composition was determined by chemical analysis.

M^{II} össbauer spectra of the austenite were recorded at room temperature. The samples were then cooled in situ to -193°C in a liquid nitrogen dewar, causing a partial transformation of the austenite to martensite; the spectrum of virgin martensite was recorded at the low temperature. The sample was returned to room temperature for aging, and at various time intervals was re-cooled to -193°C for M^{II} össbauer measurements for comparison with the virgin spectrum. For aging experiments at 100°C , M^{II} össbauer spectra were taken at room temperature, before and after the heat treatment for various times. The hyperfine parameters of the distinguishable site environ-

ments in all of the phases identified are given in Table (II. 1).

A constant acceleration Mössbauer spectrometer (Austin Science Associates) with a ^{57}Co in copper γ -ray source was used in this study (Appendix B). The Doppler velocity was calibrated with a laser interferometer¹³ and checked with an α -iron reference. Thus, all Mössbauer spectra could be plotted point for point on the same velocity scale.

Direct comparison of Mössbauer spectra taken before and after each heat treatment was done by the difference-spectrum technique formulated by Choo and Kaplow.⁵ For these comparisons, the following restraints must be observed:

1. Channel to channel variation of the Doppler velocity between the two spectra must be eliminated. Drift as small as ± 1 channel between measurements can cause serious distortion of the difference spectrum in the vicinity of sharp peaks. The laser interferometer enables us to satisfy this criterion. (Appendix C contains a more detailed discussion of error analysis relevant to the results in this thesis.)

2. Statistical fluctuations in the data must be minimized. Fluctuations in the difference spectrum are approximately $\sqrt{2}$ as large as in either spectra being compared. As the difference spectrum is

TABLE II.1

MOSSBAUER PARAMETERS OF IRON ATOM ENVIRONMENTS

Structure Iron Atom Type	interstitial composition (y)	relative fraction of spectrum	T	isomer shift (mm/sec)	quadrupole splitting (mm/sec)	hyperfine magnetic field (KOe)
Fe 1.86 wt.% C Austenite	0.0875		20°C			
C neighbor		0.505		-0.29	0.63	----
no C neighbor		0.495		-0.33	----	----
Fe 1.86 wt.% C V. Martensite	0.0875		-193°C			
INN of C		0.175		0.05	-0.15	279
2NN		0.350		0.04	-0.04	331
3NN		0.475		-0.04	0.0	361
Fe ₄ C* (20°C Aged)	0.25		-193°C			
face-centered		0.75		0.096	0.011	280
corner		0.25		0.097	0.008	386
ε-carbide*			20°C			240
Fe 2.34 wt.%N Austenite	0.0956		20°C			
N neighbor		0.45		-0.18	0.29	----
no N neighbor		0.55		-0.39	----	----
Fe 2.83 wt.% N V. Martensite	0.116		-193°C			
1NN or N		0.221		-0.11	-0.32	316
2NN		0.306		-0.12	0.12	346
3NN		0.298		-0.06	0.0	370
no N neighbor		0.175				340
Fe ₁₆ N ₂	0.125		20°C			
1NN of N		0.25		-0.15	-0.17	288
2NN		0.50		-0.06	0.09	314
3NN		0.25		-0.09	-0.09	399

* Ref. 5

monitoring small effects (approximately 1% of the transmitted level) large numbers of counts per channel are necessary. For example, if each spectrum contains a transmitted intensity of 10^6 counts per channel ($\sigma = N^{-1/2} = 0.1\%$), the fluctuation in the difference spectrum will be as large as 20% of an effect totaling 1% of the transmitted intensity.

3. The source-absorber-detector geometry must be maintained for both spectral measurements. This prevents any change in the angular broadening due to the alignment of the spectrometer. In addition, the absorber must be positioned in the spectrometer identically for both measurements to ensure that the rate of "background" radiation detection is the same.

The spectra are then normalized at the regions of maximum gamma-ray transmittance. The difference spectrum is obtained by subtracting the spectrum taken after aging from the spectrum taken before aging. Positive peaks in the difference spectrum correspond to iron-atom environments which have increased in number during aging; negative peaks correspond to environments which have decreased in number.

II. 3 Experimental Results

The idealized Mossbauer pattern is the result of the convolution:¹⁴

$$P_{th}(E_s) = \int_{-\infty}^{\infty} I(E, E_s) [1 - \exp(-k \Sigma(E))] dE \quad (II.1)$$

where

$P_{th}(E)$ = theoretical resonant absorption

$I(E, E_s)$ = Lorentzian energy distribution of the gamma-radiation source

k = function of: cross section for resonant absorption, recoilless fraction, number of nuclei/cm² and thickness of the absorber

and

$$\Sigma(E) = \sum_{i=1}^N \frac{g_i \Gamma_a^2}{4(E - E_i)^2 + \Gamma_a^2} \quad (II.2)$$

The latter term is the sum of the series of Lorentzian curves each representing one distinct absorption energy in the sample. Γ_a is the width of a Mössbauer line ($\Gamma_a = 0.095$ mm./sec. for ⁵⁷Fe); E_i and g_i are the positions and fractional weights of the i -th line respectively.

Instrumental broadening was compensated for by convolving the theoretical resonant absorption with a normalized Gaussian curve, G , i. e.,

$$P(E_s) = \int_{-\infty}^{\infty} P_{th}(E) \cdot G(E - E_s) dE \quad (II.3)$$

The appropriate width for the broadening was determined by comparison of $P(E_g)$ with the experimental Mössbauer spectrum of α -iron. This procedure differs from other attempts to correct for instrumental broadening which have employed the use of artificially large line-widths in Equation (II.2). The Gaussian form is more likely than a Lorentzian for instrumental effects and appears to account adequately for the experimental shapes. In addition, in our modelling, the positions and fractional weights of related spectral lines in all hyperfine split spectra followed the physical constraints outlined by Wertheim.¹

While Equation (II.3) was used as the basic theoretical model, certain spectra, particularly virgin martensite, are more complex. Not only are the readily distinguishable peaks in virgin martensite broader, but within each ferromagnetic spectrum the peak width varies as a function of the magnitude splitting of the nuclear state; i. e., peaks furthest from the center of the spectrum are broader than the inner peaks. Close fits between model and experimental spectra for both iron-carbon and iron-nitrogen martensites were obtained by the following procedure: for each ferromagnetic spectrum, each individual absorption peak (each term in Equation (II.2)) was broadened by convolving it with a Gaussian curve whose width was proportional to the distance of the peak from the center of the spectrum. This is

equivalent to assuming a small spread of the effective field, H , associated with each of the separate spectra included. Thus, Equation (II.2) would become:

$$\Sigma(E) = \sum_{i=1}^N \left(\int \frac{g_i \Gamma_a^2}{4(E-E_i)^2 + \Gamma_a^2} G(E, E_i) dE \right) \quad (\text{II.4})$$

where $G(E, E_i)$ represents a Gaussian curve whose width is a function of peak position E . A listing of the computer program of this model is provided in Appendix D.

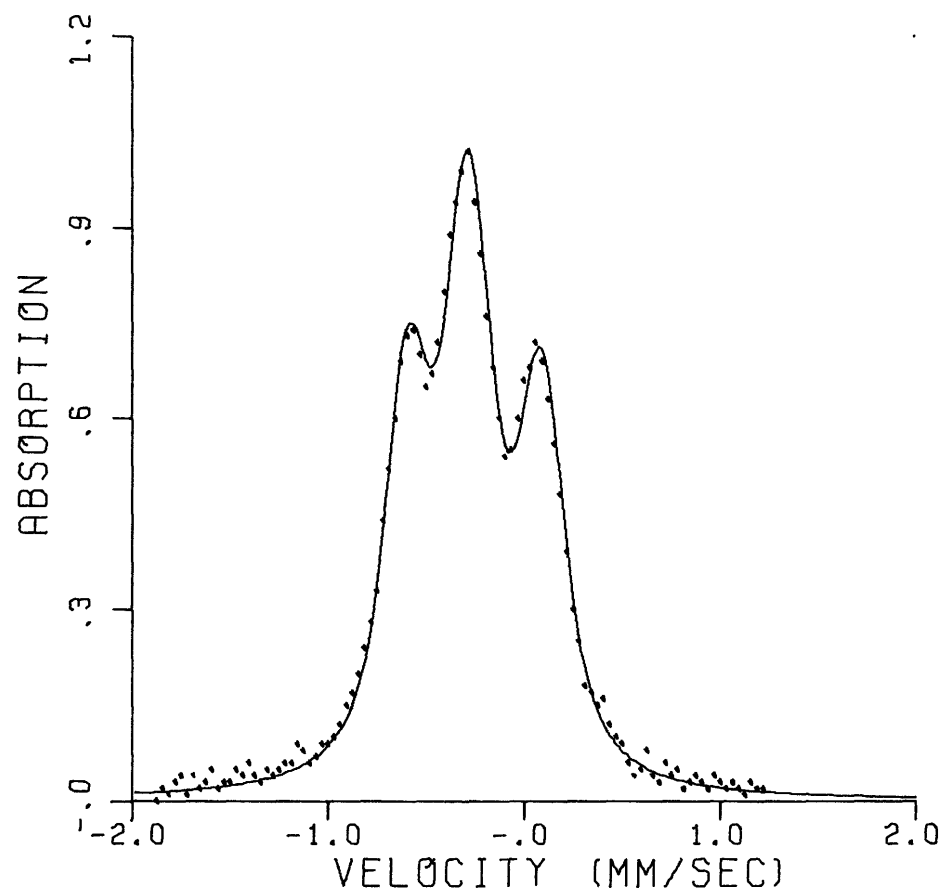
II. 3. 1 Iron-Carbon Alloys

II. 3. 1. 1 Carbon-Austenite

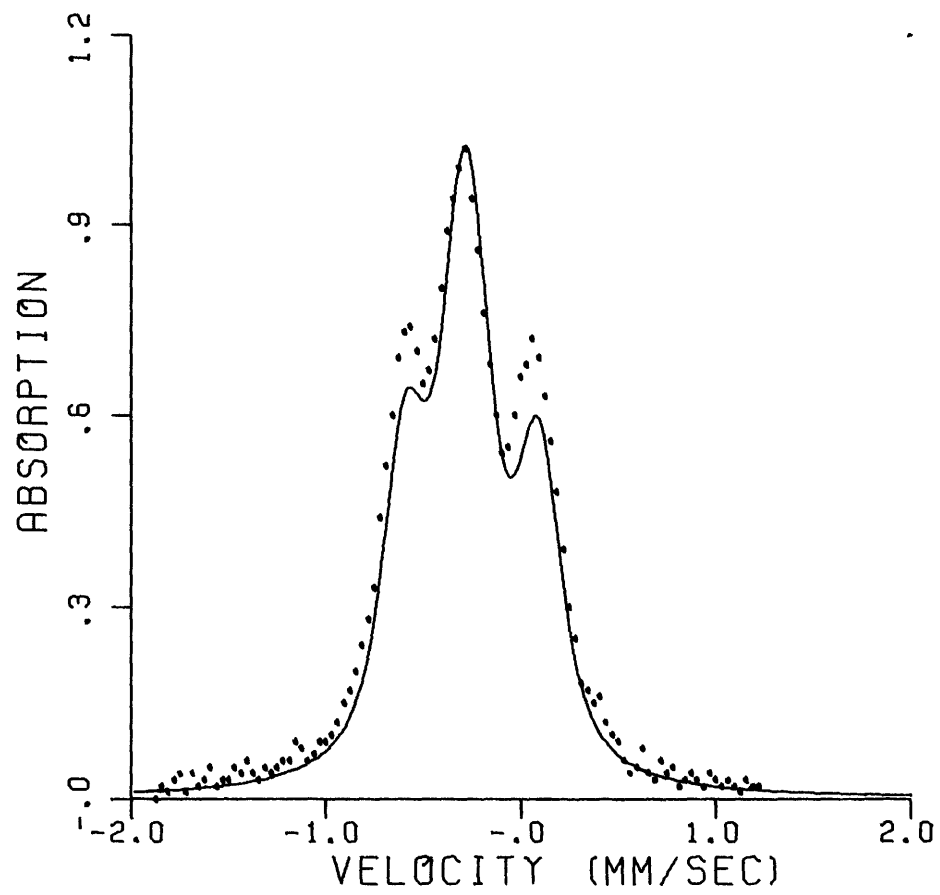
The Mössbauer spectrum of iron 1.86 wt. % carbon austenite (Figure II.2a, b) taken at room temperature, is interpreted, as earlier, as being comprised of: (a) a quadrupole split doublet due to the six iron atoms which are the nearest neighbors of each interstitial carbon atom, and (b) a central peak due to the remaining iron atoms. From the relative intensities of the doublet and the single peak, it was determined that 0.505 ± 0.008 of the iron atoms neighbor a carbon interstitial and 0.495 do not. (The precision of this measurement is determined in Appendix C.) For an alloy of this composition, in which 0.0975 of the octahedral interstitial sites are occupied by carbon atoms, the relative populations indicate that the carbon atoms are not randomly

Figure II.2 Mössbauer Spectrum of Fe-1.86 wt. % C Austenite (points)
II.2 a Compared to "separated" Model of Carbon Atoms (line)
II.2 b Compared to "random" Model of Carbon Atoms (line)

II, 2 a



II.2 b



arranged on the interstitial sites, but rather are separated such that relatively few iron atoms are the nearest neighbor of more than one carbon atom. Computer-generated comparisons of the "separated" and "random" models to the experimental data are shown in Figures (II. 2a) and (II. 2b) respectively.

II. 3. 1. 2 Virgin Carbon Martensite

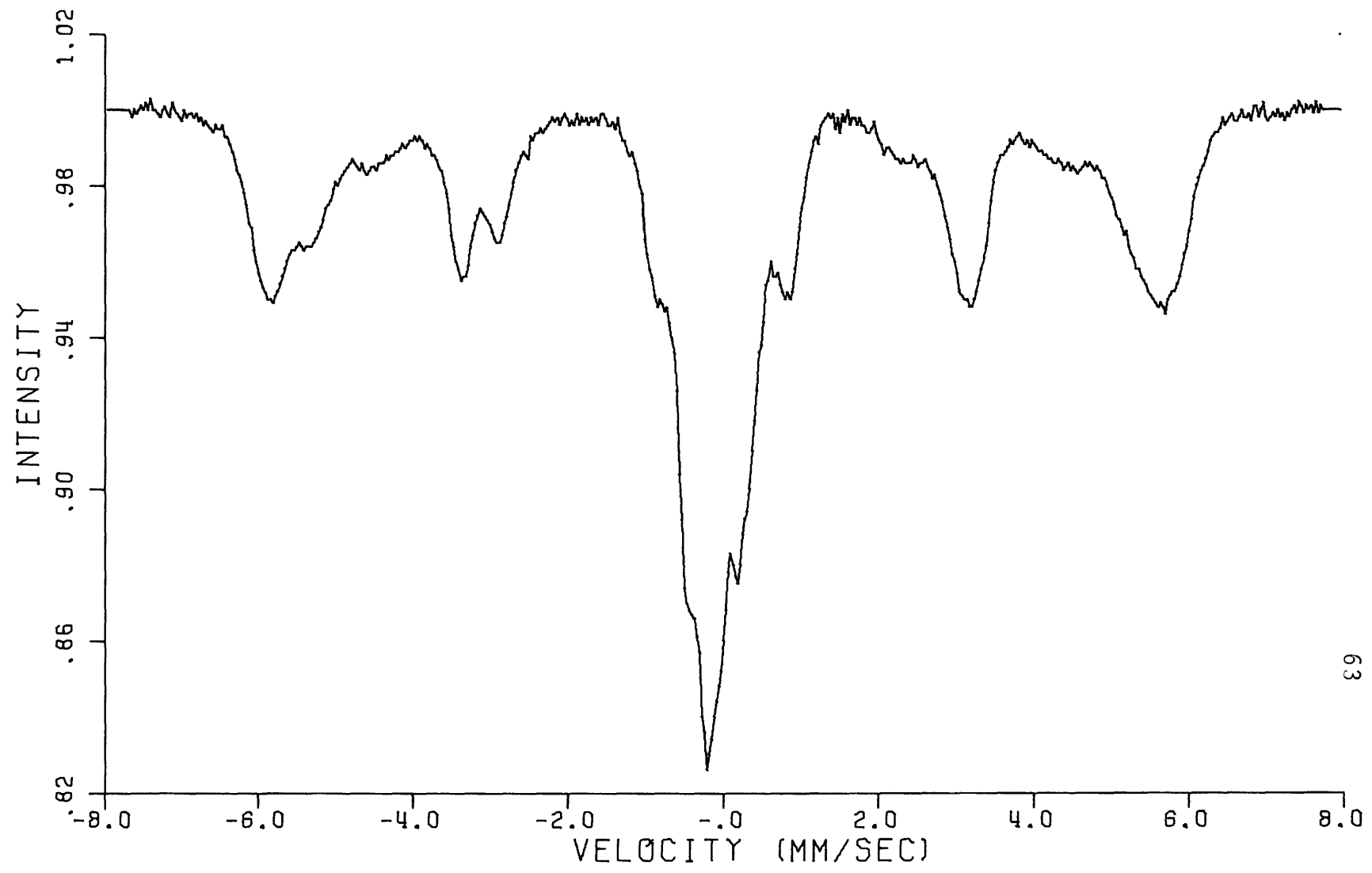
Virgin martensite was produced by quenching the austenite sample described above in a liquid-nitrogen dewar on the spectrometer. Figure (II. 3a) is the Mössbauer spectrum measured at -193°C immediately after that temperature had been reached. The spectrum displays the paramagnetic Mössbauer peaks of untransformed austenite as well as the more complex ferromagnetic spectrum of virgin martensite.

From room temperature aging of martensite, Choo and Kaplow⁵ were able to deduce that the broad, asymmetric peaks associated with virgin martensite were actually comprised of three distinguishable ferromagnetic patterns due to three different iron atom environments in the bct martensite structure. These were interpreted as iron atoms for which the closest carbon atom was in the first-, second-, or third-nearest neighbor position.

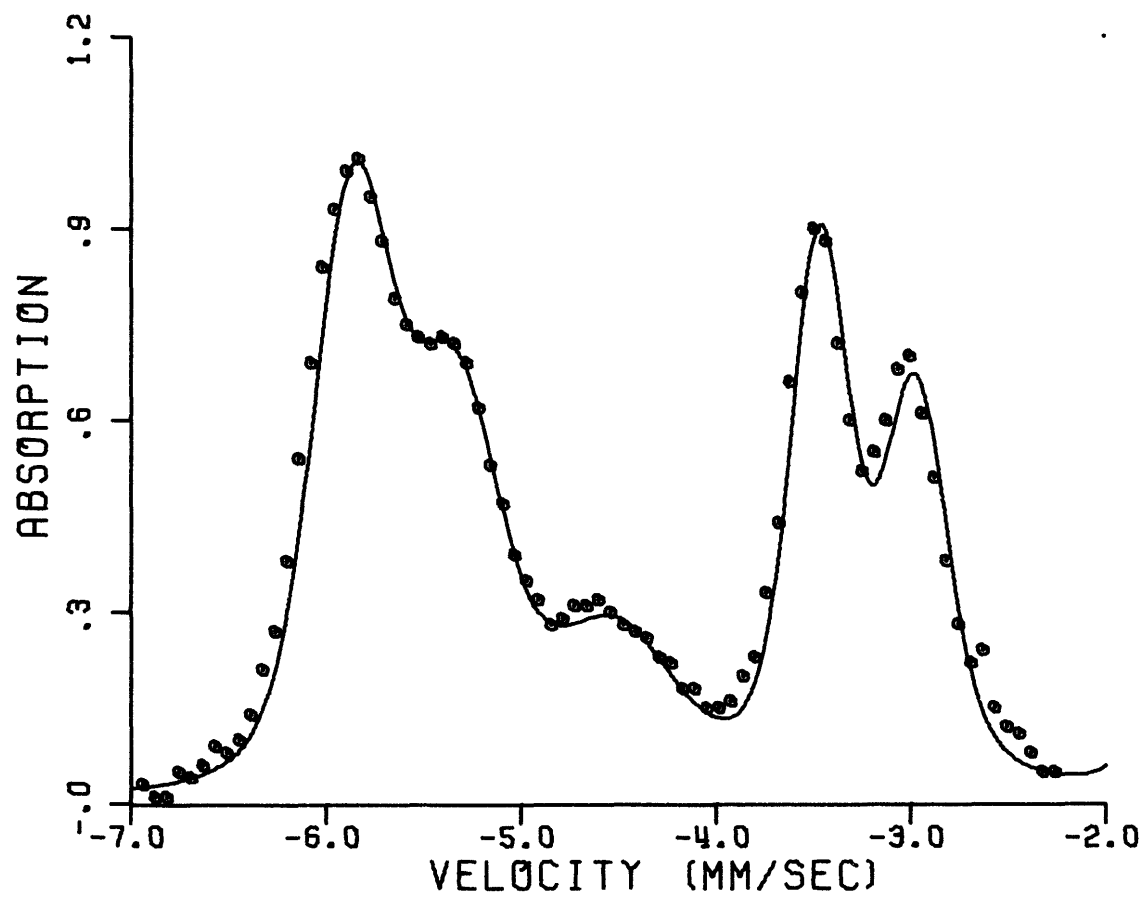
As in the case of the austenite, the relative intensities of the three spectra reveal the arrangement of carbon atoms on the

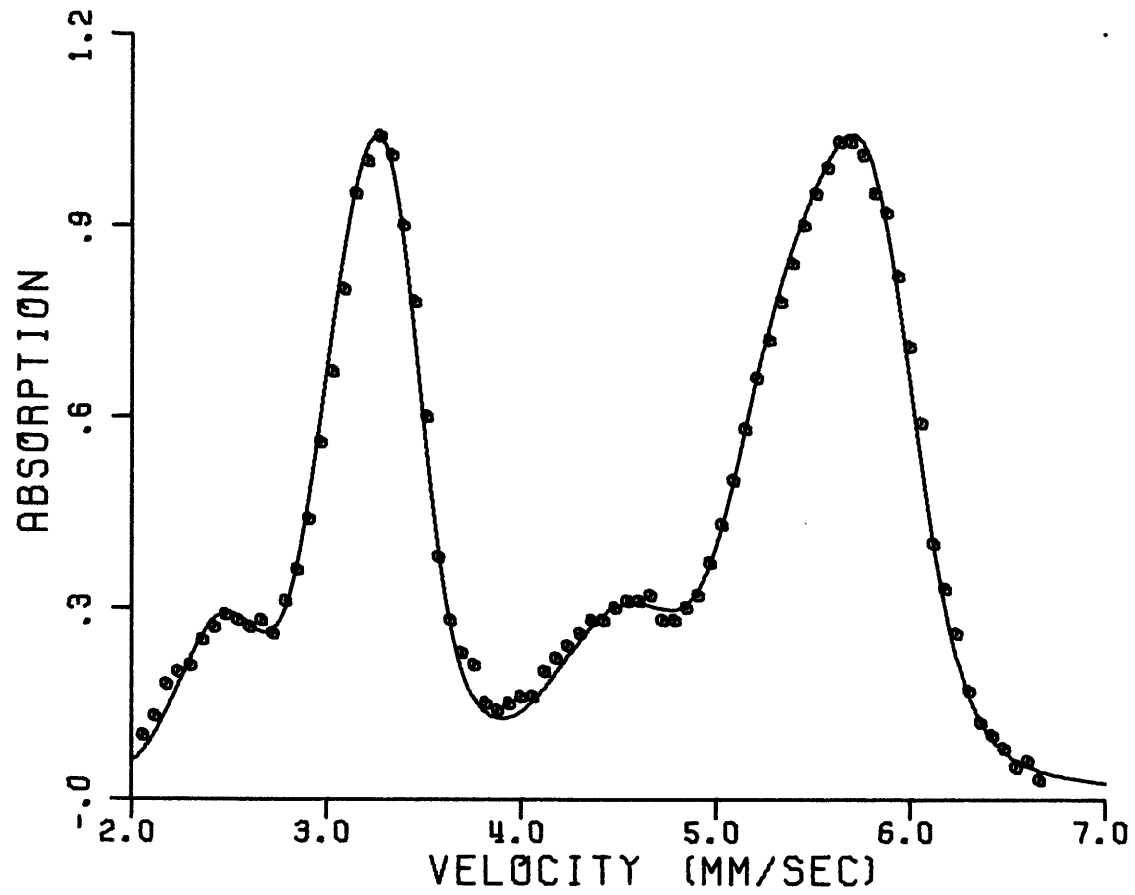
Figure II. 3 a ⁵⁷Mössbauer Spectrum of Fe - 1.86 wt. % C
Virgin Martensite
II. 3 b, c Comparison of Virgin Martensite Spectrum (points)
to "separated" Model of Carbon Atoms (line)

II.3 a



II.3 b





interstitial sublattice. Computer-generated patterns closely fit experimental data when the intensities of the first, second, and third neighbors are set at 0.175, 0.350, and 0.475 respectively, as demonstrated in Figures (II.3b) and (II.3c). These fractions imply that carbon atoms occupy positions on only one set of octahedral interstitial sites in bct martensite, and that they are situated apart from one another, as in the parent-phase austenite.

At such high-carbon contents (and nitrogen contents, in the next example), some iron atoms will inevitably have more than one close interstitial neighbor. Although the nearest of the neighboring interstitial atoms has the greatest effect on the iron atom and is the principal determinant on the hyperfine parameters, more distant interstitial atoms will cause slight perturbations. For example, a first-neighbor-type iron atom with another interstitial atom at a second- or third-neighbor distance will behave slightly differently than a first-neighbor iron with no other nearby interstitial atoms. This effect would explain the observed excess broadening of the martensite peaks. More specifically, slight variations in the hyperfine magnetic field account not only for the general broadening but also for the observed variation in widths as a function of transition energy. The excess

broadening is greatest for the spectrum associated with iron atoms which are first neighbors of an interstitial. This effect may be attributed to the relatively stronger secondary effect (as above) of variations in second-near neighbors.

II. 3. 1. 3 Aging of Martensite

Choo and Kaplow's Mössbauer measurements on the aging of iron-carbon martensite⁵ yielded the following results:

1. Carbon atoms in virgin martensite agglomerate at room temperature and regions of ordered Fe_4C are believed to result.
2. At 80°C , the spectra of virgin martensite and the room temperature aged structure decrease in intensity, indicating the disappearance of these arrangements and the spectrum of ϵ -carbide¹⁵ is observed to appear.
3. Above 160°C , Fe_3C precipitates.

Additional Mossbauer measurements by this author¹⁶ done in conjunction with the experimental work of Choo on the aging of austenite indicate that this phase decomposes by the formation of ϵ -carbide below 160°C and by the precipitation of Fe_3C above 180°C .

II. 3. 2 Iron-Nitrogen Alloys

II. 3. 2. 1 Nitrogen-Austenite

The Mössbauer spectrum of iron 2.34 wt. % nitrogen

austenite, Figure (II. 4a, b), differs from that of iron carbon austenite in the following respects:

- (a) iron atoms which are first neighbors of nitrogen interstitials show a smaller quadrupole splitting than in the iron-carbon case,
- (b) these first-neighbor iron atoms have a smaller negative isomer shift (with respect to the iron in the copper host of the source) than do iron atoms with no nitrogen neighbors.

The relative intensities of the doublet and the single peak indicate that 0.45 ± 0.008 of the iron atoms neighbor a nitrogen interstitial and 0.55 do not. As this alloy has 0.0956 of its interstitial sites occupied by nitrogen atoms, these fractions reveal that, unlike carbon, the nitrogen atoms are randomly arranged on the octahedral sites.

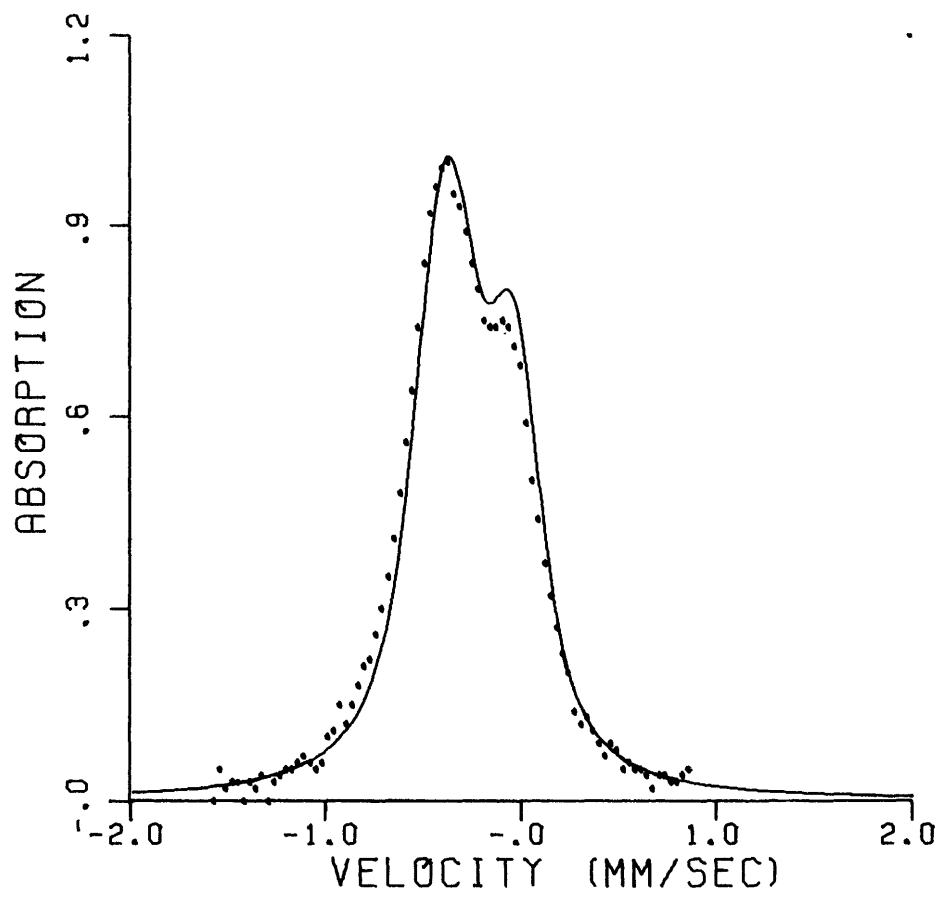
Computer-generated models of the "separated" (as in the case of iron-carbon austenite) and "random" configurations of nitrogen atoms are compared to experimental data in Figure (II. 4a and 4b).

II. 3. 2. 2 Virgin Nitrogen Martensite

Virgin martensite in an iron 2.83 wt. % nitrogen austenite alloy was produced as described for iron-carbon alloys. The Mössbauer spectrum recorded at -193°C , Figure (II. 5a) was interpreted in the

Figure II.4 ⁵⁷Mossbauer Spectrum of Fe-2.34 wt. % N Austenite
 (points)
II.4 a Compared to "separated" Model of Nitrogen Atoms
II.4 b Compared to "random" Model of Nitrogen Atoms

II.4 a



II.4 b

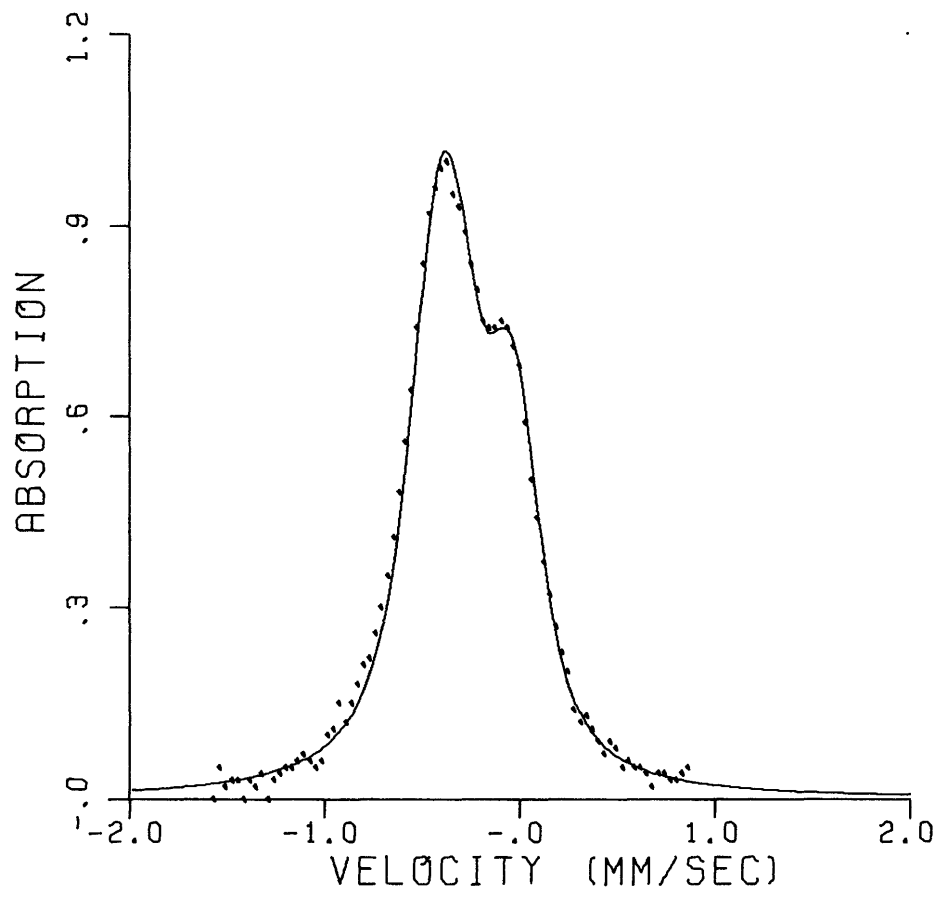
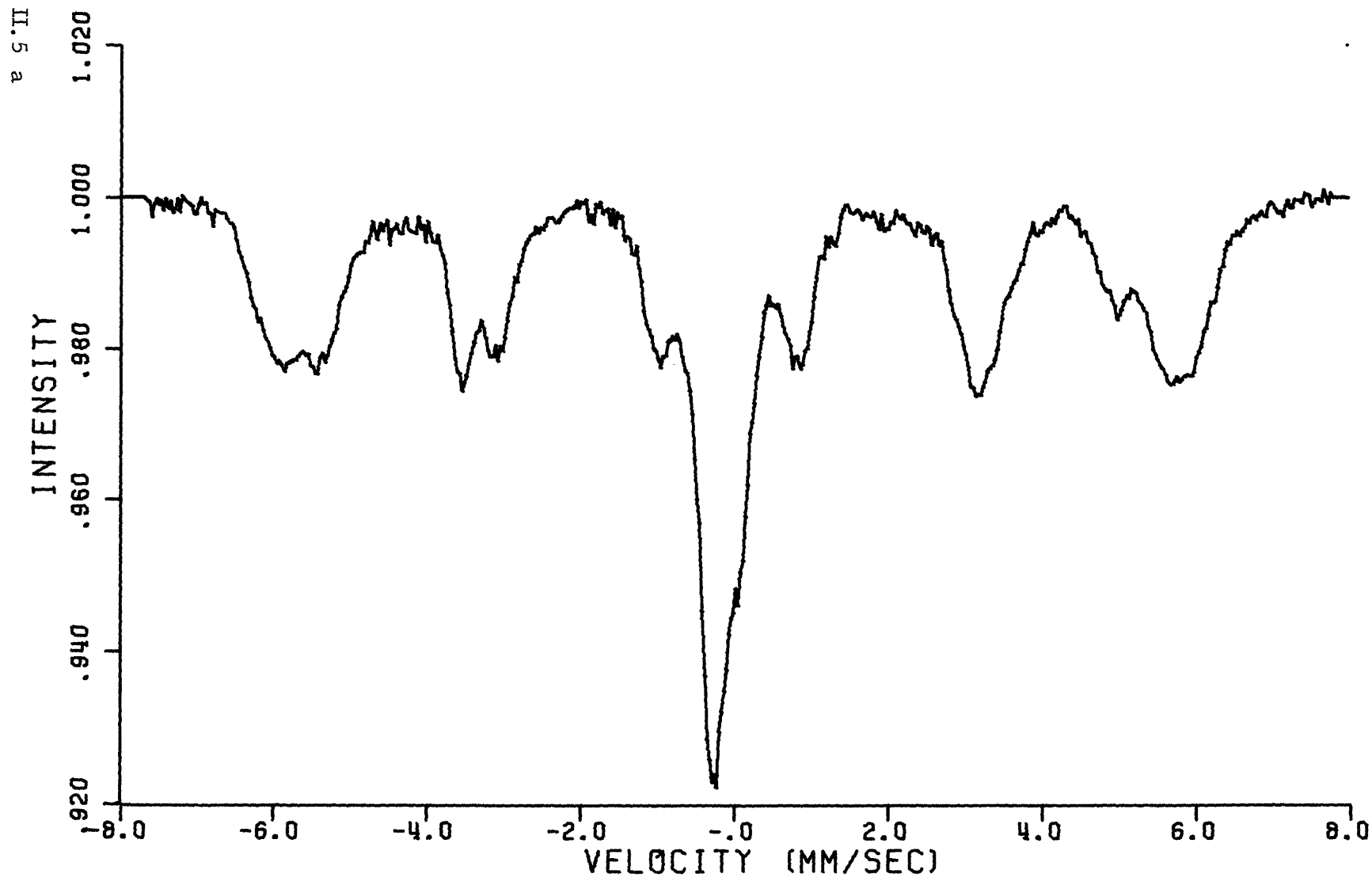
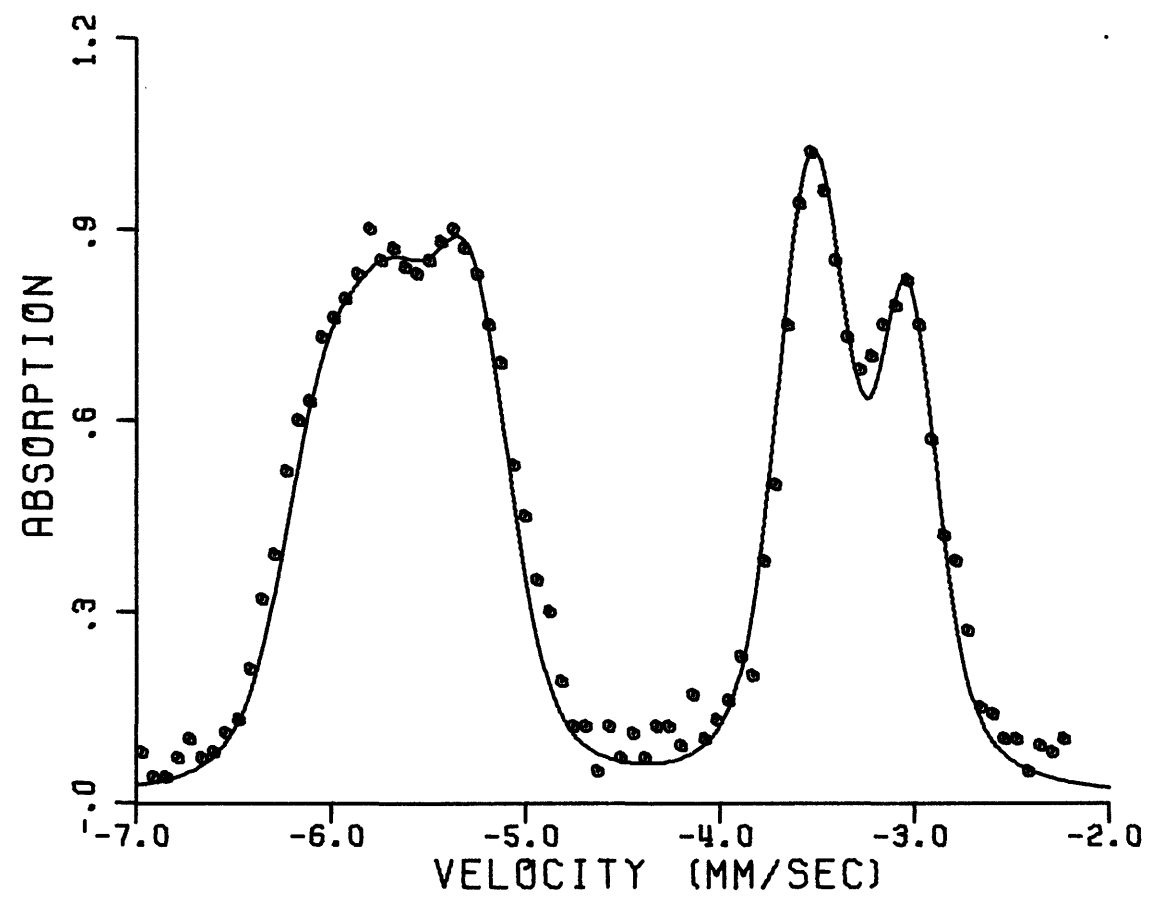


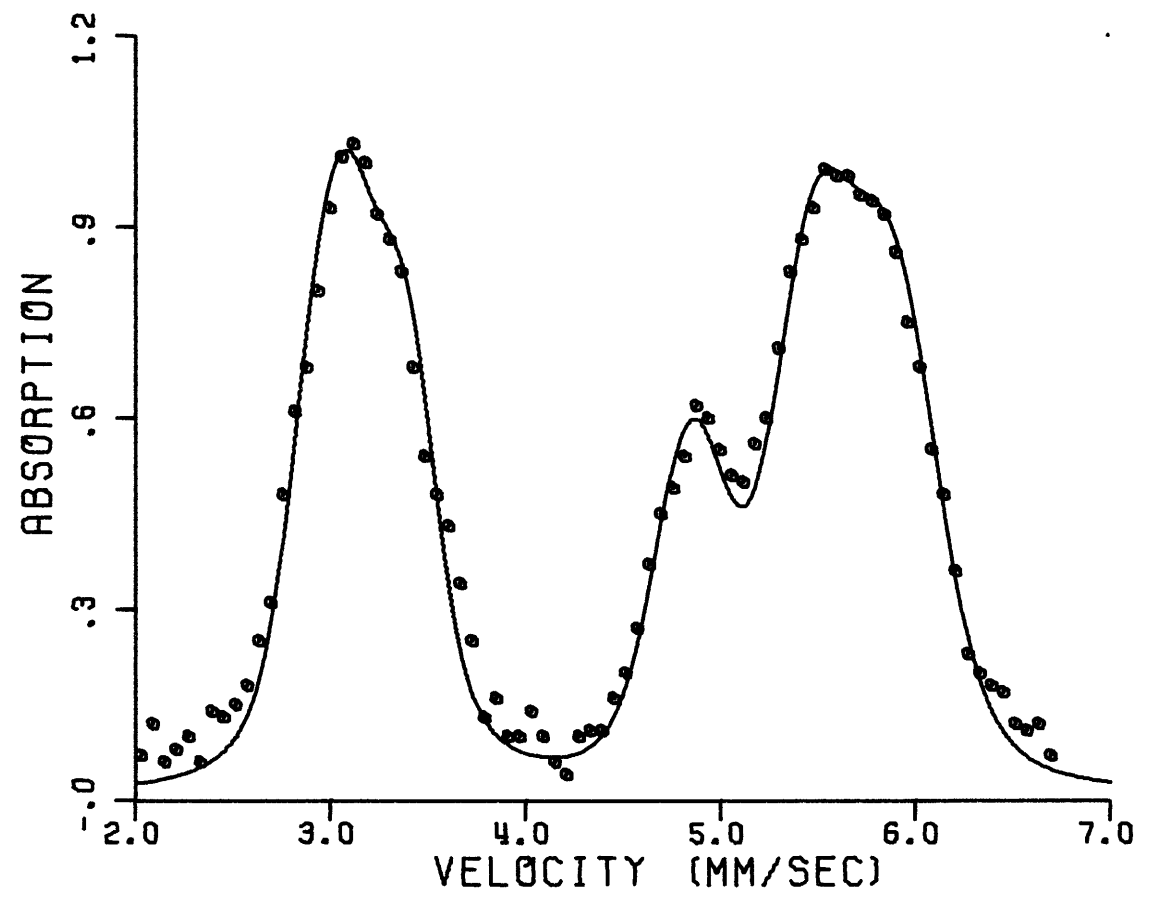
Figure II. 5 a Mössbauer Spectrum of Fe - 2.83 wt. % N
Virgin Martensite
II. 5 b, c Comparison of Virgin Martensite Spectrum (points)
to "random" Model of Nitrogen Atoms (line)



II.5 b



II.5 c



same manner as for iron-carbon martensite, with peaks being due to iron atoms which were first-, second-, and third-neighbors of a nitrogen atom. This procedure revealed that another ferromagnetic spectrum, whose line positions were virtually that of pure iron, was required to fit the virgin martensite data, indicating that some of the iron atoms are further than third-neighbor distances from nitrogen atoms. For this alloy, a close fit of a computer-generated pattern to experimental data (Figures (II.5b, 5c)) was for a model in which 0.221, 0.306 and 0.298 of the iron atoms were first-, second-, and third-neighbors of a nitrogen interstitial, with the remaining 0.175 having no nitrogen close neighbors. The relative fractions of the four spectra comprising the virgin martensite pattern indicate that the nitrogen atoms are randomly arranged on one of the three octahedral interstitial sublattices. Thus, the atom configuration in virgin nitrogen martensite is also inherited from the parent phase.

While the hyperfine parameters of the spectrum for "no nitrogen neighbors" closely resemble those of α -iron, the peak widths are greater. This effect is to be expected as iron atoms in virgin martensite described as having "no neighbors" actually have nitrogen atoms at 4th, or further-neighbor distances. The direct interactions, as well as indirect effects through intervening atoms, create small

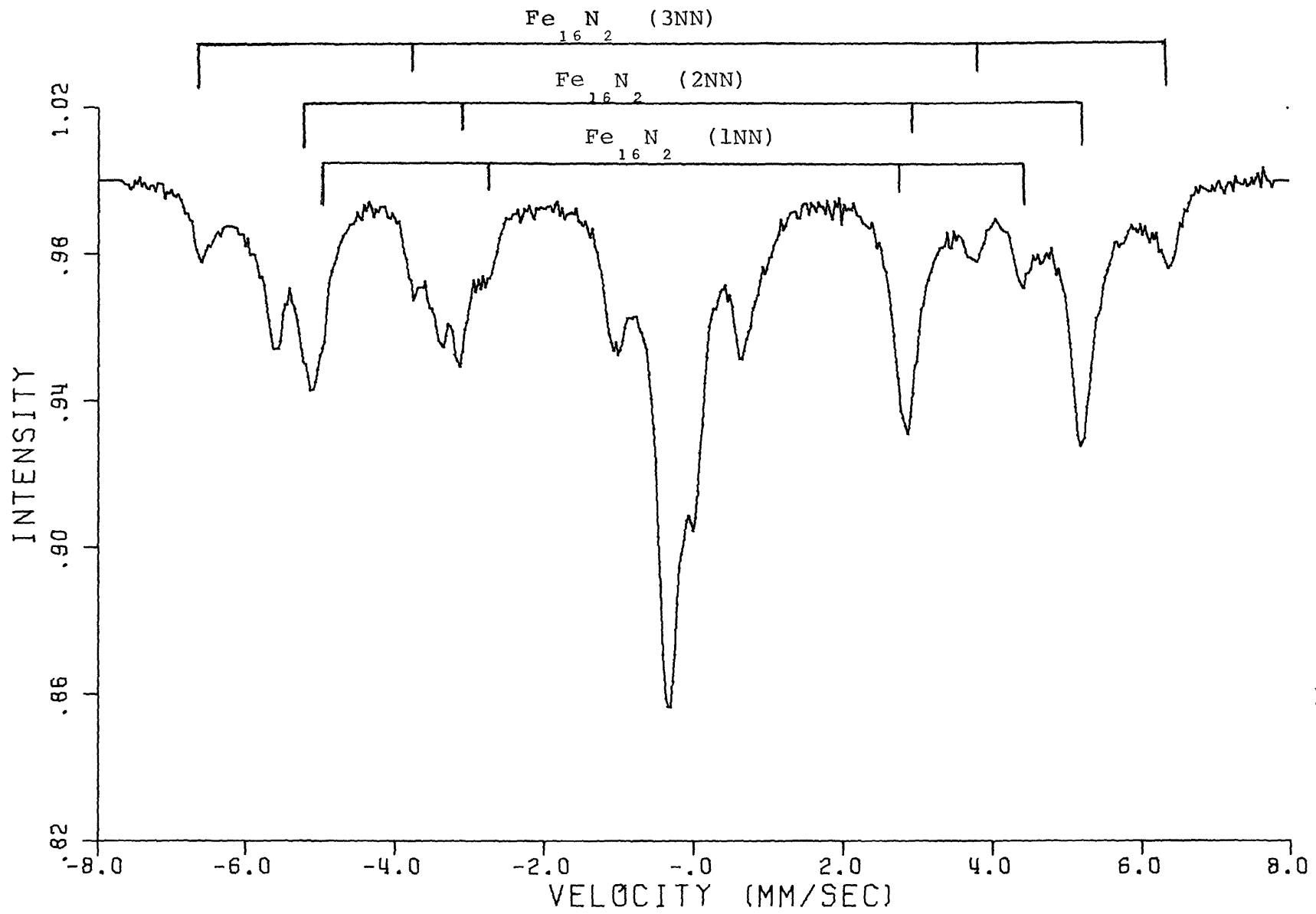
but finite perturbations on the electronic and magnetic properties of the iron atoms, which cause Mössbauer peak broadening.

II. 3. 2. 3 Aging of Nitrogen-Martensite

K. H. Jack¹⁷ reported that iron-nitrogen martensite decomposes below 200°C by the formation of α -iron and α' -Fe₁₆N₂, an ordered arrangement of nitrogen atoms in body-centered-tetragonal iron. A more recent electron microscopic investigation¹⁸ has shown that the α and Fe₁₆N₂ phases precipitate in a lamellar structure independent of the martensitic substructure. The authors suggest that the reaction is homogeneous and similar to spinodal decomposition.

To determine the Mössbauer spectrum of Fe₁₆N₂, an iron 2.34 wt. % nitrogen austenite sample was quenched in liquid nitrogen to create martensite, and tempered at 100°C for 24 hours. The sharp ferromagnetic spectra resulting from the decomposition of the martensite, appearing in Figure (II.6), indicate the presence of α -iron and three new iron-atom environments. These appear in a 1:2:1 ratio and are attributed to the first-, second-, and third-neighbor of a nitrogen atom in ordered Fe₁₆N₂, which exist in the same relative numbers. Aging above 100°C showed that the α + Fe₁₆N₂ structure

Figure II.6 ^{57}Fe Mössbauer Spectrum of Fe - 2.83 wt. % N Martensite
Aged 24 Hours at 100°C. Indicated is the spectrum of
 $\alpha'' - \text{Fe}_{16}\text{N}_2$.



was stable to 160°C , above which the precipitation of Fe_4N occurs.

In order to trace the effects of room temperature aging of virgin martensite, the iron 2.83 wt.% nitrogen sample (whose Mossbauer spectrum at liquid-nitrogen temperature was illustrated in Figure (II. 5a) was aged for one month at room temperature. The Mossbauer spectrum, taken after aging, is shown in Figure (II. 7), and the difference spectrum, obtained from Figures (II. 5a) and (II. 7), in Figure (II. 8). The difference spectrum shows that, while the iron-atom environments associated with the virgin martensite structure have been disappearing, three ferromagnetic iron atom spectra have appeared during the month at room temperature. Although these peaks are broad, the hyperfine parameters, measured at -193°C , are consistent with those of the Fe_{16}N_2 , formed at 100°C , and measured at room temperature. Furthermore, when the detailed effects on the difference spectrum of the decomposed virgin martensite are considered, the ratio of intensities of the three new spectra are approximately 1:2:1. Thus, the formation of new iron environments at room temperature is associated with the development of regions of ordered Fe_{16}N_2 . The spectrum of α -iron is not easily observed in this experiment as the alloy is sufficiently close to the stoichiometric Fe_{16}N_2 composition

Figure II.7 ^{57}Fe Mossbauer Spectrum of Fe - 2.83 wt. % N Martensite
Aged One Month at Room Temperature.

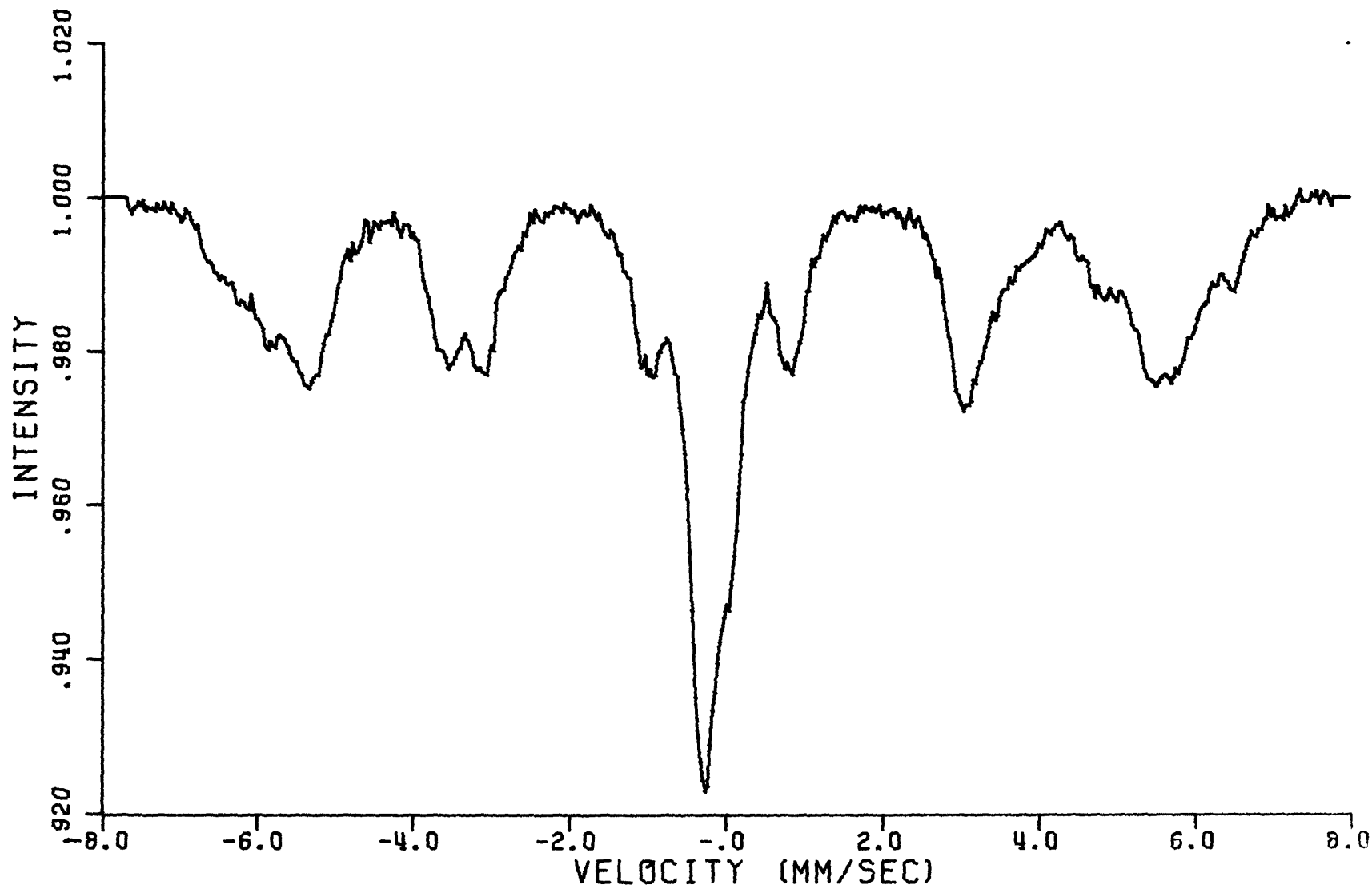
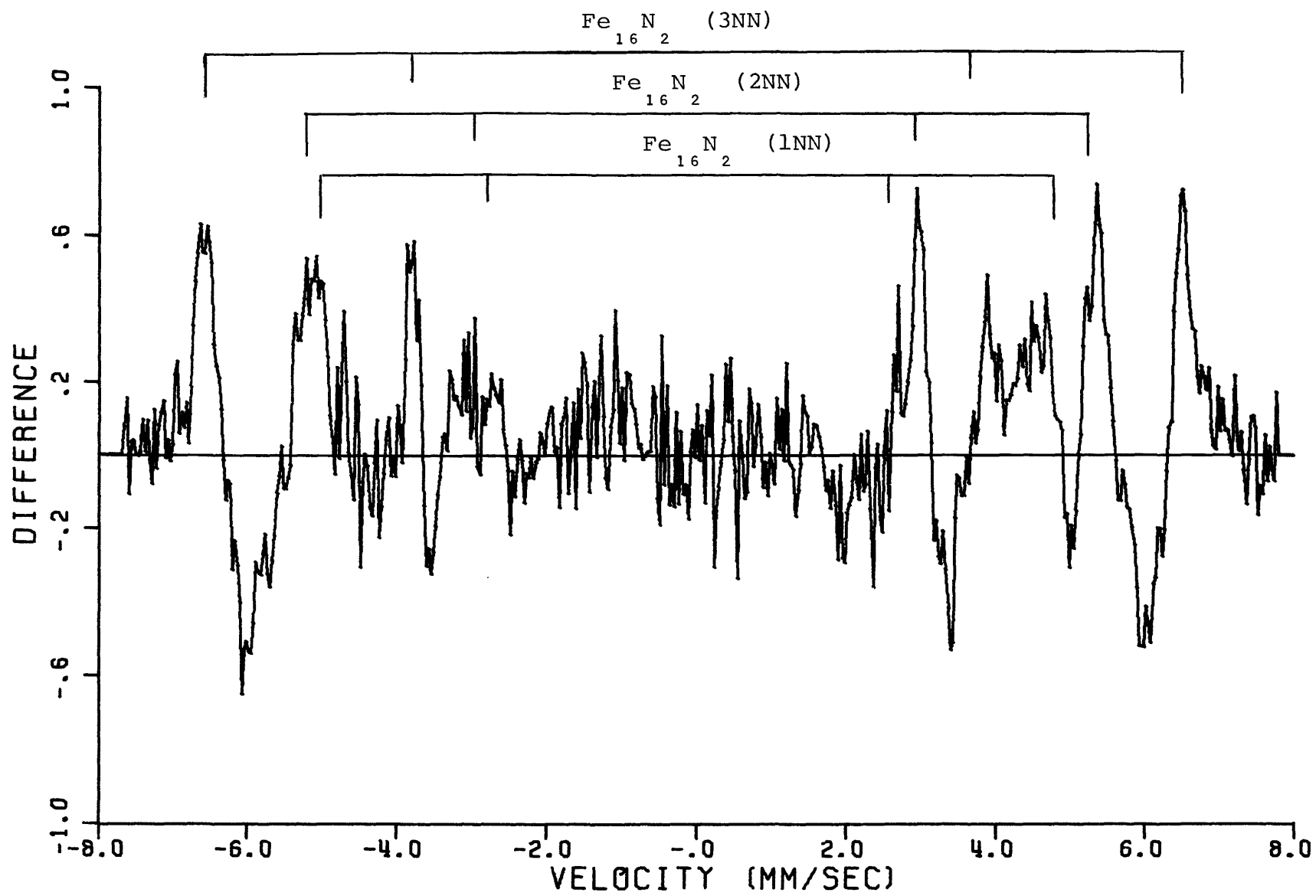


Figure II. 8 Difference Spectrum for Aging Fe - 2.83 wt. % N
Martensite at Room Temperature (from Figures
II. 5 and II. 7) indicating the Formation of Fe_{16}N_2 Spectrum



that only small amounts of α are formed. By the same token, this particular experiment helps to stress that aging in both the carbon- and nitrogen-containing alloys occurs, in general, by an agglomeration and an ordering of the interstitials.

The relatively large width of the room temperature Fe_{16}N_2 Mössbauer peaks (0.35 mm./sec. as compared to 0.30 for Fe_{16}N_2 formed at 100°C) may be related to the spinodal nature of its formation. Garwood and Thomas¹⁸ have shown that Fe_{16}N_2 lamellae formed at room temperature are only 50A wide and are not clearly detectable by electron microscopy until aging times of six months. If the reaction is indeed spinodal in nature, for aging times as short as one month the Fe_{16}N_2 region may not have completely reached the stoichiometric nitrogen content, and therefore, would also not be fully ordered. Such effects would result in a broadening and a distortion of the relative intensities of the Mössbauer peaks of the phase, as observed.

II.4 Austenite Configurational Models and Thermodynamic Data

In comparing the behavior of carbon and nitrogen atoms in austenite, both random and nonrandom configurational models need to be considered.

For a perfectly random solution of atoms on interstitial sites, in which y represents the fraction of interstitial sites occupied, the probability that a given site will be occupied is y and the probability that a site will be empty is $(1-y)$.

In face-centered-cubic austenite, there exists one octahedral interstitial site per iron atom, with each iron atom having six neighboring interstitial sites. For a perfectly random solution, the probability that an iron atom will have no interstitial neighbors is:

$$P_0 = (1-y)^6$$

while

$$P_1 = 1 - P_0$$

is the probability that an iron has at least one neighbor.

Moon¹⁹ proposed two types of repulsive solute atom interactions in interstitial solid solutions which could cause deviation from random behavior. Solute-solute repulsions might arise from coulombic interaction between solute atoms on nearest-neighboring sites. Carbon has been observed to behave as a heavily-charged particle in austenite.^{20,21} In the face-centered-cubic structure, this would cause blocking of twelve sites. A second type of repulsion would occur because the solute atom is too large for the interstitial hole. The solvent atom ligands would then be pushed outward, tending

to block the interstitial sites directly beyond them. In austenite, this would block the six second nearest neighboring interstitial sites.

If both of these interactions are operative, and a solute atom in austenite blocks its twelve first-nearest-neighboring and six second-nearest-neighboring interstitial sites from occupation by other solute atoms, no iron atom would neighbor more than one solute atom. With solute atoms being separated in this manner, each would neighbor six different iron atoms and the fraction of iron atoms neighboring a solute atom would be:

$$F_1 = 6y$$

The fraction of iron atoms not neighboring a solute would be:

$$F_0 = 1 - 6y$$

A comparison of the measured fractions of iron atoms having no interstitial neighbors to that predicted by the random and separated models for the carbon ($y_c = 0.0875$) and nitrogen ($y_n = 0.0956$) austenites is given in Table (II.2). While the nitrogen austenite behaves in a random manner, the measured value for the carbon-austenite indicates that there is a strong tendency for the carbon atoms to be separated from one another.

Darken and Smith (DS)²² and Aaronson, Domain and Pound (ADP),²³ who used the mathematical model developed by Moon,

TABLE II.2

FRACTION OF IRON ATOMS IN AUSTENITE
HAVING NO INTERSTITIAL ATOM NEIGHBORS

	<u>Fe-C</u>	<u>Fe-N</u>
Composition (y)	0.0875	0.0956
Random Model	0.577	0.547
Separated Model	0.472	0.426
Measured Value	0.495±0.008	0.55±0.008

both considered only first-neighbor interactions to calculate the energy required to bring carbon atoms onto adjacent interstitial sites. Ban-ya, Elliott and Chipman^{24,25} have shown that both the (DS) and (ADP) models are consistent with their more comprehensive measurements of the activity of carbon in iron as a function of temperature and composition, and both yield a calculated repulsive energy of 8367 joules (2000 calories) per mole, independent of temperature. If we consider the possibility that carbon blocks only its twelve nearest-neighboring interstitial sites, an iron atom can have two carbon neighbors only if they are on opposite sides of the iron. Assuming a random arrangement of carbon atoms on all but the blocked sites and permitting overlap of blocked sites, an alloy of this composition would have approximately 0.50 of the iron atoms not neighboring a carbon. This value is within experimental error of the measured fraction, and in fact, is closer than the totally separated model predicts.*

Both the (DS) and (ADP) models have blocking parameters

* An iron atom with carbon atoms symmetrically disposed on either side would probably not show the quadrupole splitting of the iron atoms normally associated with at least one carbon neighbor, and would probably contribute to the central, "no neighbor" peak. If this is true, the probability of an iron atom having oppositely-disposed carbon atoms is also less than random.

which are temperature-dependent. The probability that a carbon atom may occupy any of the twelve neighboring sites of another carbon atom is approximately $12y \exp(-\Delta E/RT)$,²² where ΔE is the calculated interaction energy. At 22°C, this probability is only 0.03 for the carbon-austenite, indicating that blocking of the twelve nearest neighbor sites is essentially complete.

A number of other mathematical models for the configurational entropy associated with the arrangement of carbon atoms on the interstitial sites also can accommodate the nonideal behavior of carbon in austenite.^{26,27,28,29} Although many of these adequately represent the Ban-ya et al data, only Lee's²⁹ is consistent with the configuration revealed in this study.

As nitrogen atoms in austenite appear to be randomly situated rather than separated like their carbon counterparts, the interactive forces between nitrogen atoms must be either much smaller or perhaps even slightly attractive. The physical size of carbon and nitrogen as interstitial atoms can be considered virtually identical,¹⁷ since their relative atomic radii can only be readily differentiated by substituting carbon for nitrogen in hexagonal-close-packed iron of high interstitial-atom content.³⁰ Thus, their contrasting behavior must be due to electronic and chemical differences rather than simple

size affects. It has been observed that carbon atoms diffusing interstitially in iron under an applied voltage behave as positively charged particles,^{20,21} while other evidence exists that nitrogen in iron may be negatively charged.^{30,31,32} The major difference between the Mössbauer patterns of carbon and nitrogen austenites is the much larger positive isomer shift in the nitrogen alloys of the peaks due to atoms with interstitial neighbors relative to the peak due to the neighborless atoms. Gielen² attributes this behavior to bonding differences: carbon atoms contribute electrons to the iron 4s band, which will not greatly affect the isomer shift, while the presence of nitrogen leaves iron in a $3d^8$ state, reflecting a covalent bond as in Fe_4N .

II.5 Crystallographic Symmetries in Carbide and Nitride Structures

Nitrogen shows a much stronger preference to remain at the center of a regular octahedron of iron atoms than does carbon. Essentially all known nitrides have this structure on the atomic scale.³⁰ This is true even in body-centered-cubic and body-centered-tetragonal iron structures, since occupation of the octahedral interstitial site causes the two closest iron atoms to be displaced a substantial distance, thereby making the distances between the interstitial atom and all neighboring iron atoms approximately the same.³⁴ Interstitial nitrogen

also stabilizes the hexagonal-close-packed structure of iron over a wide range of temperature and composition,³⁵ (the octahedral interstitial site in hexagonal-close-packed is equivalent to that in face-centered-cubic).

Carbon atoms rapidly alter their octahedral environment at relatively low temperatures. ϵ -carbide, which may be orthorhombic rather than hexagonal-close-packed,³⁵ is observed to be the first precipitate from both room-temperature-aged martensite and retained austenite. The fact that the same metastable carbide is formed from two crystallographically different structures may be due to the formation of Fe_4C clusters in martensite, approximating the face-centered-cubic structure. With the formation of the most stable carbide, Fe_3C cementite, octahedral coordination is completely destroyed. The carbon atom is located in the center of a trigonal prism of six iron atoms. However, although two crystallographically distinct iron atom sites exist in the cementite structure, their ^{57}Fe Mössbauer spectra are indistinguishable.³⁷ Thus, despite the structural asymmetry, all iron atoms in cementite must be nearly identical, both electronically and magnetically. This is not the case for Fe_3B , which is isostructural with Fe_3C , and for which the ^{57}Fe Mössbauer spectra clearly differentiates the two crystal sites of iron.³⁸

II.6 Summary

Earlier work in this laboratory on the Mössbauer spectroscopy of iron-carbon alloys^{5, 16} has yielded the following results:

1. Three separate spectra can be distinguished in virgin martensite, due to iron atoms which are first-, second-, and third-nearest neighbors of a carbon interstitial.
2. At room temperature, carbon atoms in virgin martensite agglomerate and regions of ordered Fe_4C are believed to result.
3. ϵ -carbide precipitates from the martensite at temperatures as low as 80°C .
4. Austenite decomposes by the formation of ϵ -carbide below 160°C and Fe_3C above 180°C .

In this current work, Mössbauer spectroscopy of iron-carbon and iron-nitrogen alloys has yielded the following new information concerning interstitial atom configurations:

1. Carbon atoms in austenite and virgin martensite are widely separated on the octahedral interstitial sublattice.
2. The Mössbauer pattern of iron-nitrogen virgin martensite is composed of distinct spectra from iron

atoms which are the first-, second-, and third-nearest neighbors of a nitrogen atom and from iron atoms with no nitrogen neighbors.

3. Nitrogen atoms in austenite and virgin martensite are randomly arranged on the octahedral interstitial sites.
4. At room temperatures, nitrogen atoms in virgin martensite undergo local ordering to form regions of Fe_{16}N_2 .
5. The Mössbauer pattern of Fe_{16}N_2 is composed of distinct spectra from iron atoms which are first-, second-, and third-nearest neighbors of a nitrogen atom.
6. At the temperatures studied, the decomposition of iron-nitrogen austenite shows no other products than the equilibrium phases α -iron and Fe_4N , which are also eventually formed at higher temperatures in the decomposition of martensite.

References

1. G. Wertheim: Mössbauer Effect: Principles and Applications, Academic Press, New York, 1964.
2. P. M. Gielen and R. Kaplow: Mössbauer Effect in Iron-Carbon and Iron-Nitrogen Alloys, Acta Met., 1967, vol. 15, p. 49.
3. H. Ino, T. Moriya, E. Fujita, Y. Maeda, Y. Ono and Y. Inokuti: A Study of the Mössbauer Effect during the Tempering of Iron-Carbon Martensite, J. Phys. Soc. Japan, 1968, vol. 25, p. 88.
4. J. M. Genin and P. Flinn: Mössbauer Effect Study of the Clustering of Carbon Atoms during the Room Temperature Aging of Iron-Carbon Martensite, Trans. A.I.M.E., 1968, vol. 242, p. 1419.
5. W. K. Choo and R. Kaplow: Mössbauer Measurements on the Aging of Iron-Carbon Martensite, Acta Met., 1973, vol. 21, p. 725.
6. M. Lesoille and P. M. Gielen: Mössbauer Spectroscopy Study of Iron-Carbon Austenite and Virgin Martensite, Met. Trans., 1972, vol. 3, p. 2681.
7. M. Cohen: The Strengthening of Steel, Trans. A.I.M.E., 1962, vol. 224, p. 638.
8. G. V. Kurdjumov and A. G. Khachaturyan: Nature of Axial Ratio Anomalies of the Martensite Lattice and Mechanism of Diffusionless $\gamma \rightarrow \alpha$ Transformation, Acta Met. 1975, vol. 23, p. 1077.
9. Y. Yamaoka, M. Mekata and H. Takaki: Mössbauer Effect Study of Face-Centered Cubic Fe Nitrides, J. Phys. Soc. Japan, 1973, vol. 35, p. 1378.
10. J. M. Genin and J. Foct: Mössbauer Spectroscopy of Disordered and Ordered Iron-Nitrogen Solid Solutions, Phys. Stat. Sol. (a), 1973, vol. 17, p. 395.
11. T. Moriya, Y. Sumitomo, H. Ino, E. Fugita and Y. Maeda: Mössbauer Effect in Iron-Nitrogen Alloys and Compounds J. Phys. Soc. Japan, 1973, vol. 35, p. 1378.

12. T. Bell and W. S. Owen: The Thermodynamics of the Martensite Transformation in Iron-Carbon and Iron-Nitrogen, Trans. A.I.M.E., 1967, vol. 239, p. 1940.
13. J. Cosgrove and R. Collins: Mössbauer Velocity Calibration via Interferometry, Nuc. Inst. Meth., 1971, vol. 95, p. 269.
14. S. Hanna and R. Preston: Mössbauer Cross Section of Fe⁵⁷ in Iron, Phys. Rev., 1965, vol. 139, 3A, p. 722.
15. R. A. Arents, Yu. V. Maksimov, I. P. Suzdalev, V. K. Imshennik, and Yu. F. Krupyanskiy: Mössbauer Study of the Local Magnetic Structure of Iron ϵ -Carbide and the Intermediate Carbides which Arise during $\epsilon \rightarrow \chi \rightarrow \theta$ Transformations, Phys. Metal. and Metallog., 1973, vol. 36, p. 46.
16. N. DeCristofaro: The Aging of Martensite and Austenite, S.M. Thesis, M.I.T., 1973.
17. K. H. Jack: The Occurrence and the Crystal Structure of α' -Iron Nitride, Proc. Roy. Soc. (London) 1951, vol. 208A, p. 216.
18. R. D. Garwood and G. Thomas: Tempering of Martensite in an Fe - 1.5 Pct. N Alloy, Met. Trans., 1973, vol. 4, p. 225.
19. K. Moon: Thermodynamics of Interstitial Solid Solutions with Repulsive Solute - Solute Interactions, Trans. A.I.M.E., 1963, vol. 227, p. 1116.
20. T. Okabe and A. G. Guy: Steady State Electrotransport of Carbon in Iron, Met. Trans., 1970, vol. 1, p. 2705.
21. T. Okabe and A. G. Guy: Constancy of Z^* for Electrotransport of Carbon in Austenite, Met. Trans., 1973, vol. 4, p. 2673.
22. L. S. Darken and R. P. Smith: Equilibrium of Iron-Carbon Alloys with Gases, J. Am. Chem. Soc., 1946, vol. 63, p. 1172.

23. H. I. Aaronson, H. A. Domain and G. M. Pound: Thermodynamics of the Austenite \rightarrow Proeutectoid Ferrite Transformation .I, Fe-C Alloys, Trans. A.I.M.E., 1966, vol. 236, p. 753.
24. S. Ban-ya, J. Elliott and J. Chipman: Activity of Carbon in Fe-C Alloys at 1150°C, Trans. A.I.M.E., 1969, vol. 245, p. 1199.
25. S. Ban-ya, J. Elliott and J. Chipman: Thermodynamics of Austenite Fe-C Alloys, Met. Trans., 1970, vol. 1, p. 1313.
26. L. Kaufman, S. Radcliffe and M. Cohen: Decomposition of Austenite by Diffusional Process, V. F. Zackay and H. I. Aaronson, eds., Interscience, New York, 1962.
27. R. McLellan, T. Garrard, S. Horowitz and J. Sprague: A Model for Concentrated Interstitial Solid Solutions: Its Applications to Solutions of Carbon in Gamma Iron, Trans. A.I.M.E., 1967, vol. 239, p. 528.
28. P. Gallagher, J. Lambert and W. Oates: Carbon Activity in Austenite by Monte Carlo Computations, Trans. A.I.M.E. 1969, vol. 245, p. 887.
29. H. M. Lee: Carbon Activity in Austenite, Met. Trans., 1974, vol. 5, p. 787.
30. D. H. Jack and K. H. Jack: Carbides and Nitrides in Steel, Mater. Sci and Eng., 1973, vol. 11, p. 1.
31. N. Elliott: X-Ray Scattering Factor of N in Fe_4N , Phys. Rev., 1963, vol. 129, p. 1120.
32. S. Nagakura: Electronic Structure of Iron Nitrides Studied by Electron Diffraction, I. Fe_4N , J. Phys. Soc. Japan, 1968, vol. 25, p. 488.
33. S. Nagakura and K. Tanehashi: Electronic Structure of Iron Nitrides Studied by Electron Diffraction. II. ϵ - Fe_2N and ξ - Fe_2N , J. Phys. Soc. Japan, 1968, vol. 25, p. 840.

34. S. C. Moss: Static Atomic Displacements in Iron-Carbon Martensite, *Acta Met.*, 1967, vol. 15, p. 1815.
35. K. H. Jack: The Iron-Nitrogen System: The Crystal Structures of ϵ -Phase Iron Nitrides, *Acta Cryst.*, 1952, vol. 5, p. 404.
36. Y. Hirotsu and S. Nakagura: Crystal Structure and Morphology of the Carbide Precipitated from Martensitic High Carbon Steel during the First Stage of Tempering, *Acta Met.*, 1972, vol. 20, p. 645.
37. T. Shinjo, F. Itoh, H. Takaki, Y. Nakamura and N. Shikazono: Mossbauer Effect in Fe_2B , FeB and Fe_3C , *J. Phys. Soc. Japan*, 1964, vol. 19, p. 1252.
38. W. K. Choo and R. Kaplow: (private communication).

III. THE KINETICS OF CARBON CLUSTERING IN MARTENSITE

ABSTRACT

The rate of clustering of carbon atoms into regions of ordered Fe_4C has been studied by Mössbauer spectroscopy. The activation energy associated with this process is $89,525 \pm 12,000$ joules per mole.

III. 1 Introduction

The segregation and redistribution of carbon atoms in martensitic steels prior to purposeful treatment at elevated temperatures is a well recognized phenomenon.¹ "Auto-tempering" is an example of such a process occurring in low-carbon, low-alloy steels with high M_s temperatures. During the quench, carbon atoms in the freshly formed martensite in these alloys migrate to sites at lattice defects such as dislocations since the interstitial atom mobility is high and the stress fields associated with the defects provide low-energy environments. This type of process also may occur in steels with subambient M_s temperatures when the existing martensitic phase is allowed to age at room temperature, since the jump frequency of carbon in martensite is still rapid enough to permit local rearrangement.² Measurements of the resistivity of iron-carbon alloys as a function of carbon content have shown that the preferential defect-related sites become saturated with carbon atoms when the carbon content exceeds 0.20 wt. %.

The substructure of plate martensite, which starts to form in steels with more than 0.2 wt. % carbon, consists of fine twins and a dislocation density significantly smaller than that of the low-carbon, lath martensite. Estimates of the density of low-energy, defect-related sites in plate martensite indicate that less than 0.2 wt. % carbon should be sufficient to saturate them. However, the behavior of the resistivity of high-carbon steels on aging in the vicinity of room temperature reveal that additional changes are occurring. Activation energies derived from those measurements vary between 75,300 joules (18 kcal) and 100,400 joules (24 kcal) per mole, and the authors report that the probable value is 87,850 joules.^{3,4} This value is consistent with the activation energy for the diffusion of carbon in martensite.⁵ Mössbauer measurements of the room-temperature aging of martensite unambiguously indicate that a substantial redistribution of carbon atoms takes place, and have yielded a structural model for the process.^{6,7} In virgin martensite, formed below room temperature, carbon atoms occupy interstitial sites apart from one another, a configuration inherited from the parent-phase austenite. The room-temperature aging of martensite proceeds by a redistribution of carbon atoms to produce carbon-rich and carbon-depleted regions.

The carbon-rich regions are interpreted as being of an ordered Fe_4C stoichiometry, similar to Fe_4N in structure. Such a structure also has been proposed on the basis of electron-diffraction measurement.⁸ This process only occurs within a narrow temperature range; the Fe_4C regions begin to disappear on aging at temperatures at or above 80°C , and ϵ -carbon is observed to form at their expense.⁶ Below room temperature, the diffusion rate slows to the point that inordinately long times are required for significant fractions of this transformation.

Nonetheless, unambiguous transformation-rate studies can be made by Mössbauer spectroscopy since the spectra of the iron atoms in virgin martensite can be clearly differentiated from those due to carbon-rich and carbon-depleted regions of the aged product.

III.2 Experimental Procedure

The preparation of virgin martensite in an iron - 1.86 wt.% carbon alloy and the method of monitoring its aging have been described elsewhere.⁶ The Mössbauer spectra of virgin martensite (and of the retained austenite) in each sample was measured at -193°C immediately after its formation in situ. The sample was then allowed to age at a specific temperature and periodically re-cooled to -193°C for measurement and comparison with the virgin spectrum. The

fraction of the martensite transformed as a function of aging time was calculated from the relative peak intensities in the regions of the first and sixth Mössbauer peaks corresponding to the relevant, ferromagnetically-split spectral lines.

III.3 Experimental Results

The Mössbauer spectrum of virgin martensite, measured at -193°C , is shown in Figure (III.1a). The spectra associated with the three iron-atom environments comprising the virgin martensitic structure [iron atoms which are at first (1NN), second (2NN) and third (3NN) nearest-neighboring distances from an interstitial carbon atom] are indicated. The Mössbauer spectrum of the martensite aged at 50°C for a total of 25 hours is shown in Figure (III.1b). The difference between those spectra, Figure (III.1c), allows a quantitative measurement of the fraction of iron atoms whose local environments have changed from those characteristic of the virgin structure to those present in the altered regions. (Such difference spectra also serve, initially, to clarify the individual spectra that characterize the two sets of atomic environments.) The fraction of the virgin martensite transformed as a function of total aging time at 50°C is shown in Figure (III.2). Additional data for room-temperature (22°C)

Figure III.1 a ^{57}Fe Mössbauer Spectrum of Iron - 1.86 wt.% Carbon
Virgin Martensite plus Austenite, Measured at -193°K

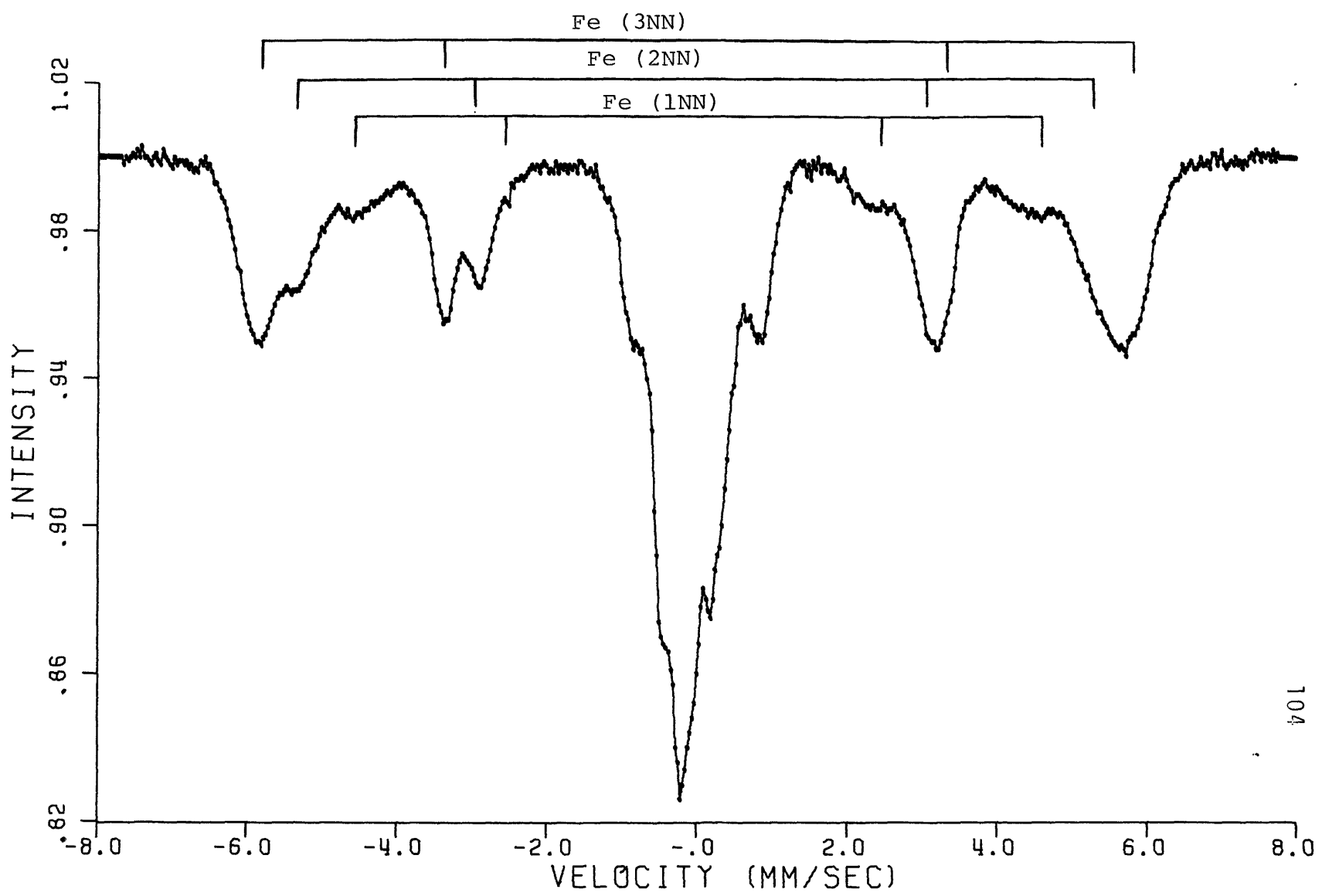


Figure III.1 b ⁵⁷Fe Mössbauer Spectrum of Martensite Aged at 323°K
for 25 Hours, Measured at -193°K.

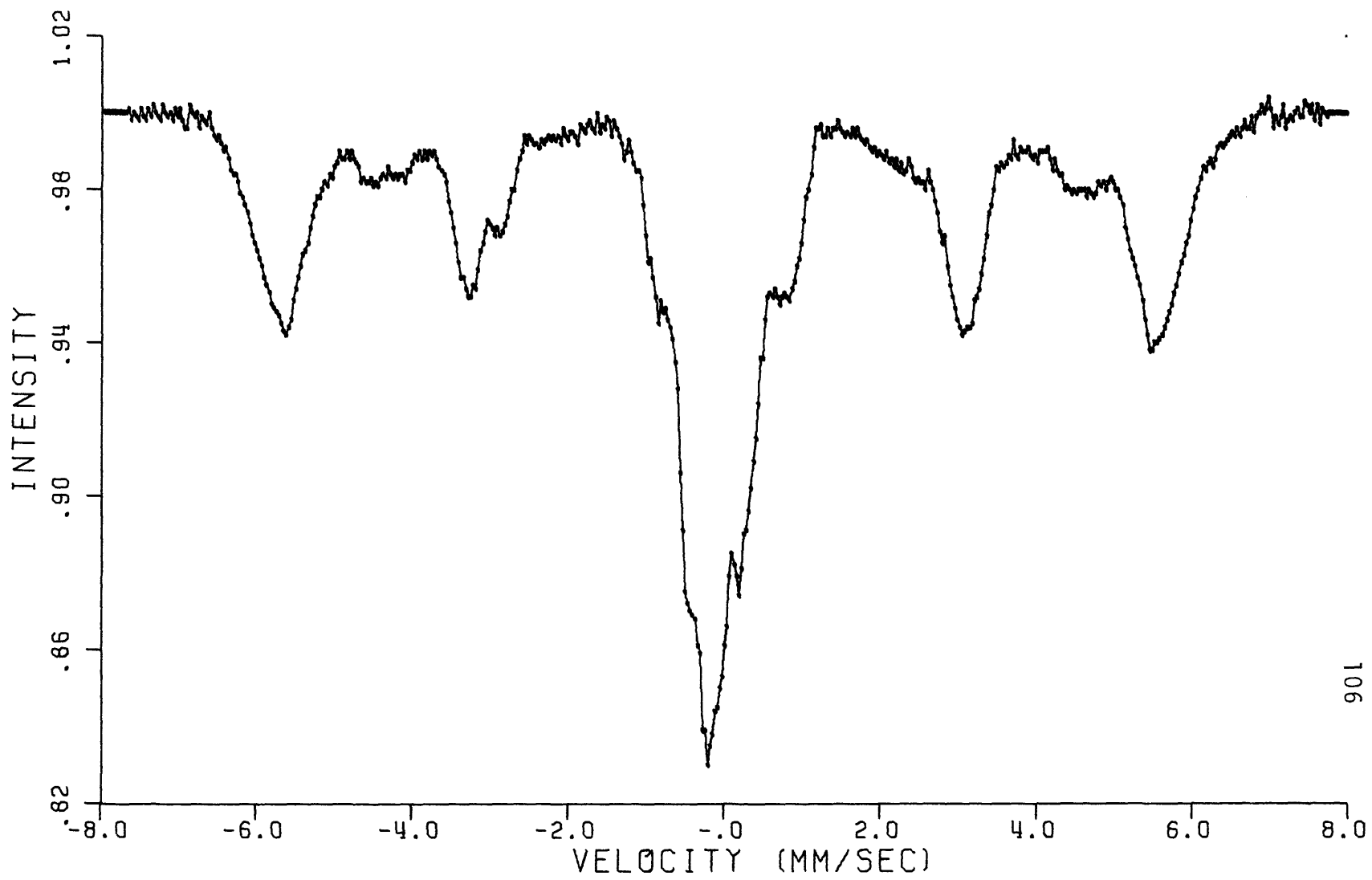


Figure III. 1 c Difference Spectrum of Martensite: Changes Occurring during 25 Hours of Aging at 323°K, Measured at -193°K. Indicated are the spectra from the two iron atom sites in Fe_4C and the spectrum of the "pure iron" in the carbon depleted regions.

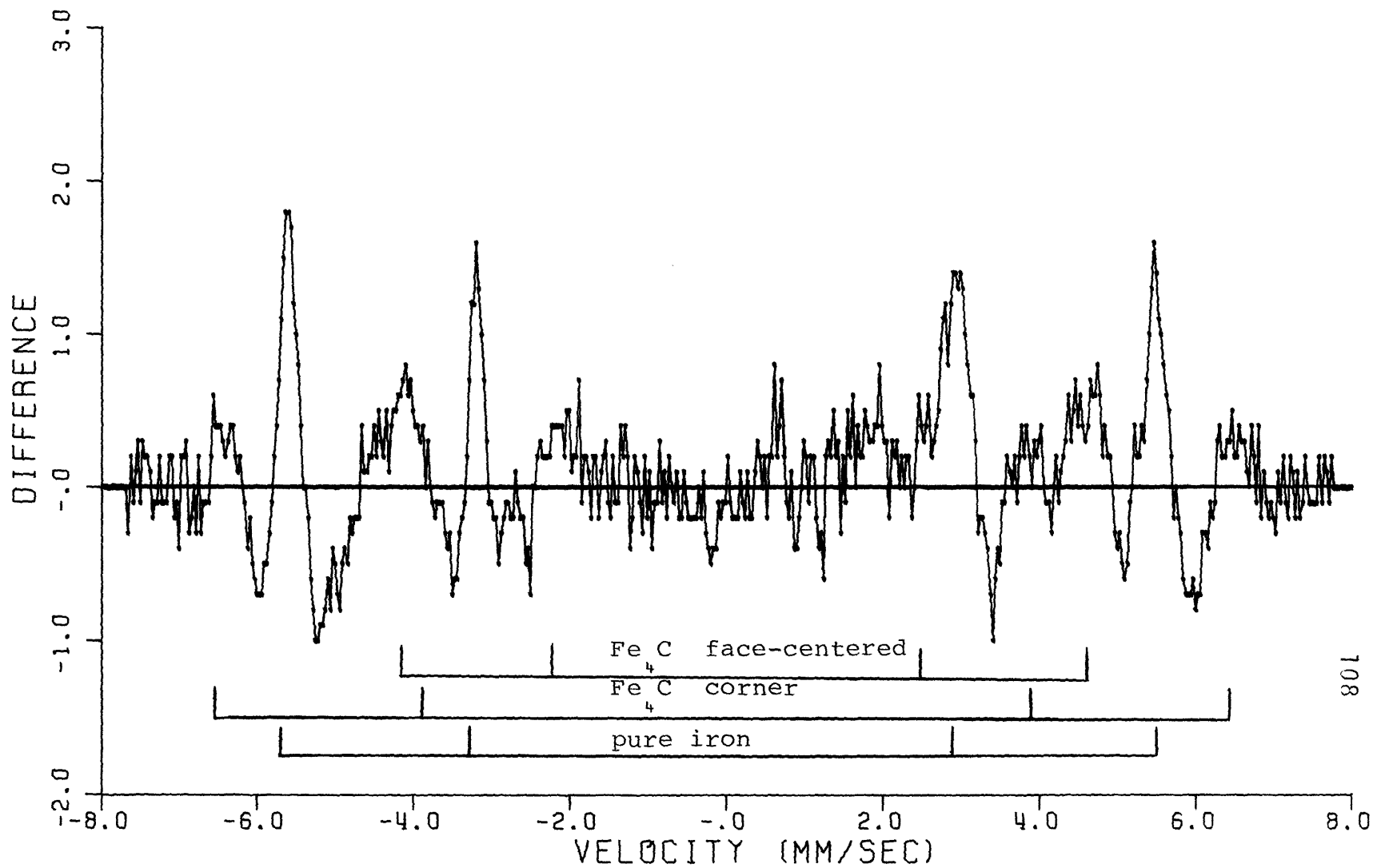
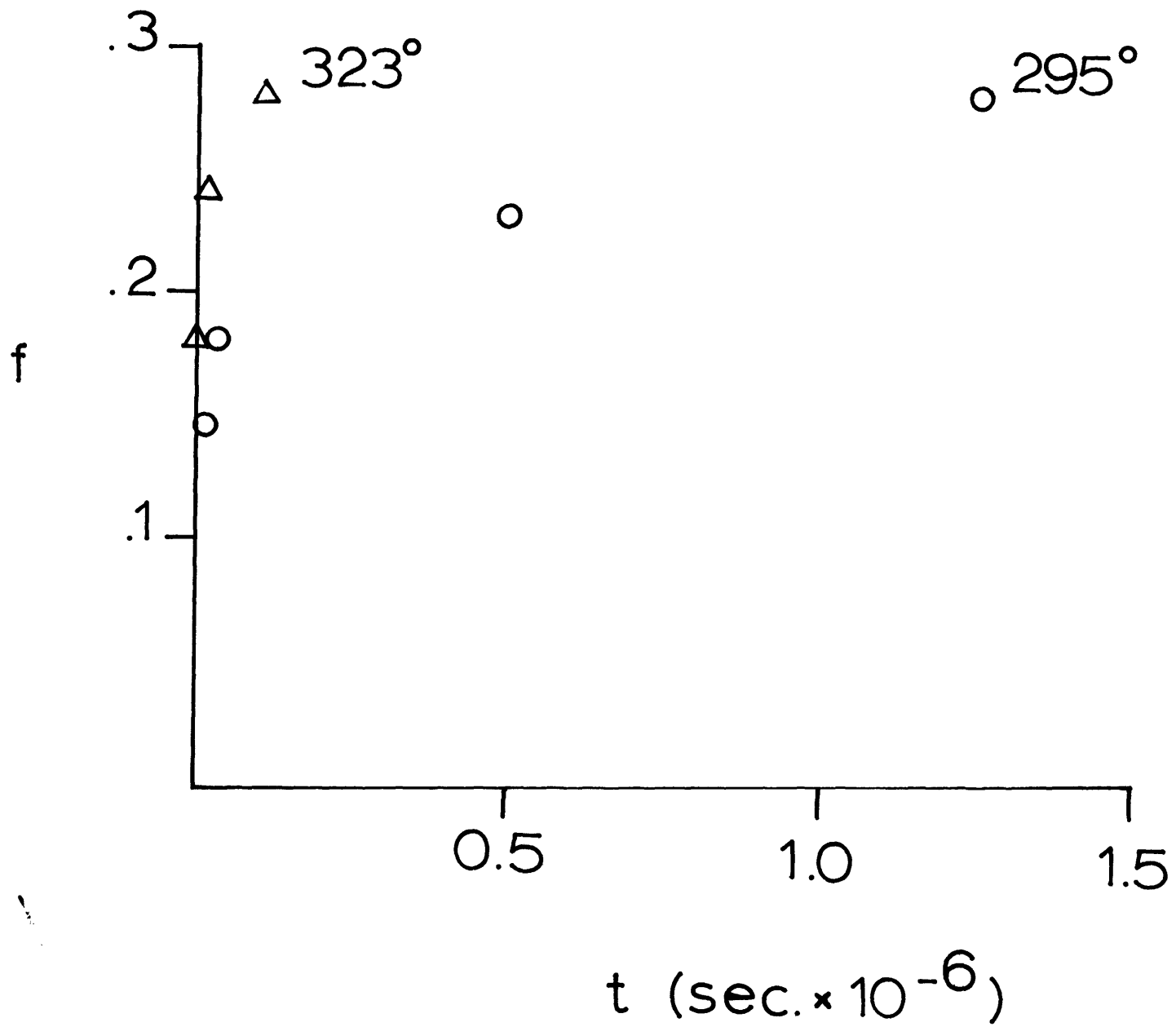


Figure III.2 Isothermal Transformation Curves for the Clustering of Carbon Atoms in Martensite Based on Mossbauer Measurements: Fraction transformed, f , vs. time, t .



aging, obtained from earlier work,⁶ are also given in Figure (III.2).

III.4 Discussion

A kinetic equation that is often used to represent the fraction transformed, f , as a function of time, t , for a thermally activated process is

$$f = 1 - \exp [- (\kappa t)^n] \quad (\text{III. 1})$$

where κ is the reaction-rate constant, n is the time exponent, and,

$$\kappa = \kappa_0 \exp [- Q/RT] \quad (\text{III. 2})$$

where Q is the activation energy, R the gas constant, and T the temperature.

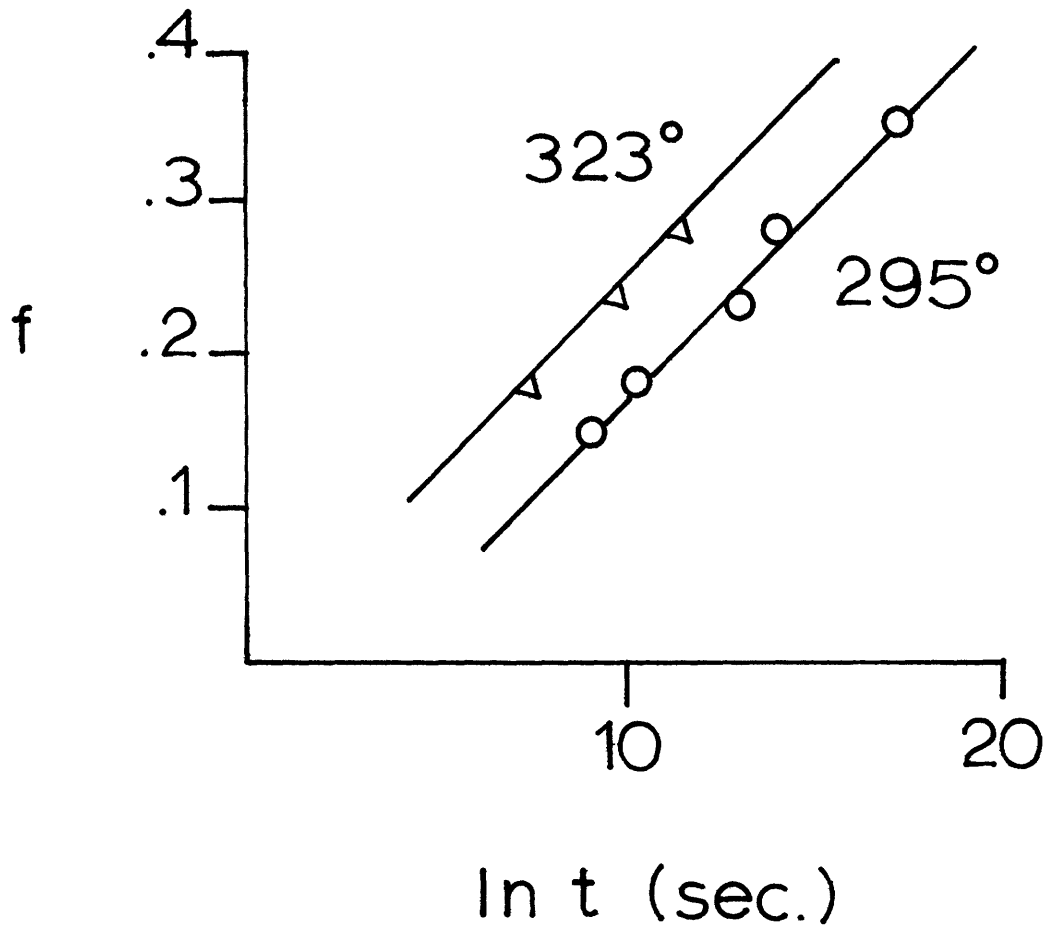
The plot of the fraction transformed vs. the natural logarithm of the time appears to be linear for both temperatures (Figure III.3). Least-squares analysis indicate that the lines are nearly parallel. This linear behavior is not analytically consistent with Equation (III.1), of course, but the two forms can be mutually consistent over the limited range of f values which were experimentally accessible.

The linear behavior of f vs. $\ln(t)$ does permit application of the Arrhenius relationship in the form,

$$\ln(\text{rate}) = \text{constant} - Q/RT \quad (\text{III. 3})$$

to calculate the activation energy for the carbon-clustering process.

Figure III. 3 Isothermal Transformation Curves for the Clustering of Carbon Atoms in Martensite: f vs. $\ln t$.



When the rate is expressed as the reciprocal of the time required to complete a given fraction of the reaction (rate = $1/t_R$), differentiating Equation (III. 3) yields:

$$\frac{\partial \ln (t_R)}{\partial (1/T)} = \frac{Q}{R} \quad (\text{III. 4})$$

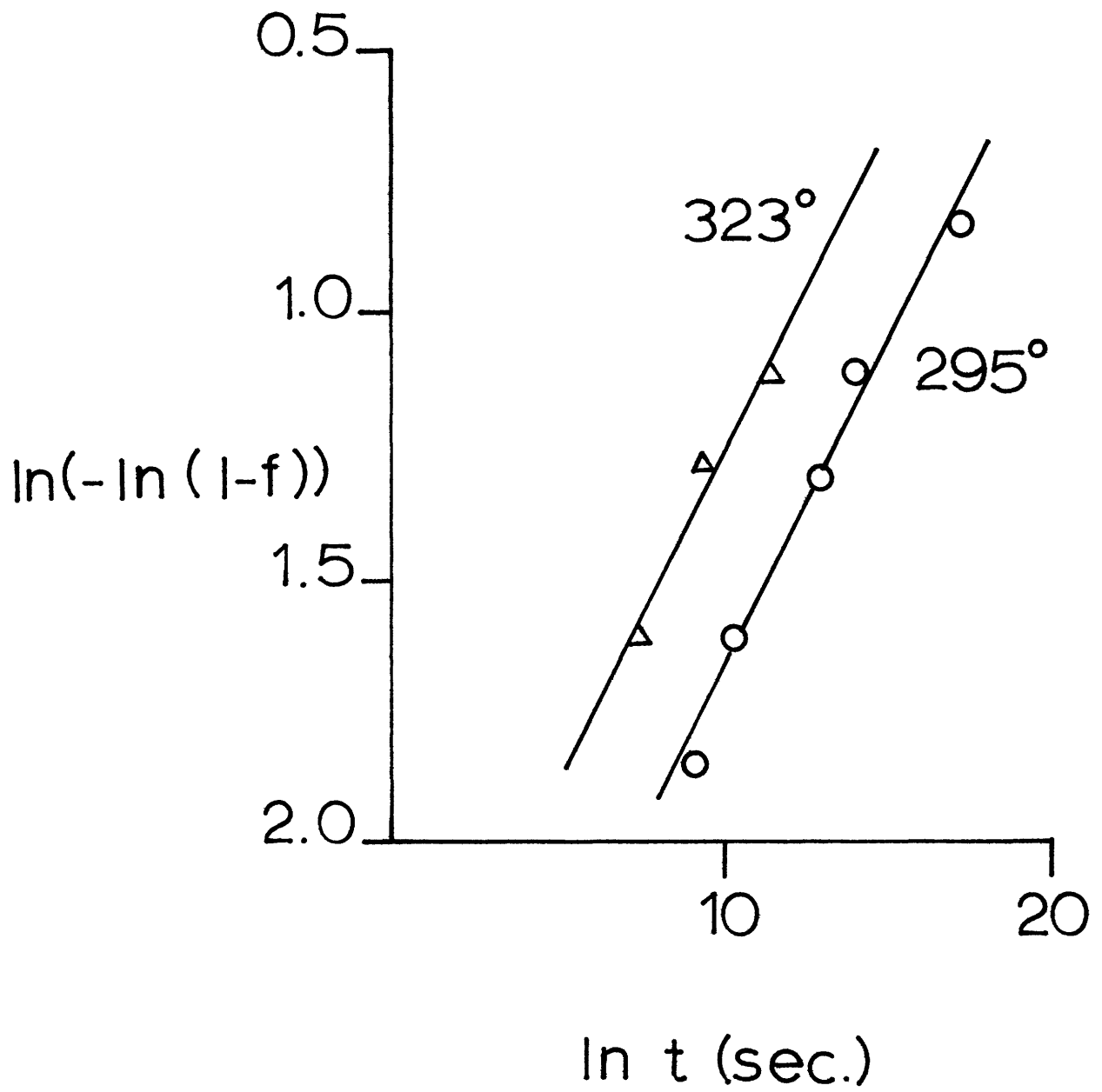
Equation (III. 3) yields an activation energy of $89.525 \pm 12,000$ joules per mole. (For an analysis of the error approximation, see Appendix C).

A least-squares analysis of Equation (III. 1), written in the form:

$$\ln \{ -\ln (1-f) \} = \ln (\kappa^n) + n \ln t \quad (\text{III. 5})$$

was also done for both temperatures (Figure III. 4) yielding values of n equal to 0.125 and 0.127, for 22° and 50°C respectively. With Equation (III. 2), the activation energy, Q , was calculated as 95,170 joules per mole. Although values of n this small ($\sim 1/8$) are not interpretable in terms of the conventional nucleation and growth processes, similar values have been obtained for the clustering and ordering of nitrogen atoms into the Fe_{16}N_2 structure in nitrogen martensites.⁹ The value of Q obtained here is in the range of activation energies calculated from resistivity measurements made in this temperature range⁴ and which are probably being determined by the same structural change.

Figure III.4 Isothermal Transformation Curves for the Clustering of Carbon Atoms in Martensite: $\ln(-\ln(1-f))$ vs. $\ln t$.



This value of Q is just slightly greater than the activation energy for the diffusion of carbon in ferrite ($Q_{\text{ferrite}} = 83,660$ joules per mole¹⁰), determined by internal friction. If the process is diffusion controlled, this may verify the belief that the energy barrier which a carbon atom must overcome to jump to an adjacent interstitial site is not affected much by the tetragonality of the lattice. Hillert⁵, however, argues that the activation energy for the diffusion of carbon in martensite is increased by the tetragonality and is a function of carbon content in the form:

$$Q_{\text{mart.}} = Q_{\text{ferrite}} + (14140) \cdot (\text{wt. \% C})$$

This relationship predicts a value of 109,966 joules per mole for an alloy of 1.86 wt. % carbon.

If Hillert's theory is correct, the activation energy calculated here may nonetheless be consistent with the process being controlled by interstitial atom diffusion, with the primary diffusion occurring across local regions of nearly pure, body-centered-cubic iron. The Mössbauer spectrum of the partially aged martensite indicates that this structure contains three types of regions: (a) iron atoms which are still in a virgin martensite-like environment, (b) iron atoms which are part of carbon-rich (Fe_4C) clusters, and (c) iron atoms which have lost

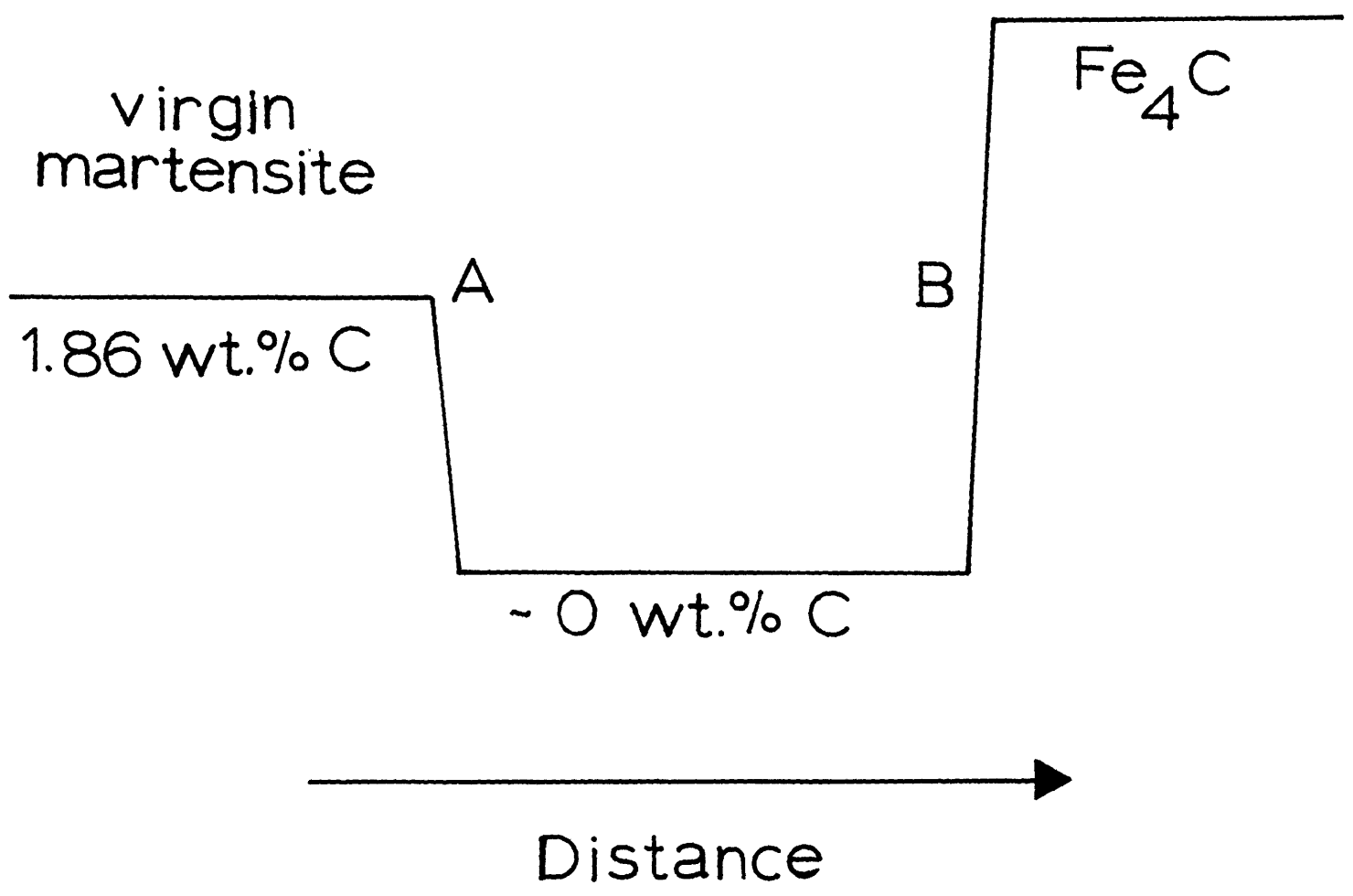
their carbon neighbors and have a ferrite-like environment. If the carbon-concentration profile of the aged martensite (on a local scale) is of the form illustrated in Figure (III.5), the Fe_4C regions are surrounded by the carbon-depleted regions. For such a model, the growth of the Fe_4C regions would occur by the diffusion of carbon atoms from region A, across the depleted region, to region B.

With diffusion occurring across a region essentially devoid of carbon, an activation energy close to Q_{ferrite} would be expected (independent of Hillert's model), and is, in fact, observed.

III.5 Summary

Mössbauer spectroscopy was employed to study the aging of martensite at 20° and 50°C . At both of these temperatures, the relevant process is the clustering and ordering of carbon atoms into high-carbon regions (Fe_4C) and the simultaneous creation of carbon-depleted regions. The activation energy associated with this redistribution is $89,525 \pm 12,000$ joules per mole, indicating that the process is controlled by the diffusion of carbon atoms.

Figure III.5 A possible Carbon Concentration Profile of the Aged Martensite Indicating Regions Still Possessing the Virgin Structure, Carbon Depleted Regions, and Fe₄C Regions.



References

1. G.R. Speich and W.C. Leslie: "Tempering of Steel", Met. Trans., 1972, vol. 3, p.1043.
2. M. Cohen: "The Strengthening of Steel", Trans. A.I.M.E., 1962, vol. 224, p. 638.
3. G.T. Eldis: "Ausform Strengthening of High Alloy Steels", Ph.D. Thesis, M.I.T., 1971.
4. A.M. Sherman: "The Structure and Aging of Martensite", Ph.D. Thesis, M.I.T., 1972.
5. M. Hillert: "The Kinetics of the First Stage of Tempering", Acta Met., 1959, vol. 7, p.653.
6. W.K. Choo and R. Kaplow: "⁵⁷Fe Mossbauer Measurements on the Aging of Iron-Carbon Martensite", Acta Met., 1973, vol. 21, p. 725.
7. N. DeCristofaro and R. Kaplow: "Interstitial Atom Configurations in Iron-Carbon and Iron-Nitrogen Solid Solutions", Chapter II of this thesis.
8. V. Izotov and L. Utervskii: "Structure of the Martensite Crystals of High-Carbon Steel", Phys. Metal. and Metallog., 1968, vol. 25, No. 1, p. 86.
9. R.D. Garwood and G. Thomas: "Tempering of Martensite in an Fe-1.5 Pct. N Alloy", Met. Trans., 1973, vol. 4, p. 225.
10. C. Wert: "Diffusion Coefficient of C in α -Iron", Phys. Rev., 1950, vol. 79, p. 601.

IV. ⁵⁷MOSSBAUER SPECTROSCOPY OF HEXAGONAL IRON-NITROGEN ALLOYS

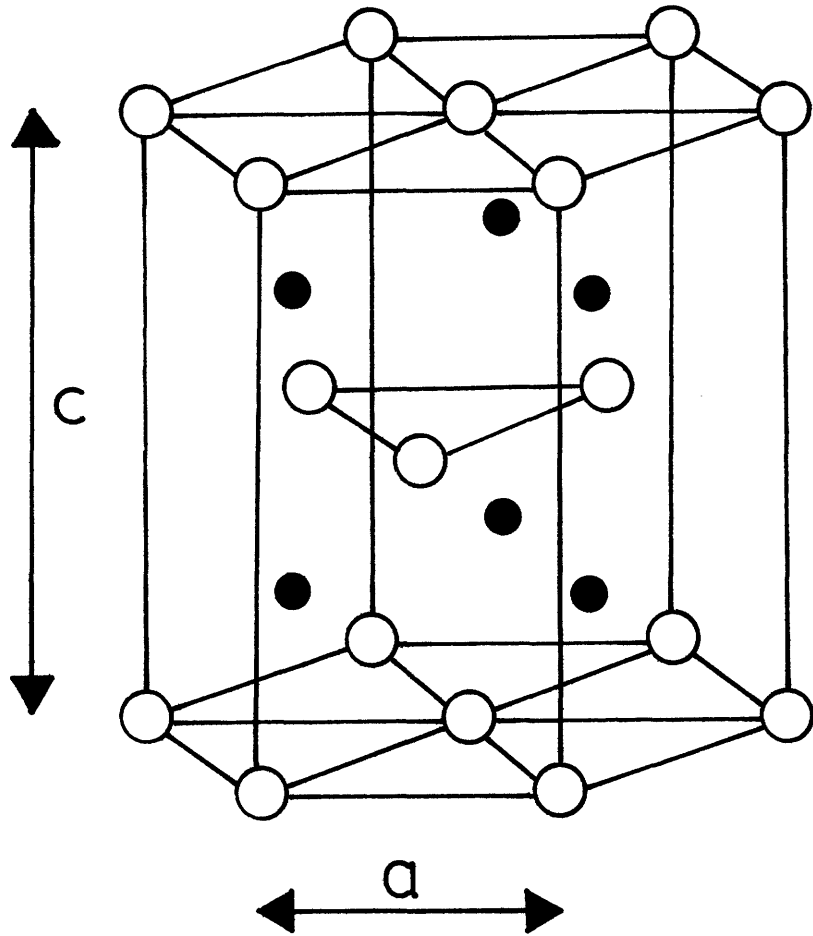
ABSTRACT

In Fe-N alloys, the hexagonal-close-packed phase can be completely retained metastably at room temperature by rapid quenching from 700°C, with nitrogen contents ranging from about 17 to 27 at. % N; (between the latter composition and 33 at. % N, the hexagonal phase is stable at room temperature). The phase is ferromagnetic; the Curie temperature is a sharp function of nitrogen content, with the maximum Curie point (about 300°C) occurring at 24 at. % N. The Curie point is below room temperature in the hexagonal phase for nitrogen contents less than 17 or greater than 31.8 at. % N. For alloys of the Fe₃N composition quenched from various temperatures, ⁵⁷Mössbauer spectroscopy indicates that the hexagonal phase undergoes ordering of nitrogen atoms on interstitial sites.

IV.1 Introduction

The knowledge of an hexagonal-close-packed phase of iron, ϵ -nitride, stabilized by high interstitial-nitrogen contents, dates back to the 1920's.¹⁻⁴ However, the equilibrium temperatures and compositional extent of this structure was not fully recognized until the development of the presently accepted iron-nitrogen phase diagram by Paranjpe⁵ and Jack.⁶ In those reports, the nitrogen atoms were described as occupying the octahedral interstitial positions in hcp iron (Figure IV.1). The interstitial sites are arranged in layers perpendicular to the c-axis with spacing $c/2$ such that each layer is equidistant between two basal planes of iron and each iron atom is

Figure IV.1 Hexagonal Close-Packed Structure



IRON ATOM



OCTAHEDRAL INTERSTITIAL SITE

adjacent to six interstitial sites (only some of which are filled). The lattice parameters of ϵ -nitride are a function of nitrogen content, with the c/a ratio decreasing continuously from approximately 1.65 at 15.5 at. % nitrogen to 1.60 at 33.0 at. % nitrogen. (The ideal close-packed ratio is 1.633.) Values at the low-nitrogen end of this range have been calculated by indirect methods, as it remains difficult to retain the hcp structure for nitrogen contents much less than 26.4 at. %, which represents the phase boundary at room temperature. As a result, virtually all investigations of ϵ -nitride have been focused on the upper end of its composition range.

ϵ -nitride has received much attention because of its interesting magnetic properties. Bridelle⁷ has shown the Curie temperature of this phase to decrease with increasing nitrogen content, from a maximum of 294°C at 24. at. %, to below room temperature for compositions greater than 30.5 at. %.

Mössbauer spectroscopy has been a particularly useful tool in studying ϵ -nitride's magnetic properties. Collectively, Eickel⁸, Takaki⁹, and Chabanel¹⁰ have demonstrated the Curie point behavior for alloys of greater than 24. at. % nitrogen. Separately resolvable

Mössbauer spectra have been identified for iron atoms with one (Fe_I), two (Fe_{II}), and three (Fe_{III}) of the adjacent interstitial sites occupied by nitrogen atoms. The hyperfine magnetic field, H , characterizing these sites when the material is well below the Curie temperature are reported as 298, 238, and 140 KOe respectively. The effect of the hyperfine magnetic field decreasing with increasing nitrogen coordination is also observed in Fe_4N .¹¹ On the basis of the Mössbauer parameters and the magnetic moments of the iron atoms comprising the Fe_4N structure (the latter values being proportional to the hyperfine magnetic field), Shirane¹¹ proposed that the nitrogen atoms in this structure act as electron donors to the nearest-neighboring iron atoms. However, the scattering factor for nitrogen in both Fe_4N and ϵ , as determined by X-ray¹² and electron^{13, 14} diffraction data, indicates just the opposite: that the nitrogen atom appears to be negatively charged. These authors suggest that covalent bonds are formed between nitrogen atoms and their nearest iron neighbors with electrons from the iron atoms being close enough to the nitrogen atom to contribute to its scattering power.

In this report, we have used Mössbauer spectroscopy to study the magnetic behavior of ϵ -nitride of nitrogen content less

than 25 at. % and to investigate the ordering of nitrogen atoms on the interstitial sites at 25 at. % nitrogen.

IV.2 Experimental Procedure

IV.2.1 Sample Preparation

Alloys of iron and nitrogen were prepared by flowing mixtures of ammonia and hydrogen over a pure iron (99.9%) foil (thickness = 0.001 inch) at elevated temperatures. The nitriding furnace contained a quartz tube in which the sample was suspended from a support wire. Samples were rapidly quenched directly from the nitriding atmosphere into an iced-brine bath by melting the support wire. The nitrogen content of the alloy was controlled by varying the relative fractions of ammonia and hydrogen in the nitriding mixture. As indicated by Lehrer,¹⁵ the nitrogen content of the alloy is increased with the ammonia fraction in the mixture. Samples were nitrided for one hour at 700°C to reach equilibrium.

The nitrogen content of all alloys was measured by chemical analysis. X-ray diffraction and Mössbauer spectroscopy were employed to determine the phases present. By quenching from 700°C, the hcp phase could be completely retained at room temperature for compositions as low as 17 at. % nitrogen. ϵ -nitride between 17 and 27 at. % nitrogen is metastable at room temperature, and

decomposes to $\alpha+\gamma'$, γ' or $\gamma'+\epsilon$ (27 at. % nitrogen) when heated. Between 27 and 50 at. % nitrogen, ϵ -nitride is stable.

Foils nitrified at 700°C to 25 at. % nitrogen (Fe_3N) were also furnace-cooled and annealed at lower temperatures while under the same nitriding atmosphere prior to quenching at this composition. The hcp phase could be completely retained on quenching with annealing temperatures as low as 550°C. Below 550°C, two-phase mixtures of γ' and ϵ were formed, as would be expected from the equilibrium binary phase diagram.

IV.2.2 Mössbauer Spectroscopy

Mössbauer spectra were recorded on a constant acceleration spectrometer (Austin Science Associates) with a Co^{57} in copper γ -ray source. The Doppler velocities were monitored with a laser interferometer¹⁶ and calibrated with a pure-iron reference. For Mössbauer measurements below room-temperature, and for room-temperature comparisons with low-temperature data, samples were placed in a liquid-nitrogen dewar, mounted on the spectrometer. Sample temperatures could be maintained as low as -193°C in the manner.

The Mössbauer peak widths for ϵ -nitride are much greater than would be expected from the natural linewidths for Fe^{57} and

the known instrumental broadening.¹⁷ As in the case of iron-carbon and iron-nitrogen martensites, the peak widths vary as a function of the magnitude of the magnetic splitting of the nuclear state; i. e., peaks farthest from the center of the spectrum are broader than the inner peaks, indicating that the broadening is mainly due to a spread in the magnetic hyperfine fields. In calculating the relative intensities of the Fe_I, Fe_{II}, and Fe_{III} spectra, the same fitting techniques were adopted as have been used earlier for the martensite.¹⁷

The idealized Mossbauer pattern is the result of the convolution:¹⁸

$$P_{th}(E_s) = \int_{-\infty}^{\infty} I(E, E_s) [1 - \exp(-k \Sigma(E))] dE \quad (IV.1)$$

where

$P_{th}(E)$ = theoretical resonant absorption

$I(E, E_s)$ = Lorentzian energy distribution of the gamma-radiation source

k = function of: cross section for resonant absorption, recoilless fraction, number of nuclei/cm², and thickness of the absorber.

and

$$\Sigma(E) = \sum_{i=1}^N \frac{g_i \Gamma_a^2}{4(E-E_i)^2 + \Gamma_a^2} \quad (IV.2)$$

The latter term is the sum of a series of Lorentzian curves, each representing one distinct absorption energy in the sample. Γ_a is the natural energy width of a Mössbauer absorption or emission event ($\Gamma_a = 0.095$ mm./sec. for ^{57}Fe); E_i and g_i are the positions and fractional weights of the i -th line respectively.

Instrumental broadening was compensated for by convolving the theoretical resonant absorption with a normalized Gaussian curve, G , i. e.

$$P(E_s) = \int P_{th}(E) \cdot G(E - E_s) dE \quad (\text{IV. 3})$$

The appropriate width for the broadening was determined by comparison of $P(E_s)$ with the experimental Mössbauer spectrum of α -iron. To accommodate the additional internal ferromagnetic broadening, equation (IV.2) becomes:

$$\Sigma(E) = \sum_{i=1}^N \left(\int \frac{g_i \Gamma_a^2}{4(E - E_i)^2 + \Gamma_a^2} G(E, E_i) dE \right) \quad (\text{IV. 4})$$

where $G(E, E_i)$ represents a Gaussian curve whose width is a function of peak position, but corresponding to a fixed spread in fields.

IV. 3 Experimental Results

The room-temperature Mössbauer spectra of ϵ -nitrides of compositions ranging from 17.1 to 23.8 at. % nitrogen are shown in

Figure (IV.2). All samples were nitrated at 700°C and quenched from that temperature. At approximately 24 at. % nitrogen (Figure (IV.2a)), ϵ -nitride displays a spectrum characteristic of a ferromagnetic material with three types of iron-atom sites. All three iron-atom spectra previously reported for ϵ -nitride are observable: that is, iron atoms with one ($H = 284 \text{ KOe}$), two ($H = 227 \text{ KOe}$), and three ($H = 130 \text{ KOe}$) nitrogen neighbors.

As the nitrogen content of the ϵ -phase is decreased, the relative weights of the three spectra comprising the M^{II} pattern change and their hyperfine magnetic fields at room temperature decrease. At 18.2 at. % nitrogen (Figure IV.2c), the hyperfine fields have diminished to the point where resolution between the individual peaks comprising the M^{II} pattern has been lost. The pattern continues to coalesce until, at 17.1 at. % nitrogen (Figure IV.2e), only a quadrupole split doublet exists. This last spectrum is characteristic of a ferromagnetic material above its Curie point.

The M^{II} effect in three samples, those of 21.6, 18.2, and 17.1 at. % nitrogen (the latter two compositions being where the hyperfine magnetic field is either greatly reduced or absent at room temperature) was also measured at liquid nitrogen temperature. The three M^{II} spectra, shown in Figure(IV.3), are all distinctly

Figure IV.2 Mossbauer Spectra of ϵ -Nitride:

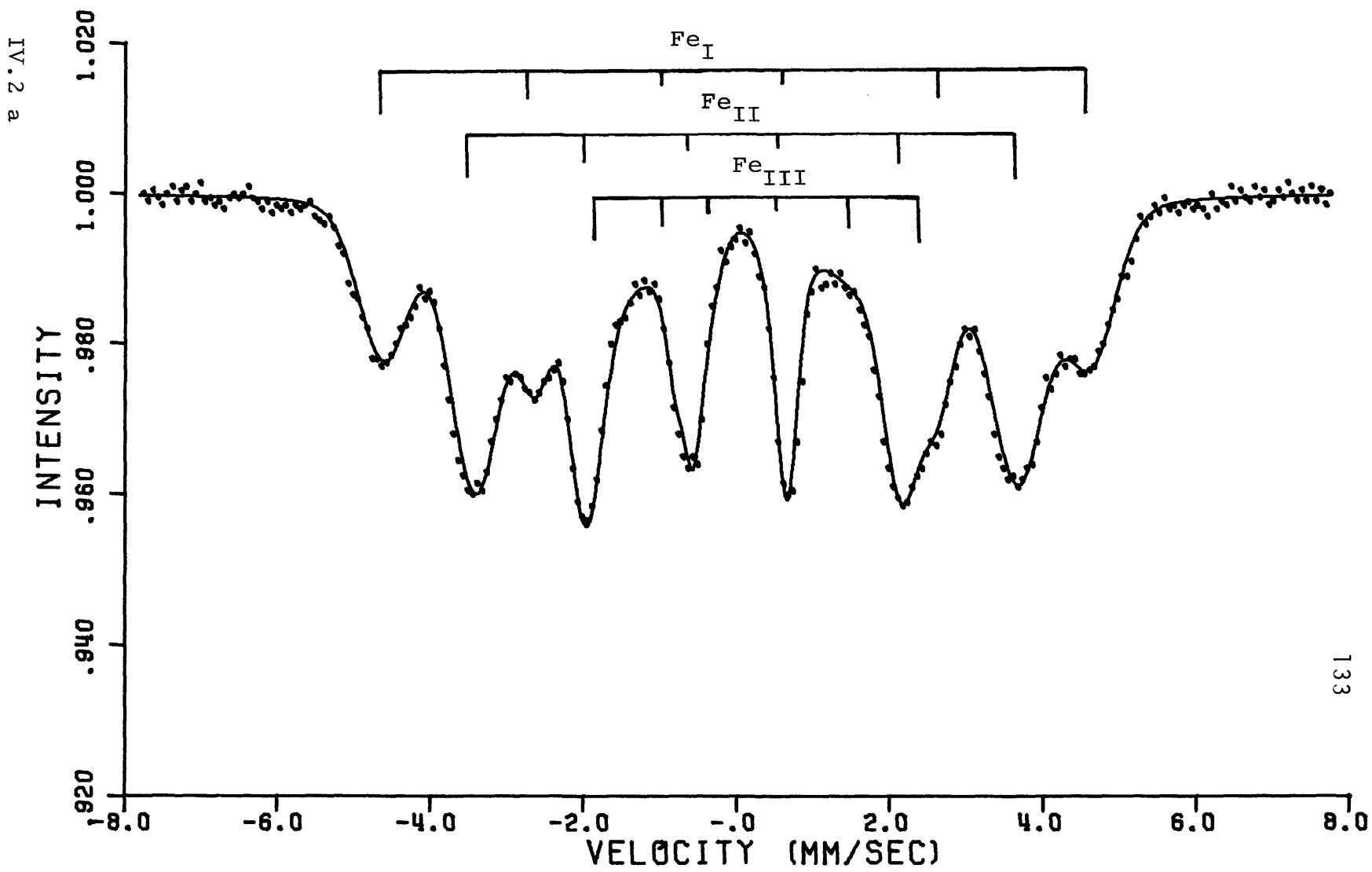
IV.2 a 23.8 at.% N

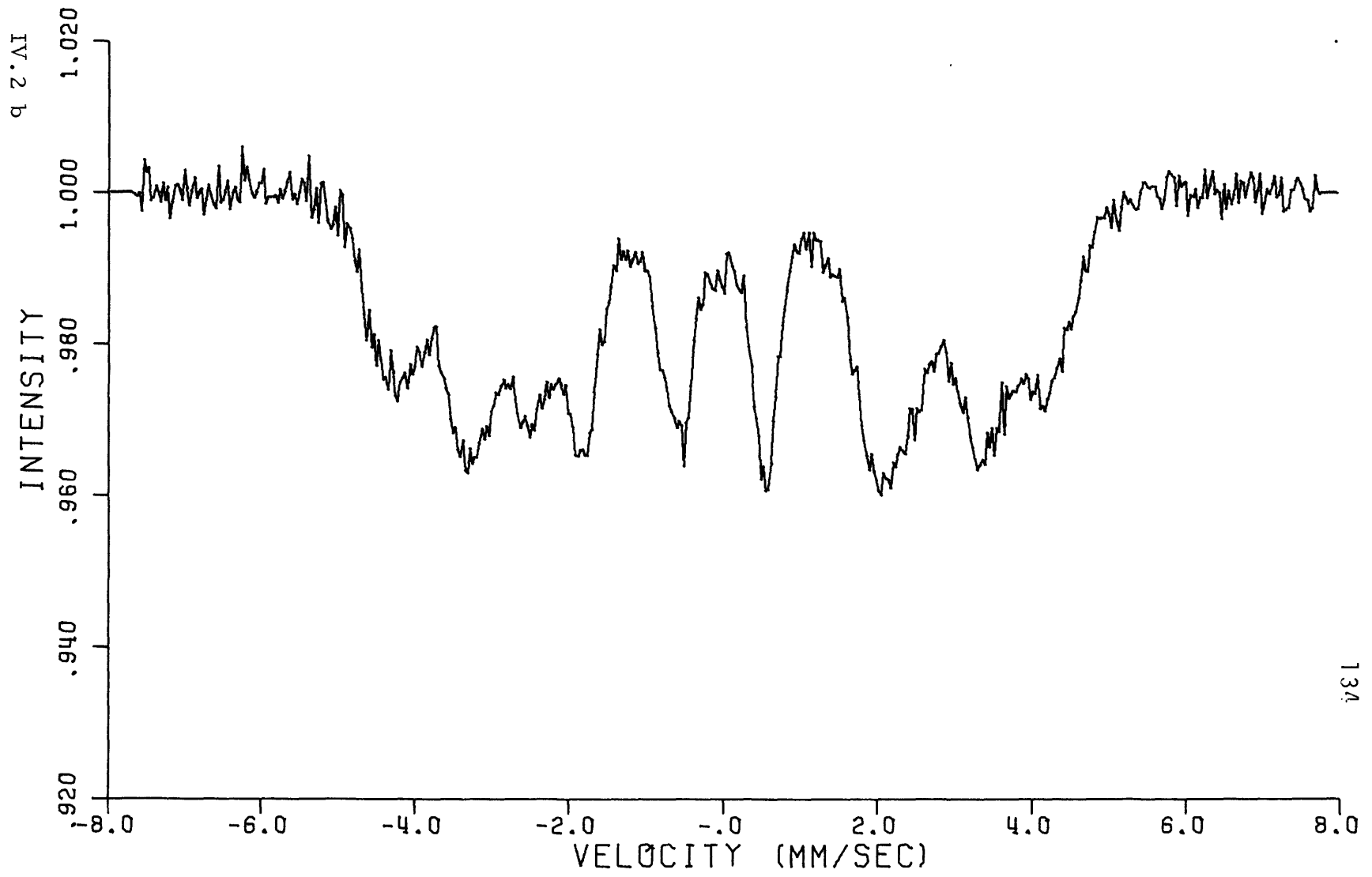
IV.2 b 21.6 at.% N

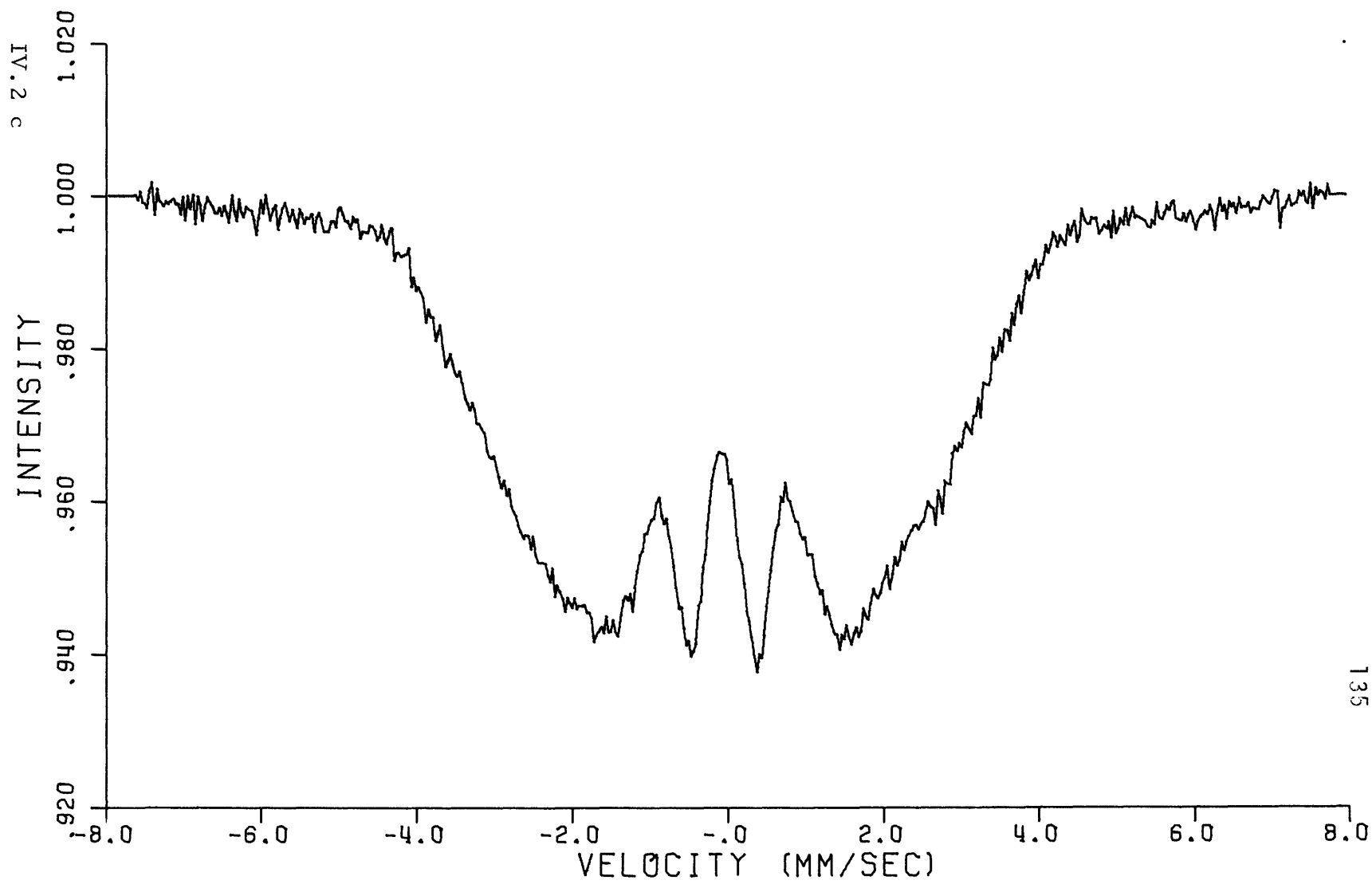
IV.2 c 18.2 at.% N

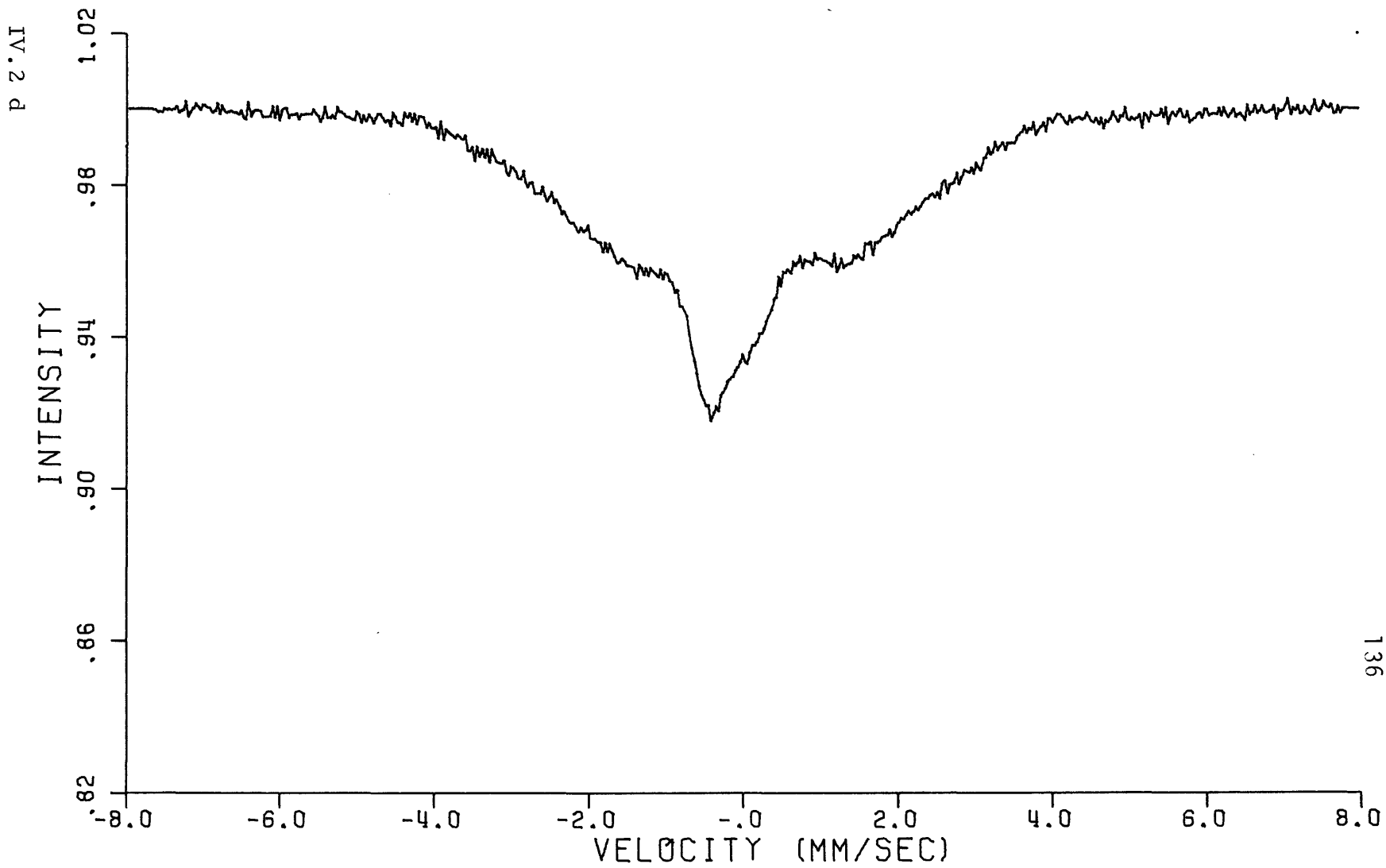
IV.2 d 17.7 at.% N

IV.2 e 17.1 at.% N









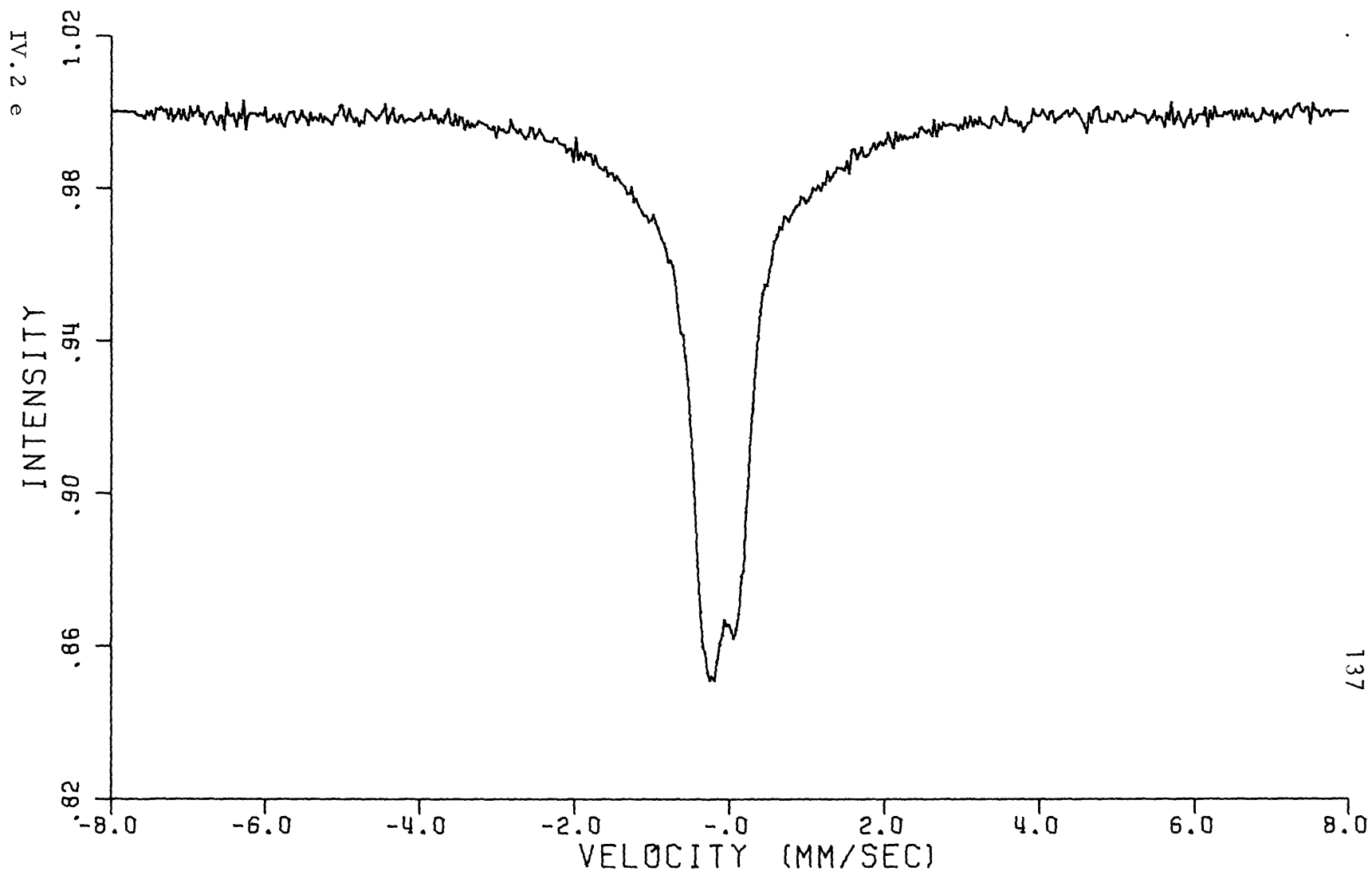
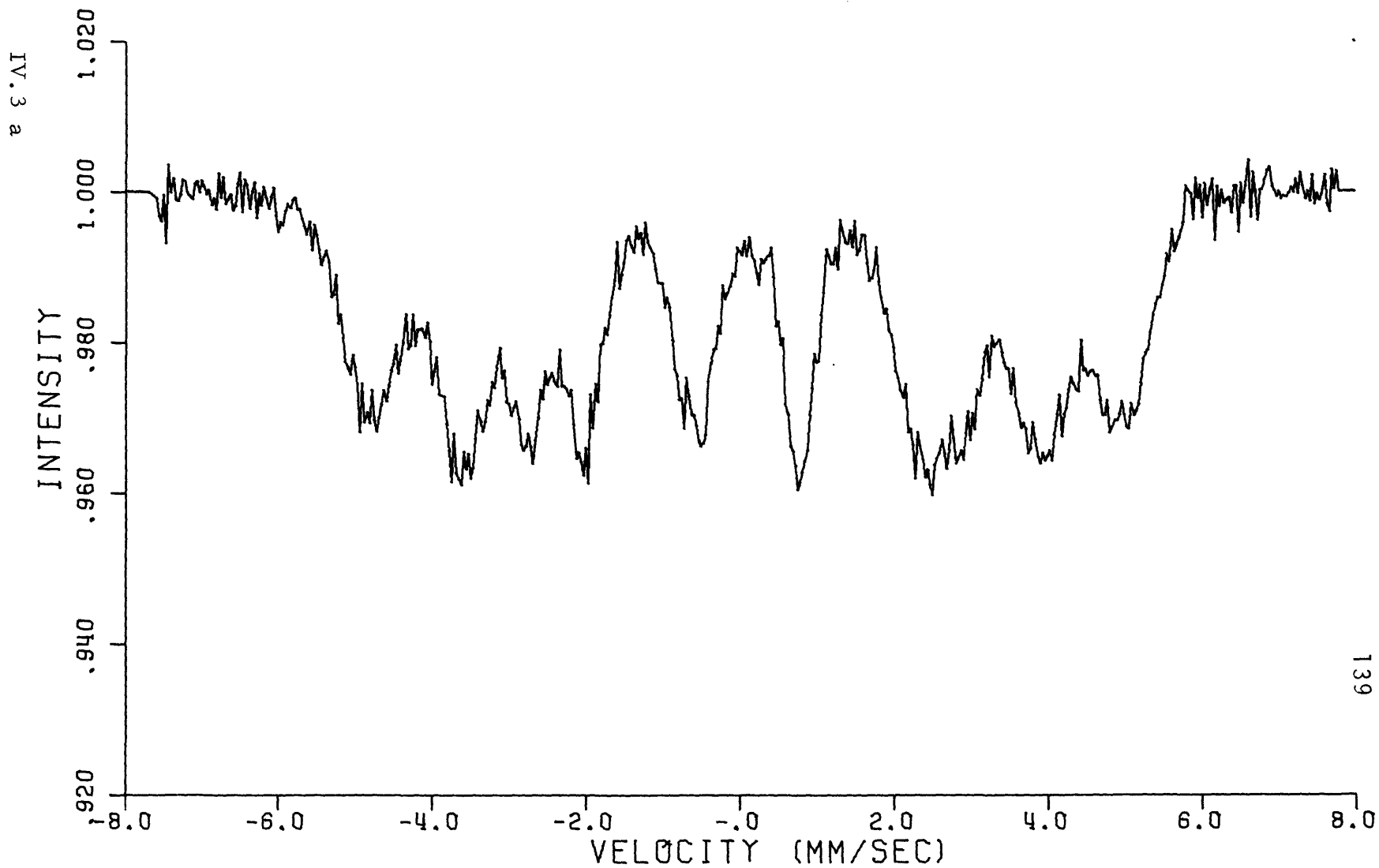
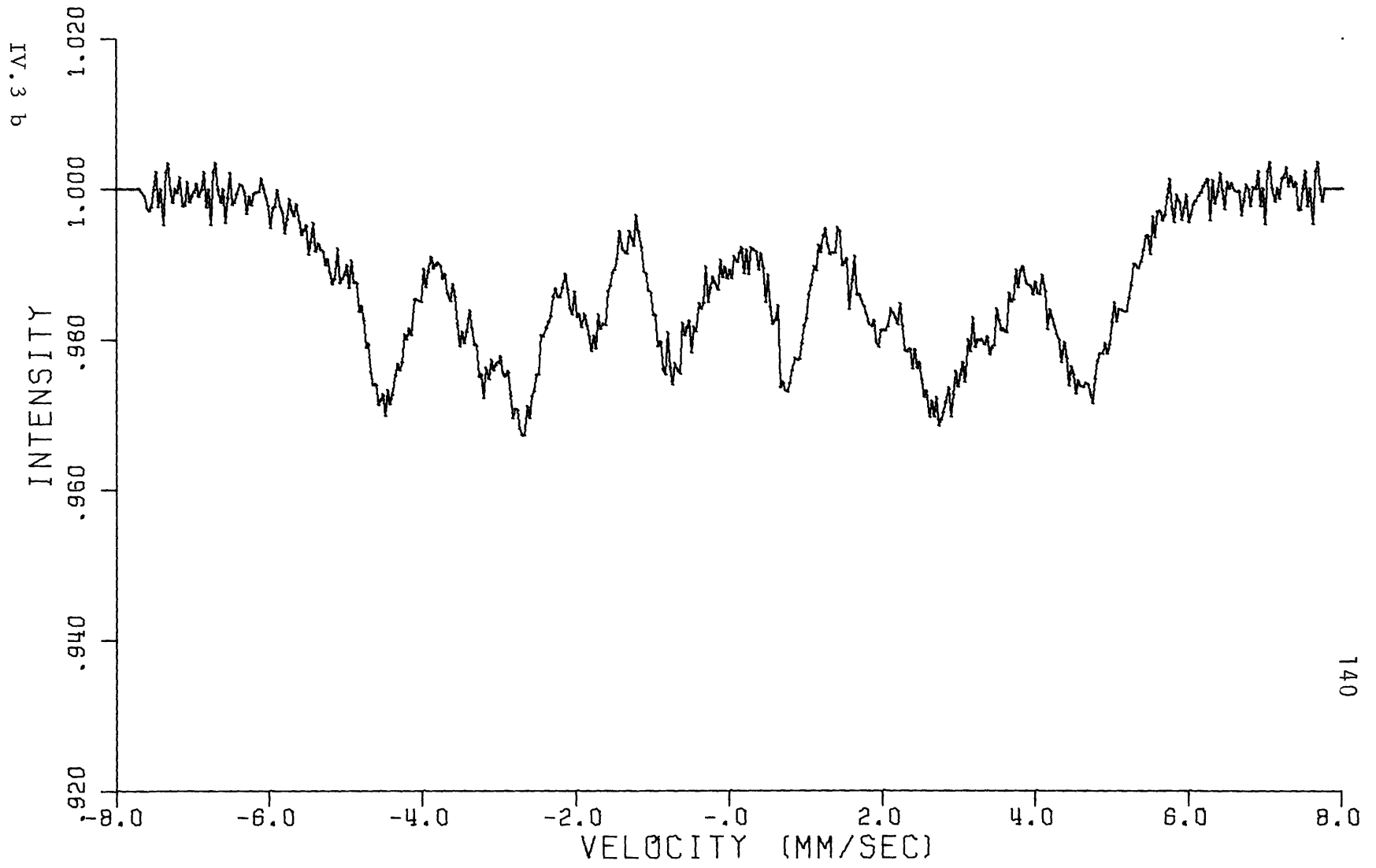
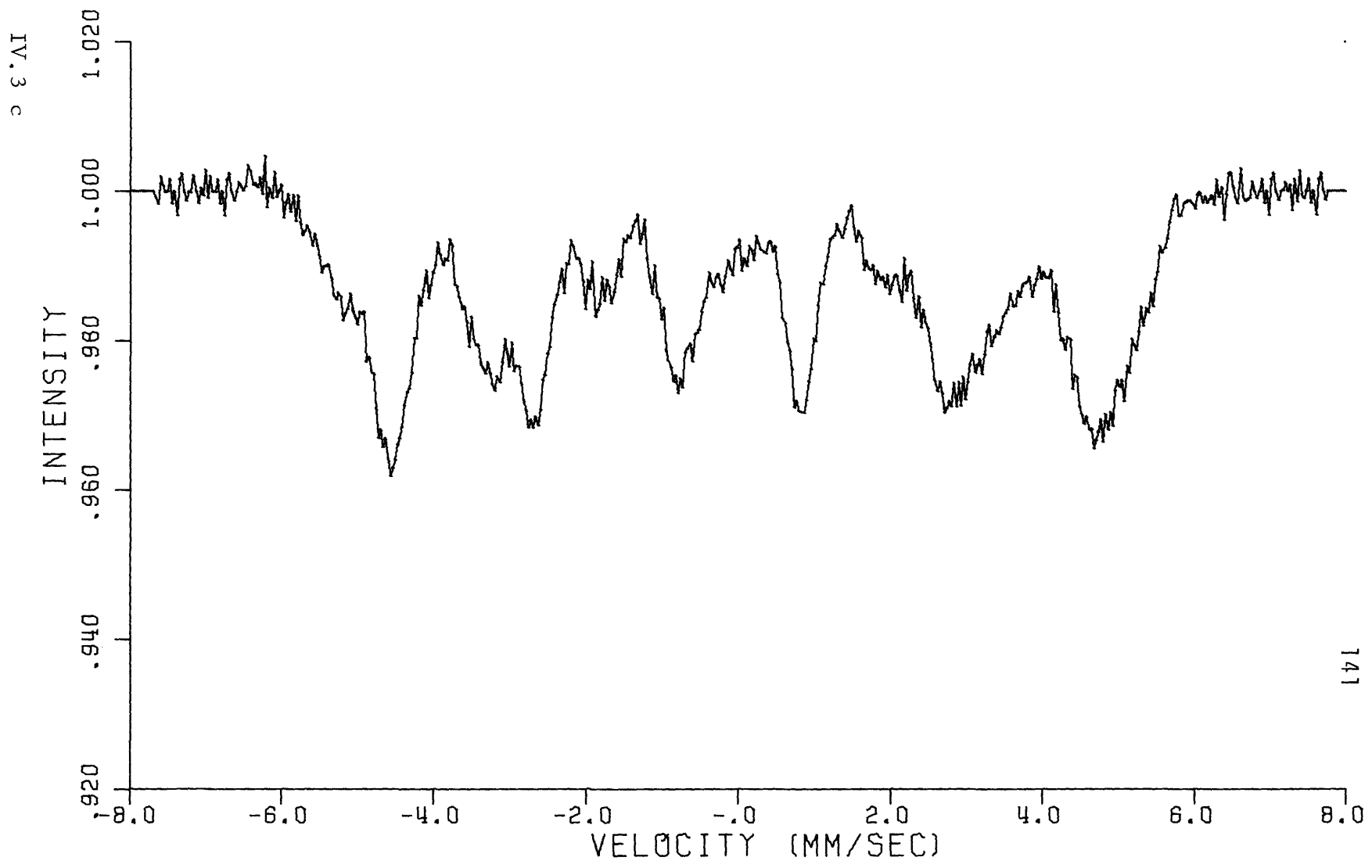


Figure IV.3 Mossbauer Spectra of ϵ -Nitride Measured at -193°C .
IV.3 a 21.6 at. % N
IV.3 b 18.2 at. % N
IV.3 c 17.1 at. % N







ferromagnetic in nature, indicating that at this temperature, all three alloys are below their Curie points. X-ray diffraction patterns of similar ϵ -nitrides were also taken at the low temperature to ascertain that no transformations had occurred.

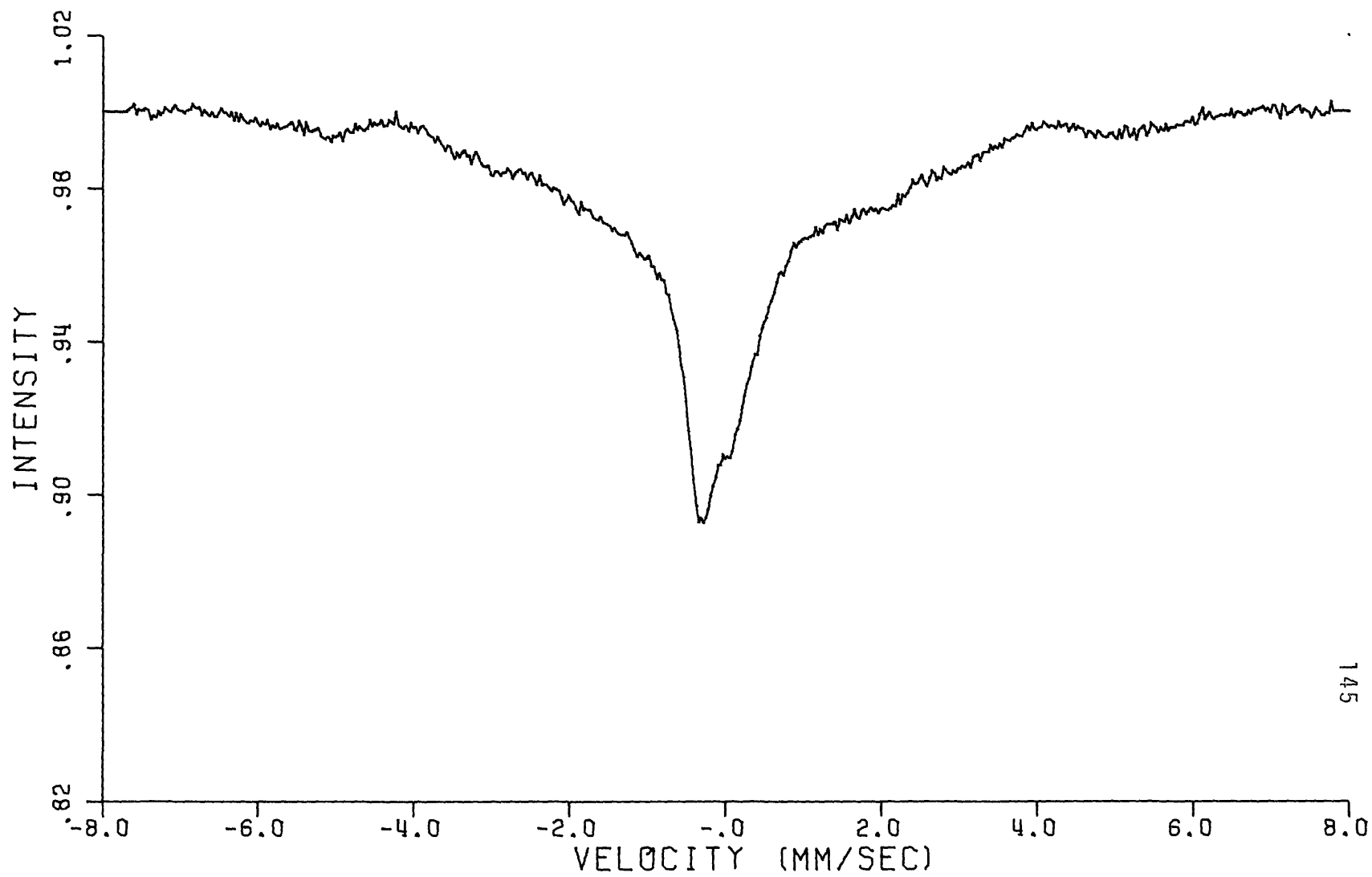
As would be expected in a ferromagnetic material, the magnetic fields associated with the iron-atom environments in the 21.6 at. % nitrogen sample are all slightly greater at the lower temperature. In the Mössbauer patterns of 18.2 and 17.1 at. % nitrogen samples, a fourth ferromagnetic spectrum with a field greater than any reported for ϵ -nitride (330 KOe) is also observed. Since these alloys are of relatively low-nitrogen content, a small but significant fraction of the iron atoms will have no nitrogen neighbors on any of the six adjacent interstitial sites, if nitrogen atoms are not ordered on the interstitial sublattice. Thus, the additional spectrum is associated with this type of iron-atom environment (Fe_\circ). The relatively large magnetic field characteristic of iron atoms with no nitrogen neighbors in this alloy is consistent with the observed decrease in field with increasing nitrogen-coordination number.

ϵ -nitride alloys which were above their Curie temperature at 22°C, and which were subsequently quenched to -193°C for

spectroscopy, show signs of residual ferromagnetism when returned to room temperature. The Mössbauer spectrum of the 17.1 at. % nitrogen sample which has undergone this thermal cycle (paramagnetic spectrum at 22°C in Figure (IV.2e) and ferromagnetic at -193°C in Figure (IV.3c)), is shown in Figure (IV.4).

In addition to the expected central paramagnetic peak, a broad region of absorption spans the central portion of the spectrum. Such a Mössbauer pattern is characteristic of a material very close to its Curie temperature. A weak, ferromagnetic spectrum, characteristic of a material well below its Curie temperature, also appears. Since one would not expect an irreversible magnetic transition, we assume that some structural changes must occur on cooling, at least in this compositional region. These changes apparently yield a nonhomogeneous material, with - at room temperature - some of it above its Curie point, some just below its Curie point, and a smaller part distinctly below its Curie point. X-ray diffraction patterns, however, show only the hexagonal Bragg lines at -193°C, and after returning to room temperature. The possibility of residual magnetism being associated with changes in the nitrogen-atom configuration (ordering) and with the development of twin or stacking faults has also

Figure IV.4 ^{57}Fe Mössbauer Spectrum of ϵ -Nitride (17.1 at. % N) at Room Temperature following Quenching at -193°C .



been considered. The Mössbauer spectrum at -193°C , where the spectra associated with the different iron types are resolvable, indicates that the nitrogen atoms are randomly arranged on the interstitial sites.

While no comparison can be made with the arrangement existing before cooling, since that structure, at room temperature, has a paramagnetic, unresolvable spectrum, it therefore appears that ordering of the nitrogen atoms below room temperature is not responsible for the experimental effects. Although detailed changes in the X-ray diffraction pattern do occur, these are not explainable in terms of basal-plane faulting, which is the most likely type of faulting expected in association with either a martensitic transformation or a transformation to the Fe_4N phase. An internally consistent and comprehensive explanation of this effect has not yet been developed.

Mössbauer spectra for samples of approximately 25 at.% nitrogen (stoichiometric Fe_3N), rapidly quenched following annealing at temperatures below 700°C , are shown in Figure (IV.5). As the annealing temperature is lowered, the predominant effect is the increasing intensity of the six-peak spectrum of Fe_{II} atoms at the expense of the F_{I} and F_{III} environments. At the same time, the peaks sharpen, especially those of the Fe_{II} atoms.

Figure IV.5 ⁵⁷Mo^{ssbauer Spectrum of Fe₃N ε - Nitride}

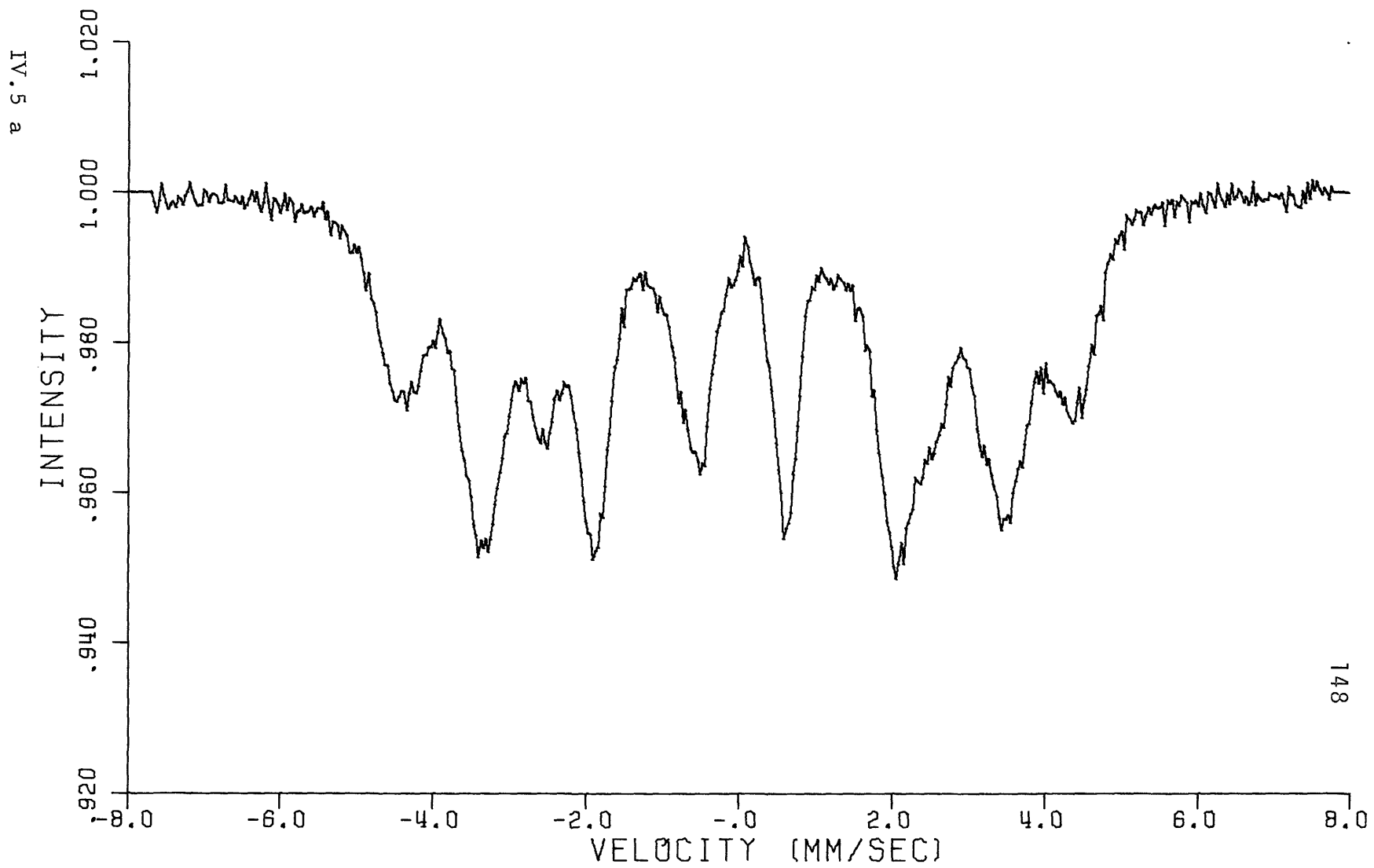
IV.5 a quenched from 640°C

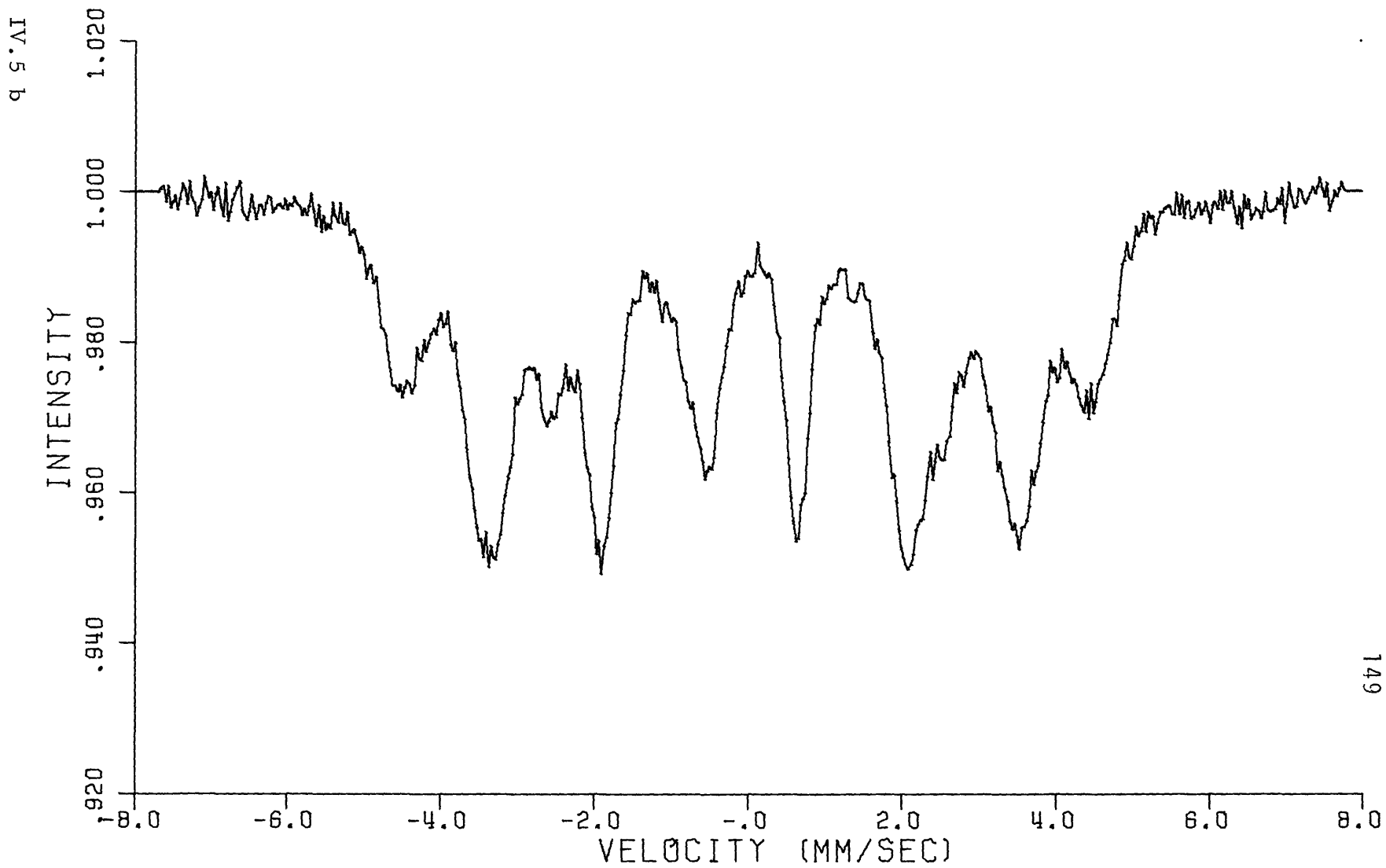
IV.5 b quenched from 625°C

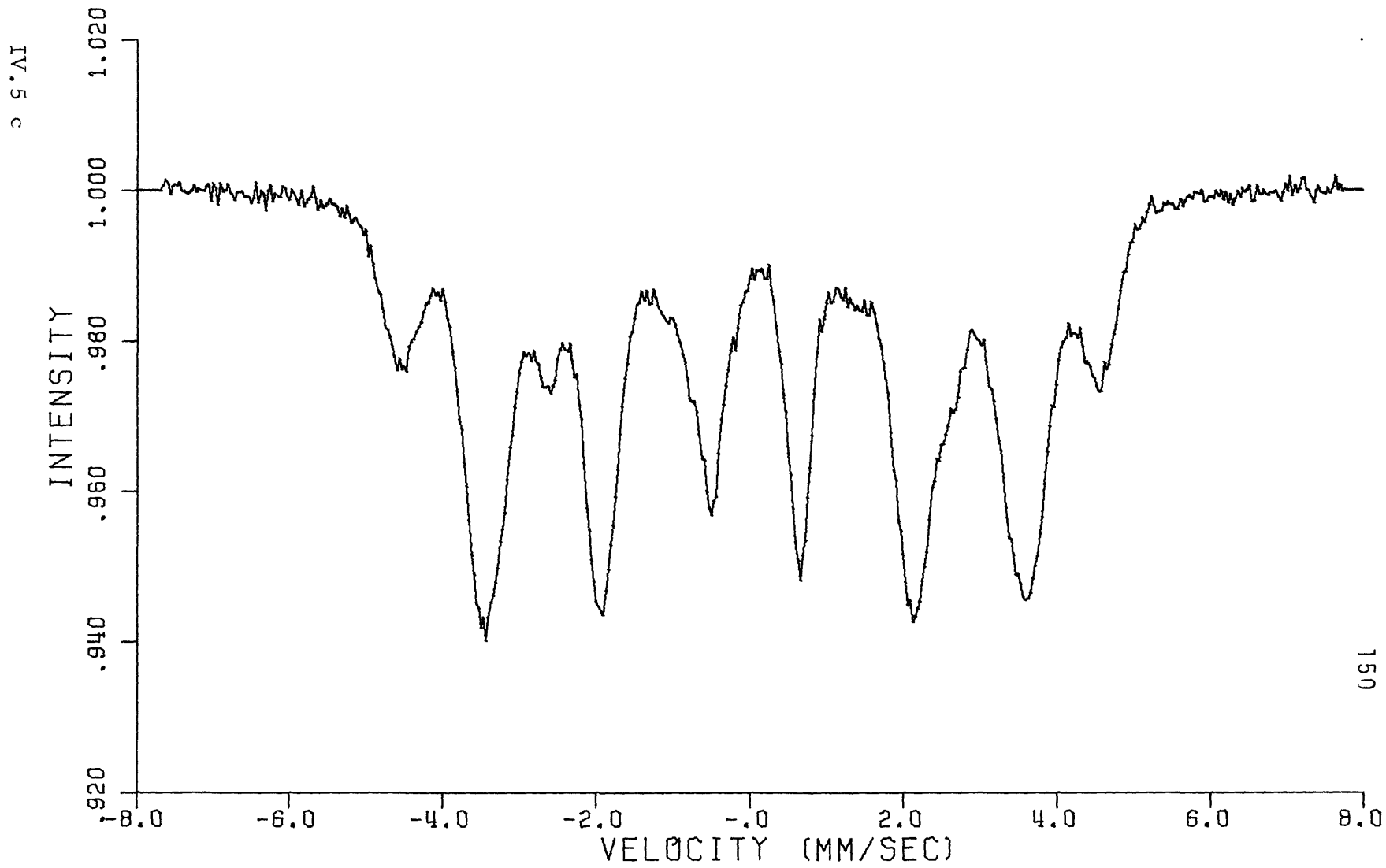
IV.5 c quenched from 610°C

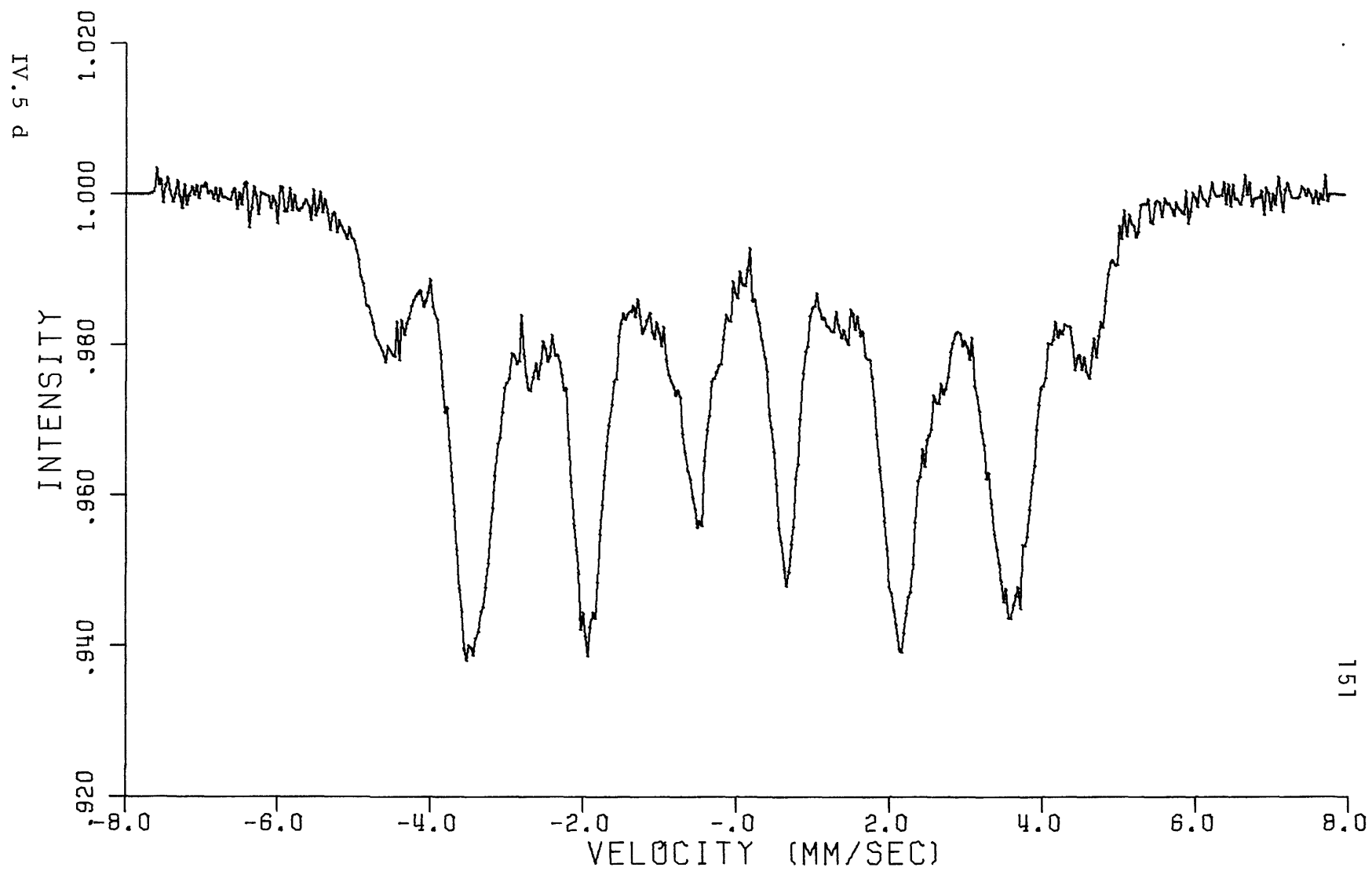
IV.5 d quenched from 580°C

IV.5 e quenched from 550°C

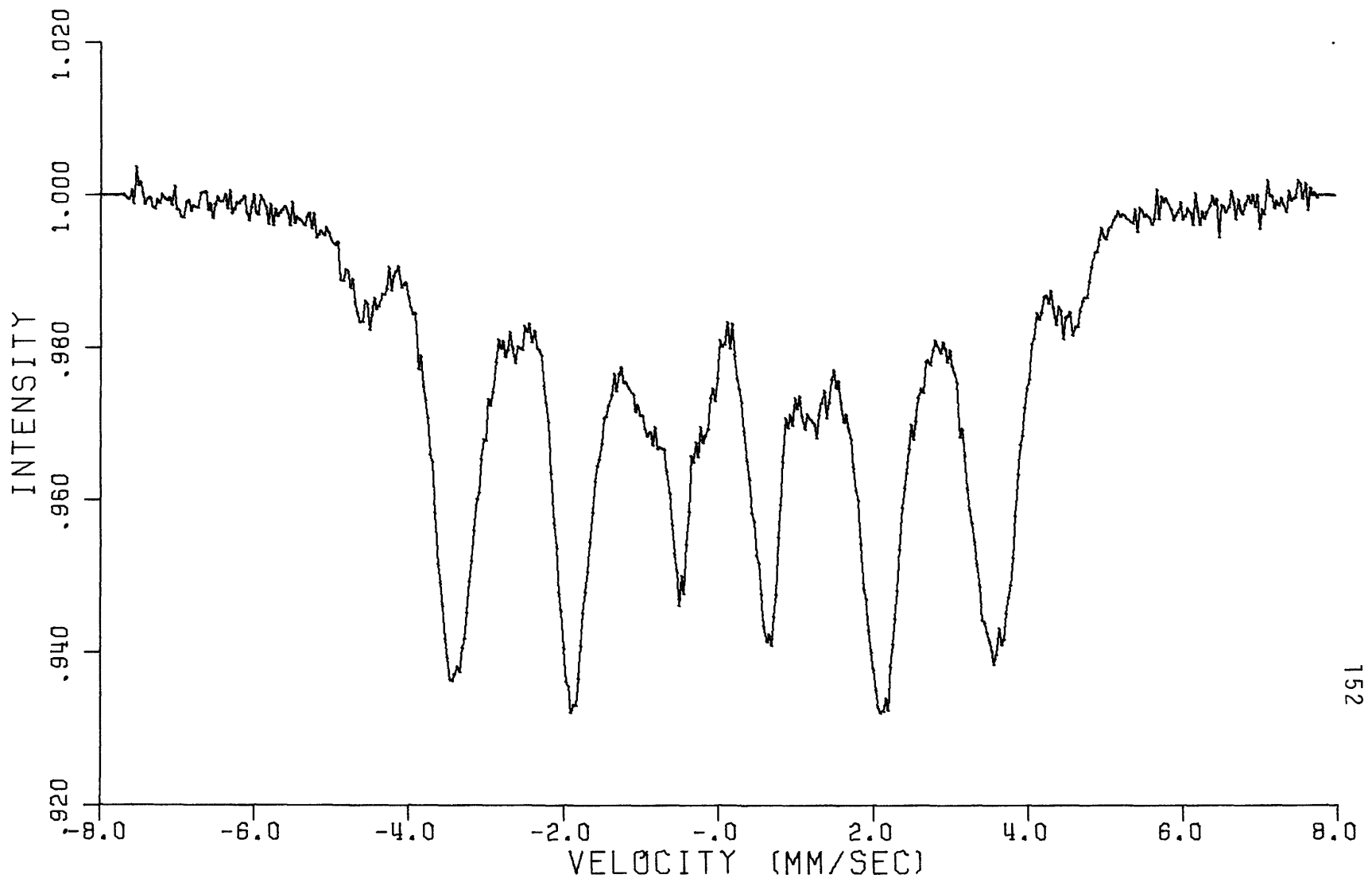








IV.5 e



IV.4 Discussion

IV.4.1 Hyperfine Magnetic Field

The hyperfine magnetic fields at room temperature of the Fe_{II} type atoms, given in Table (IV.1), are plotted as a function of composition in Figure (IV.6). Also included in Figure (IV.6) are the fields of Fe_{II} type atoms from ϵ -nitrides of higher nitrogen content, obtained by Takaki⁹ and Chabanel.¹⁰ The variation of the magnetic field with composition is roughly symmetrical about 24 at.% nitrogen, decreasing sharply as the nitrogen content is either increased or decreased.

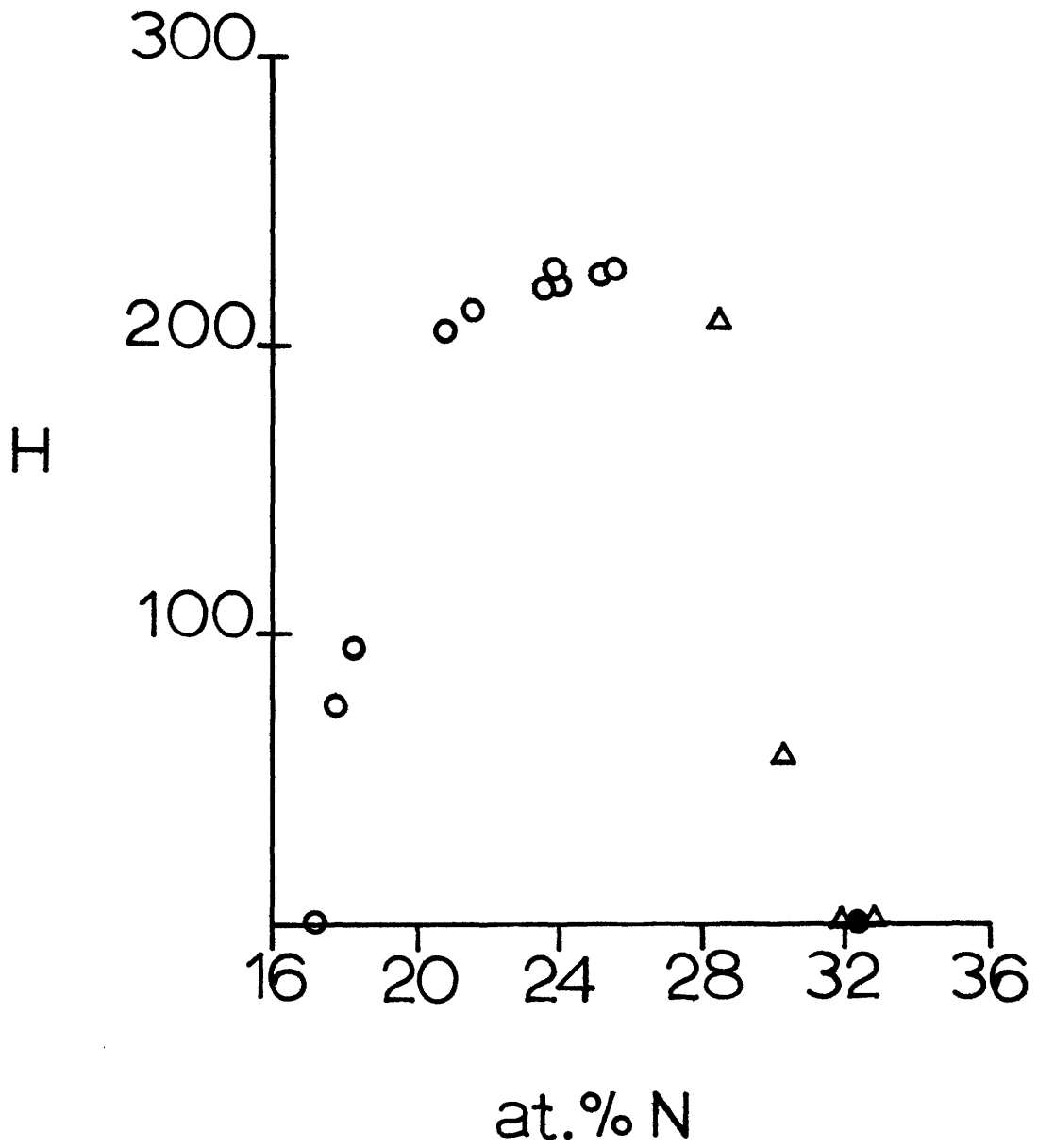
The behavior of the magnetic field as the nitrogen content is increased from 24 at.% nitrogen is related to the Curie temperature variation in this phase. Hanna¹⁹ and Ron²⁰ have demonstrated, for metallic iron and for various iron carbides, that below the Curie point the hyperfine magnetic field varies with temperature in the same manner as does the saturation magnetization, according to the Curie-Weiss law. The magnetization (or field) decreases slowly as the temperature is raised above absolute zero, drops more rapidly at higher temperatures and finally falls precipitously to zero at the Curie temperature.

TABLE IV.1

Hyperfine Magnetic Fields of Fe_{II} in ϵ -Nitride

<u>Nitride Composition (at. %N)</u>	<u>Hyperfine Magnetic Field of Fe_{II} (Koe)</u>
17.1	0
17.7	74
18.2	94
20.6	205
21.6	212
23.7	219
23.8	227
24.0	220
25.1	224.5
25.5	226

Figure IV.6 Hyperfine Magnetic Fields of Fe_{II} as a Function of Nitrogen Content



- THIS STUDY
- CHABANEL ¹⁰
- △ TAKAKI ⁹

As the Curie temperature of ϵ -nitride decreases from 294°C to below room temperature with increasing nitrogen content, the hyperfine magnetic field decreases continuously to zero in the manner expected: slowly at first, when the Curie temperature is well above room temperature, and then sharply where the Curie temperature is in the vicinity of room temperature. Paramagnetic Mössbauer spectra for ϵ -nitrides greater than 32 at.% nitrogen are consistent with the Curie temperature being below room temperature at these compositions.

Thus, the behavior of the magnetic field for nitrogen contents less than 24 at.% must also correspond to a decreasing Curie temperature. The ϵ -nitride of 17.1 at.% nitrogen, which displays a paramagnetic spectrum at 22°C , (Figure (IV.2e)), and a ferromagnetic spectrum at -193°C , (Figure (IV.3c)) demonstrate that, at this nitrogen content, the Curie point is between these temperatures. If the hyperfine magnetic field of the Fe_{II} -type atom at absolute zero is considered to be intrinsically independent of composition and determined only by the local atomic arrangement (as is the case in iron-carbon and iron-nitrogen martensites), and if the Curie-Weiss law is obeyed, then the field strength is a function only of temperature

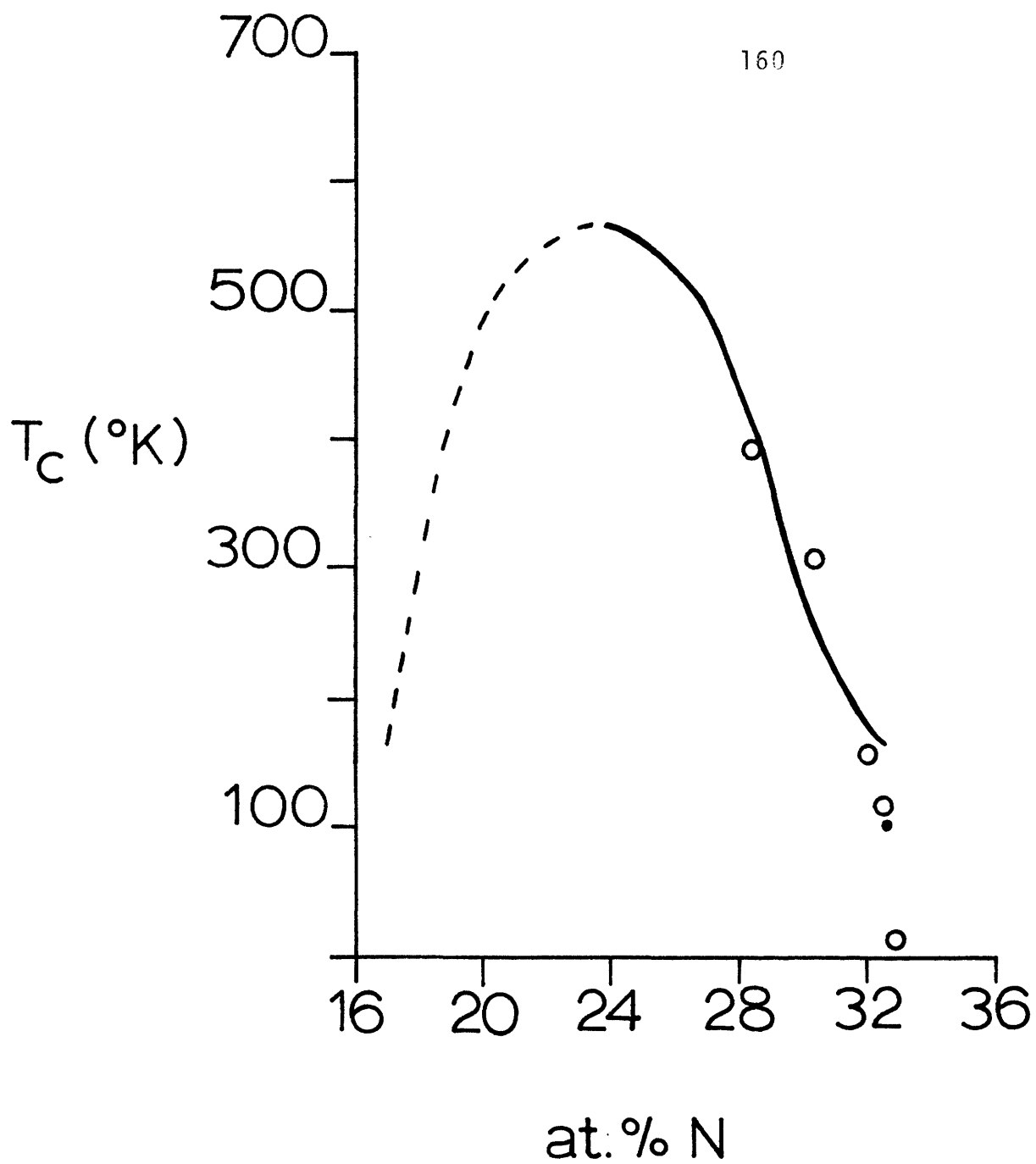
and the Curie temperature of the alloy. The Curie temperature of alloys of less than 24 at. % nitrogen may then be approximated by comparison of the hyperfine magnetic fields of their Fe_{II} -type atoms to the fields of Fe_{II} -type atoms in ϵ -nitrides of high-nitrogen content, for which the Curie temperature is known. The Curie temperature as a function of composition, derived in this manner, is shown in Figure (IV. 7).

IV. 4. 2 Ordering in Fe_3N

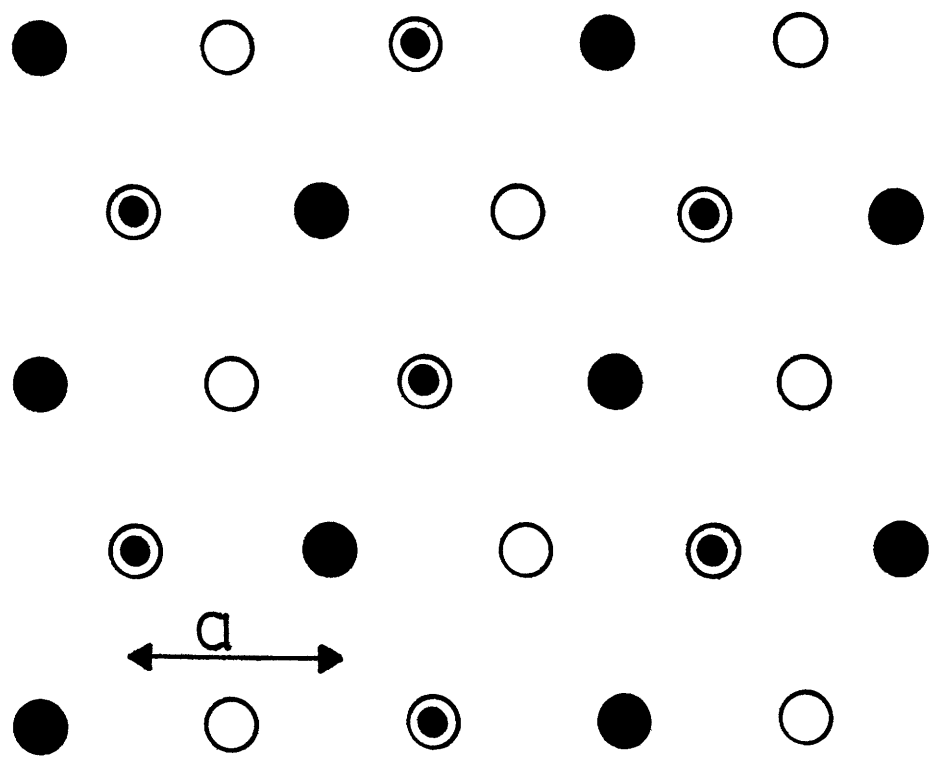
The Mössbauer spectra for ϵ -nitride of 25 at. % nitrogen indicate that as the annealing temperature decreases, the relative fraction of the Fe_{II} sites increases at the expense of the Fe_{I} and Fe_{III} . As there exists an equal number of iron atoms and interstitial sites at 25 at. % nitrogen, one-third of the interstices are occupied and two-thirds are vacant. Hendricks and Kosting³ have proposed an arrangement of nitrogen atoms for this composition such that each iron atom has two nitrogen neighbors (Figure(IV. 8)). The weak X-ray superlattice reflections reported by Jack⁶ were interpreted as being evidence for this configuration.


The progression of Mössbauer spectra indicates that as the annealing temperature is decreased toward 550°C, this type of arrangement is being approached. Complete order is not achieved,


Figure IV.7 Curie Temperature of ϵ -Nitride as a Function of Nitrogen Content



- BRIDELLE⁷
- TAKAKI⁹
- CHABANEL¹⁰
- - - THIS STUDY



 OCCUPIED IN LAYER AT HEIGHT $1/4$

 OCCUPIED IN LAYER AT HEIGHT $3/4$

 UNOCCUPIED IN LAYERS AT HEIGHTS $1/4, 3/4$

however, and phase separation to γ' and ϵ of greater than 25 at. % nitrogen occurs during annealing at temperatures below 550°C.

Additional evidence for the ordering of nitrogen atoms in the interstitial sites is the sharpening of the peaks of the Mössbauer spectra as the annealing temperature is decreased. Since the magnitude of the effect of an interstitial atom on an iron atom falls dramatically with distance, the number of nitrogen atoms in adjacent interstitial sites is the principal determinant of the hyperfine parameters of the iron. However, nitrogen atoms at greater distances can cause perturbations. The excessive breadth of the Mössbauer peaks would be due to iron atoms of a given first-neighbor type having a variety of configurations of nitrogen atoms at second- and greater-neighbor distances. The sharpening of the Fe_{II} spectrum coupled with its increasing intensity as the annealing temperature is decreased indicates that iron atoms are gaining more uniform nitrogen coordination at all near-neighbor distances.

IV. 5 Conclusions

The hexagonal-close-packed ϵ -iron nitride may be completely retained for nitrogen contents as low as 17 at. % by rapid quenching from 700°C. The Curie temperature of this phase is a maximum of 294°C at approximately 24 at. % nitrogen, and decreases

sharply as the nitrogen content is either decreased or increased from this value.

Alloys in the range of 17 at.% nitrogen, which initially are paramagnetic at room temperature, are partially ferromagnetic at room temperature after quenching below their Curie points to -193°C . This phenomena, and any structural changes which may accompany it, remain unexplained.

ϵ -nitride undergoes an ordering of nitrogen atoms on the interstitial sites at 25 at.% nitrogen, with the degree of ordering being a function of temperature. However, a perfectly ordered, Fe_3N structure has not been achieved, due to intervening phase transformations.

References

1. G. Hagg: X-Ray Studies of the Nitrides of Iron, *Nature*, 1928, vol. 121, p. 826.
2. A. Osawa and S. Iwaizomi: X-Ray Investigation of Iron and Nitrogen Alloys, *Z. Kryst*, 1930, vol. 69, p. 26.
3. S. B. Hendricks and P. Kosting: The Crystal Structure of Fe_2P , Fe_2N , Fe_3N , and FeB , *Z. Kryst*, 1930, vol. 74, p. 511.
4. O. Eisenhut and E. Kaupp: Das System Eisen-Stickstoff, *Z. Electrochem*, 1930, vol. 36, p. 392.
5. V. G. Paranjpe, M. Cohen, M. B. Bever, and C. Floe: The Iron Nitrogen System, *Trans. A.I.M.E.*, 1950, vol. 188, p. 261.
6. K. H. Jack: The Iron-Nitrogen System: The Crystal Structures of ϵ -Phase Iron Nitrides, *Acta Cryst.*, 1952, vol. 5, p. 404.
7. R. Bridelle: Sur les Nitrures et Carbonitrures de Fer, *Ann. Chimie (Paris)*, 1955, ser. 12, vol. 10, p. 824.
8. K. H. Eickel and W. Pitsch: Magnetic Properties of the Hexagonal Iron-Nitride ϵ - $\text{Fe}_{3.2}\text{N}$, *Phys. Stat. Sol.*, 1970, vol. 39, p. 121.
9. M. Mekata, H. Yoshimura and H. Takaki: Magnetic Study on Hexagonal Nitrides of 3d Transition Metals, *J. Phys. Soc. Japan*, 1972, vol. 33, p. 62.
10. M. Chabanel, C. Janot and J. Motto: Etude par effet Mossbauer des Nitrures de fer ϵ et ξ au voisinage de la composition Fe_2N , *C. R. Acad. Sc. Paris (B)*, 1968, vol. 266, p. 419.
11. G. Shirane, W. J. Takei and S. L. Ruby: Mossbauer Study of Hyperfine Fields and Isomer Shifts in Fe_4N and $(\text{Fe,Ni})_4\text{N}$, *Phys. Rev.*, 1962, vol. 126, p. 49.

12. N. Elliot: X-Ray Scattering Factor of N in Fe_4N , Phys. Rev., 1963, vol. 129, p. 1120.
13. S. Nagakura: Electronic Structure of Iron Nitrides Studied by Electron Diffraction, I. Fe_4N , J. Phys. Soc. Japan, 1968, vol. 25, p. 488.
14. S. Nagakura and K. Tanehashi: Electronic Structure of Iron Nitrides studied by Electron Diffraction. II. $\epsilon\text{-Fe}_2\text{N}$, and $\xi\text{-Fe}_2\text{N}$, J. Phys. Soc. Japan, 1968, vol. 25, p. 840.
15. E. Lehrer: Uber das Eisen-Wasserstoff-Ammoniak-Gleichgewicht, Z. Electrochem, 1930, vol. 36, p. 383.
16. J. Cosgrove and R. Collins: Mossbauer Velocity Calibration via Interferometry, Nuc. Inst. Meth., 1971, vol. 95, p. 269.
17. N. DeCristofaro and R. Kaplow: Interstitial Atom Configurations in Iron-Carbon and Iron-Nitrogen Solid Solutions, Chapter II of this thesis.
18. S. Hanna and R. S. Preston: Mossbauer Cross Section of Fe^{57} in Iron, Phys. Rev., 1965, vol. 139, 3A, p. 722.
19. S. S. Hanna, R. S. Preston and J. Heberle: The Mossbauer Effect in Metallic Iron, Phys. Rev., 1962, vol. 128, p. 2207.
20. M. Ron, H. Shechter and S. Niedzwiedz: Precipitation of Iron Carbides in Tempered Martensite, J. App. Phys., 1968, vol. 39, p. 265.

V. LOSS OF LATTICE RIGIDITY IN AUSTENITE

ABSTRACT

Mössbauer spectra were taken at and below room temperature of an iron - 2.4 wt. % nitrogen sample containing various amounts of martensite and austenite. The intensities of the martensite spectra increased with decreasing temperature as expected from the normal thermal variation of the recoilless fraction. Conversely, the intensities of the austenite spectra are smaller below room temperature corresponding to a decrease in the recoilless fraction. This is associated with a lessening of lattice resistance to excitations caused by transference of the gamma-ray recoil momentum and is thought to be related to the instability of the austenite phase.

V.1 Introduction

The fact that increasing atomic vibrations may lead to structural instabilities in a crystalline lattice during heating has long been recognized. Lindemann, in 1910, sensing that melting is determined by the vibrational amplitudes of atoms, showed that an essentially constant relationship exists between the melting point of an element, its atomic weight, its lattice parameter(s), and its characteristic vibrational frequency.¹ More recently, it has been shown that Lindemann's empirical relationship is determined by a detailed balance between the vibrational amplitudes and the size of the "passageway" available for diffusion.²

The potential instability of certain lattices with respect to interatomic displacements, on cooling, has also been recognized.

In 1948, Zener³ pointed out that the body-centered-cubic lattice is inherently unstable with respect to (110) $[\bar{1}10]$ shear if only central interatomic forces are present. Without any detailed discussion of the nature of the interatomic bonding, or of the variation with temperature of the type of bonding, he relied on the entropy dependence of the free energy to argue that a real body-centered-cubic crystal is likely to become less stable as it is cooled. More recently, the concept that various crystal lattices become structurally unstable on cooling has assumed an important role in models for martensitic or displacive transformations.

In that context, a number of anomalous effects occurring in the parent (austenite) phase at temperatures above M_s have been reported. Referred to as "premartensitic" phenomena, these include diffuse diffraction effects with X-rays and electrons,^{4,5} resistivity effects,^{6,7} and a softening of elastic constants.⁸ Mössbauer studies of three alloy systems demonstrating a martensitic transformation (Fe - 27 at.% Ni,⁹ Fe-25 at.% Ni,¹⁰ and Co - 7 wt.% Fe¹¹) all show an anomalous decrease in the recoilless fraction of the parent phase as the temperature is lowered to M_s . It has also been argued that the abnormal behavior continues to exist in the retained austenite below the temperature at which the martensitic transformation starts.¹²

The effects are undoubtedly associated with the transformation, on cooling, of austenite to martensite.^{4,13,14,15,16} In some instances, it has been suggested that they are directly related to particular models for martensite formation involving inhomogeneously distributed "embryos". In this context, it should be mentioned that "embryo" models exist which are based on (a) spatially localized, "soft" vibrational modes,¹⁷ (b) static atomic displacement waves,¹⁸ and (c) particular configurations of defects (e.g., dislocations).¹⁹

V.2 Experimental Procedure

A sample of iron 2.4 wt. % nitrogen (8.9 at. %) austenite (M_s approximately 260°K)²⁰ was produced by nitriding an iron foil (0.001 inch thick) in flowing mixtures of NH_3 and H_2 at 700°C and rapidly quenching directly from the nitriding atmosphere.

Mössbauer spectra were measured on a constant acceleration spectrometer with a gamma-ray source of Co^{57} embedded in a copper matrix. The austenite absorber was mounted in a low-temperature dewar on this spectrometer so that its temperature could be controlled in situ, without disturbing the source-sample-detector geometry.

The recoilless fraction which determines the absolute magnitude of the relevant spectra is related to a recoil energy, R ,

that would be transferred to a single free and motionless atom when its nucleus absorbs a gamma-ray, and to the effective, quantized energy increment for available lattice excitations, E^* , in the form:²¹

$$f_T = \exp(-R/E^*) \quad (V.1)$$

For the vibrational excitation of a Debye solid;

$$E^* = (1/6) k_B \theta_D \left\{ 1/4 + (T/\theta_D)^2 \int_0^{\theta_D/T} \frac{x dx}{e^x - 1} \right\} \quad (V.2)$$

where k_B is Boltzmann's constant, θ_D the Debye characteristic temperature, and T the temperature in degrees Kelvin. At low temperatures, E^* becomes $(2/3)k_B \theta_D$. The high-temperature approximation of Equation (V.2) is $k_B \theta_D^2 / 6T$. For vibrational excitations, the recoilless fraction can also be expressed in terms of atomic displacement:

$$f_T = \exp(-\bar{x}^2 k^2) \quad (V.3)$$

where \bar{x}^2 is the mean square amplitude of displacement resolved along the direction of gamma-ray propagation, and k is the gamma-ray wave number, $2\pi/\lambda$. On the basis of ordinary temperature-dependent vibrational behavior, the recoilless fraction should increase with decreasing temperature.

The effective Debye temperatures for the iron atoms are not known precisely in either the martensite or austenite phases.

The value of $\theta_D \sim 411^\circ \text{K}$, taken as an average and from interpolation and extrapolation of various data^{22,23} seems appropriate for both phases, and is... in any case... accurate enough for our purpose. The temperature dependence of the recoilless fraction, expressed in terms of f_T/f_{295} predicted by Equation (V.1) and (V.2) is illustrated as the solid curve in Figure (V.1).

The theoretical intensity of a Mössbauer absorption peak, $P_{th}(E_s)$, is related to the recoilless fraction, f_T , through the convolution:²⁴

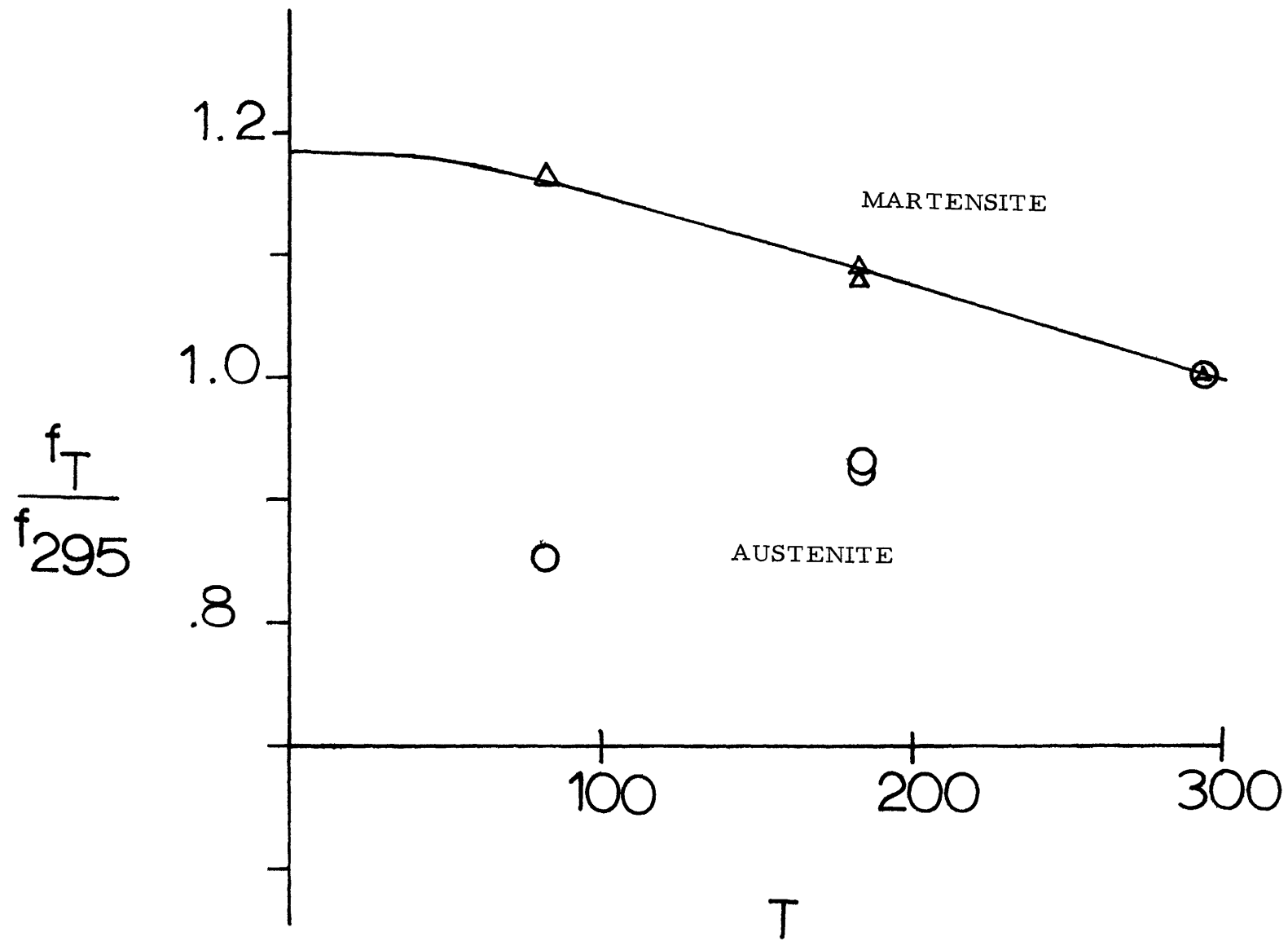
$$P_{th}(E_s) = \int_{-\infty}^{\infty} I(E, E_s) [1 - \exp(-f_T n \sigma(E))] \quad (\text{V.4})$$

where $I(E, E_s)$ is the nominally Lorentzian energy distribution of the gamma-ray source, n is the effective thickness of the absorber in nuclei per cm^2 , and $\sigma(E)$ is the cross section for resonant absorption. In practice, the proper absorption intensities and shapes, $P(E_s)$ are obtained through the convolution:

$$P(E_s) = \int P_{th}(E_s) \cdot G \quad (\text{V.5})$$

where G is a Gaussian curve which compensates for instrumental broadening.²⁵ Thus, since the nuclear parameters are constant, the temperature variation of the magnitude of resonant absorption is dependent only on f_T , if the n associated with each type of atom environment is constant also.

Figure V.1 The Temperature Dependence of the Recoilless Fraction, as Calculated by the Debye Theory and Measured by Experiment.

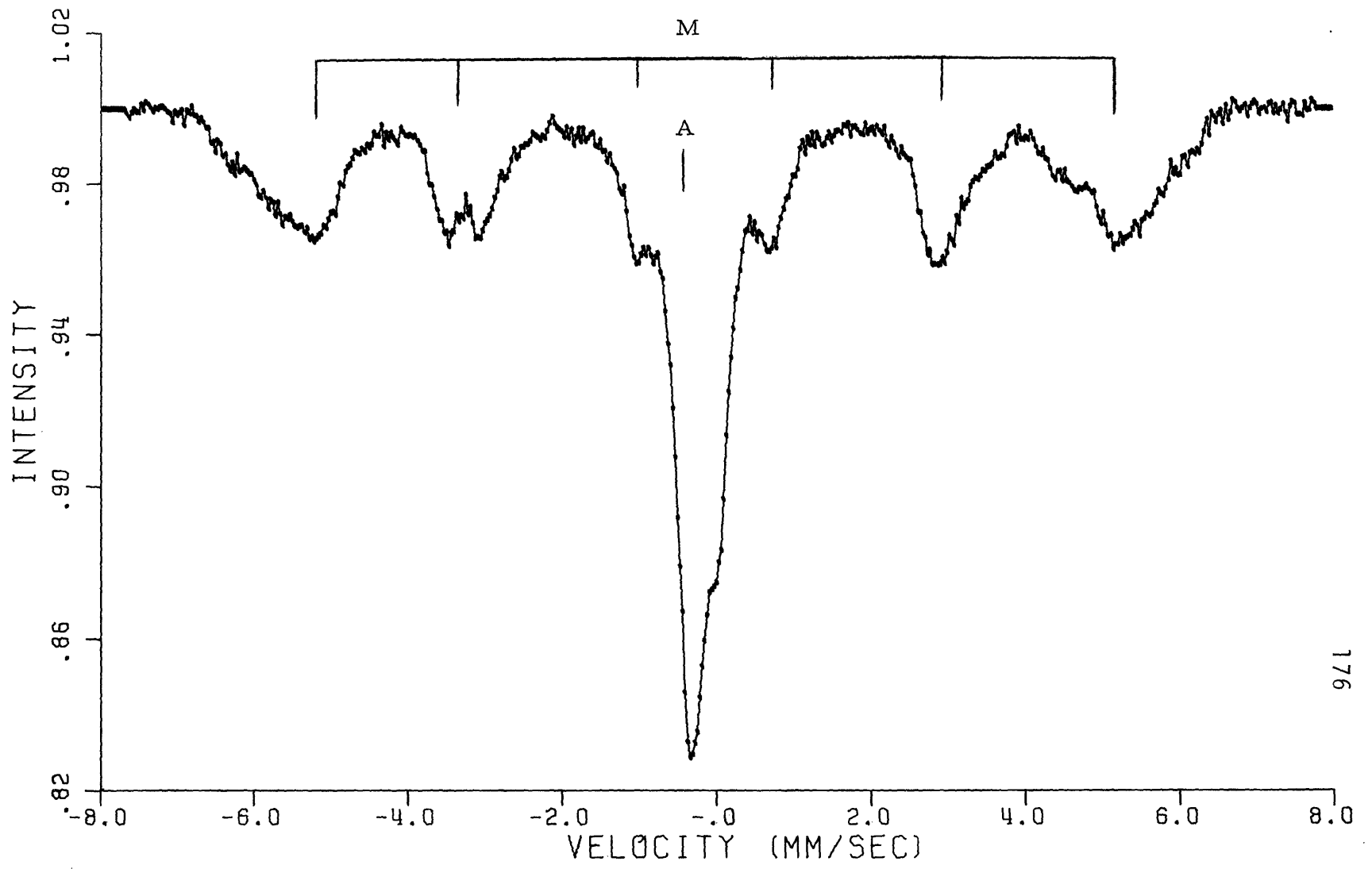


When the argument of the exponential term in Equation (V.4) is small, the depth of the Mössbauer peaks, $P(E)$, may be approximated as being directly proportional to f_T . As each of the different iron atom environments in the complex, aged martensite structure contributes a distinct ferromagnetically-split spectrum,²⁵ the term $n \sigma(E)$ for each individual peak in the martensite spectrum is small and relative values of f_T may be calculated directly from the peak intensities. For the austenite spectrum, where the exponent is larger, the more rigorous nonlinear treatment of Equations (V.4) and (V.5) must be applied.

V.3 Experimental Results

Prior to the first series of Mössbauer measurements reported here, the austenitic sample was cycled a number of times between room temperature (295°K) and 183°K. The total time spent at 183°K exceeded 24 hours and the total time at room temperature following the first quench exceeded one week. This process served to ensure that the martensite formed was stabilized both in amount and with respect to room temperature aging for this temperature range. The Mössbauer spectrum recorded at room temperature following this thermal treatment, illustrated in Figure (V.2) indicates the presence

Figure V.2 The Mössbauer Spectrum of Fe - 2.4 wt.%N
Martensite (M) and Austenite (A).



of approximately 40% martensite (the complex, ferromagnetically-split spectrum labeled M), and 60% austenite, the spectrum in the center of the pattern, labeled A. Upon recooling the sample to 183°K, and measuring the spectrum at this temperature, the martensite peaks increase in intensity by the amount expected from the thermal increase in the recoilless fraction. The austenite peak, however, shows a decrease in intensity, corresponding to a decrease in f of approximately 9%. On the return to room temperature, the intensities revert to their original values. The data given in Table (V.1) illustrates the relative changes in f_T (and the analogous values for \bar{x}^2 as calculated from Equation (V.3)) for both phases. (This data is also reported in Appendix E.)

The sample was then quenched to 82°K and cycled between this temperature and room temperature in a manner similar to that described above. Following this treatment, another series of Mössbauer spectra were recorded. The first spectrum measured at room temperature indicated that an additional 15% of the sample had transformed to martensite during the additional cooling from 183° to 82°K, i. e., that the sample was now approximately 55% martensite. Mössbauer spectra were then recorded at 183°K, 82°K and at room temperature again. The recoilless fraction of the martensite

Table V.1 The Relative Recoilless Fractions and Mean-Square Amplitudes of Displacement for Austenite and Martensite as Estimated from Theory and Determined by Experiment.

A. Stabilized at 183°K, 40% Martensite

		<u>Debye Vibrational Theory</u>	<u>Martensite Experiment</u>	<u>Austenite Experiment</u>
T=183°K	f_T/f_{295}	1.0867	1.08	0.92
	$\overline{x^2} (A^2)$	0.00333	0.0035	0.0066

B. Stabilized at 82°K, 55% Martensite

		<u>Debye Vibrational Theory</u>	<u>Martensite Experiment</u>	<u>Austenite Experiment</u>
T=82°K	f_T/f_{295}	1.1577	1.16	0.85
	$\overline{x^2} (A^2)$	0.00207	0.0020	0.0082
T=183°K	f_T/f_{295}	1.0867	1.09	0.93
	$\overline{x^2} (A^2)$	0.00333	0.0033	0.0064

was observed to increase with decreasing temperature in the manner expected from ordinary thermal vibrations while the austenite shows a continuous decrease in f_T with decreasing temperature. Again, the Mössbauer peak intensities return to their original values when the sample is returned to room temperature. Table (V.1) also gives the f data from the Mössbauer measurements at these three temperatures.

The relative recoilless fraction measured at 82°K , 183°K and room temperature are compared to the theoretical values in Figure (V.1). An important aspect of those results is the fact that the f value for austenite at 183°K is the same (within precision) of the value obtained after the first series of treatments. Thus, the value is an intrinsic property of the temperature of the austenite and not of the immediate likelihood of martensite transformation. That sample will not form any more martensite until it is cooled more than 100°K lower.

V.4 Discussion

From these results, we can rule out the following uncertainties which might ordinarily beset such an experiment:

1. erroneously low intensities measured at low temperature (because the intensity of the spectrum of the

- martensite phase in the same sample increases);
2. additional irreversible conversion of austenite to martensite during the last cooling to low temperature (because the intensities revert to their original values when the sample is returned to room temperature);
 3. reversible conversion of austenite to martensite (because the actual increase in the intensity of the martensite spectrum is just what is expected from decreased thermal vibrations alone); and
 4. instability in the detection electronics (because of the reproducibility of values on the specimen and on standard samples).

Thus, we believe the anomalous decrease in f for the austenitic phase on cooling from room temperature to be a valid and quantitatively meaningful result.

The reduced value of the recoilless fraction in the austenite at low temperature implies an increase in the probability that a gamma-ray will create a lattice excitation, i. e., that it will be absorbed in a non-recoilless manner. This increasing probability reflects a lessening of lattice resistance to excitation.

The energy available from the gamma-ray to create an excitation is, at most, the free atom recoil energy, R . R is determined by the gamma-ray energy and the atomic mass of the atom, and equals 3.1348×10^{-15} joules (1.9567×10^{-3} eV) for the Mössbauer transition in Fe^{57} .²⁶ This value is an order of magnitude less than thermal energy at room temperature.

Since at temperatures below M_s there is a driving energy for the transformation of austenite to martensite which increases with decreasing temperature, such lattice excitations formed in the austenite structure might be related to the martensitic transformation. Without distinguishing between excitations in the form of static distortions or vibrational displacements (such as of soft normal modes) one can conceive of an excitation causing a localized change in the atomic configuration toward the martensitic structure. The behavior of the recoilless fraction of the austenite with decreasing temperature is consistent with such a proposition. The essential independence of the recoilless fraction of the austenite from both the amount of martensite already formed and the immediate tendency to form more martensite indicate that it is at least primarily an intrinsic property of the austenite. This does not necessarily mean that prior treatment (e.g., the formation of the additional amount of martensite at 82°K)

does not change the excitation probability at all, but only that such effects (e. g., as may be due to back-strains, etc.) are small in comparison to the intrinsic effect.

The temperature variation of f_T and its relationship to special localized excitations, may be interpreted in a number of ways. For example, if the localized excitations are normal vibrational modes enhanced by a lessening of certain elastic constants, a decreasing f_T would imply a decrease in the vibrational characteristic energy required to create the excitation (e. g., the Debye excitation energy given in Equation (V.2)). If the excitations are different from the normal modes and independent of them, the probability of a recoilless event would take the form:

$$f_T = f_N f_S$$

where f_T is the measured recoilless fraction at temperature T , f_N is the probability that the gamma-ray absorption will not create a normal thermal excitation, and f_S is the probability it will not create a special excitation. Since we do not have absolute values for f_T , but only values relative to 295°K , it is necessary to make certain assumptions in order to proceed further with the latter concept. For this purpose, we assume that $f_S = 1$ at 295°K and f_N is the Debye value at all temperatures. Then, the temperature variation of f_S

and E_s^* can be estimated (where E_s^* is the characteristic energy associated with the special excitation.) These values are given in Table (V.2). Although the value E_s^* decreases with temperature, the probability of such excitations existing through thermal effects, estimated through the Boltzman factor, $\exp(-E_s^*/kT)$, does not increase, since the thermal energy, kT , decreases more rapidly.

If we were to assume that the austenite tendency toward instability onsets well above M_s - say at $T = 320^\circ\text{K}$ - then the data indicates that the absolute values of the f_T 's would be slightly lower. This alternate assumption has only minor effects on the derived values, given in Table (V.3).

The anomalous decrease in f_T , which amounts to 27% at 82°K , is too large to be explained in terms of localized instabilities at small metastable regions ("embryos") which are postulated to serve as nucleation centers for martensite. An upper bound for the density of "embryos" has been estimated to be 10^7 per cm^3 , with each one including the order of 10^6 atoms.²⁷ With approximately 8.5×10^{22} atoms per cm^3 in the bulk "embryos" would comprise only 10^{-10} of the material. Even if the "embryo" estimates are small by orders of magnitude and even if all atoms in an "embryo" behave as if $f_T = 0$,

TABLE V.2 Estimated Values of f_s and E_s^* , based on $f_s=1.0$ at 295°K .

<u>T °K</u>	<u>f_T</u>	<u>f_D</u>	<u>f_s</u>	<u>$E_s^*(\text{joules})$</u>	<u>$\exp(-E_s^*/kT)$</u>
295	0.7784	0.7784	1.0		0.0
183	0.7200	0.8459	0.8512	1.945×10^{-14}	0.4630
82	0.6612	0.9012	0.7341	1.014×10^{-14}	0.4085

TABLE V.3 Estimated Values of f_s and E_s^* , based on $f_s=1.0$ at 320°K .

T $^\circ\text{K}$	f_T	f_D	f_s	E_s^* (joules)	$\exp(-E_s^*/kT)$
295	0.7473	0.7784	0.9600	$7.679 \cdot 10^{-14}$	0.1571
183	0.6912	0.8459	0.8171	$1.552 \cdot 10^{-14}$	0.5410
82	0.6351	0.9012	0.7047	$0.896 \cdot 10^{-14}$	0.4535

they could not in themselves cause the observed behavior. Thus, the loss of lattice rigidity in the austenite must be a bulk effect, reflecting the overall mechanical instability of this phase at low temperatures.

V.5 Summary

The anomalously decreasing recoilless fraction of the austenite with decreasing temperature below ambient is associated with localized lattice instabilities of this phase possibly related to its transformation to martensite. The magnitude of the effect indicates that, although the excitations themselves may be localized, these instabilities are characteristic of the bulk material and cannot be explained in terms of the conventional theory of pre-existing martensitic embryos.

References

1. F. A. Lindemann: *Über die Berechnung Molekularer Eigenfrequenzen*, *Phys. Zs.*, 1910, vol. 11, p. 609.
2. R. Kaplow, B. L. Averbach and S. L. Strong: *Pair Correlations in Solid Lead near the Melting Temperature*, *J. Phys. Chem. Solids*, 1964, vol. 25, p. 1195.
3. C. Zener: *Elasticity and Anelasticity of Metals*, p. 36, University of Chicago Press, Chicago.
4. G. D. Sandrock, A. J. Perkins and R. F. Hehemann: *The Premartensitic Instability in Near-Equiatomic TiNi*, *Met. Trans.*, 1971, vol. 2, p. 2769.
5. K. Chandra and G. R. Purdy: *Observations of Thin Crystals of TiNi in Premartensitic States*, *J. App. Phys.*, 1968, vol. 39, p. 2176.
6. C. M. Wayman, I. Cornelis and K. Shimizu: *Transformation Behavior and the Shape Memory in Thermally Cycled TiNi*, *Scripta Met.*, 1972, vol. 6, p. 115.
7. J. E. Hanlon, S. R. Butler and R. J. Wasilewski: *Effect of Martensitic Transformation on the Electrical and Magnetic Properties of NiTi*, *Trans. A.I.M.E.*, 1967, vol. 239, p. 1323.
8. S. Zirinski: *The Temperature Dependence of the Elastic Constants of Gold-Cadmium Alloys*, *Acta Met.*, 1956, vol. 4, p. 1323.
9. Ye.Ye Yurchikov and A. Z. Men'shikov: *Mossbauer Study of the State of Austenite Before the Martensitic Transformation*, *Phys. Metal. Metallog.*, 1971, vol. 32, no. 1, p. 169.
10. Ye.Ye Yurchikov, A. Z. Men'shikov and V. A. Tzurin: *Mossbauer Study of $\zeta \rightarrow \alpha$ transitions in Fe-Ni Alloys*, *Proceedings of the Conference on the Application of the Mossbauer Effect (Tihany, 1969)*, p. 413.

11. B. S. Bokshtein, Yu. B. Voitkovskii, G. S. Nikol'skii and I. M. Razumovskii: Study of the Debye-Waller Factor near the Temperature of a Phase Transition of the First Kind in Cobalt, *Sov. Phys. JETP*, 1973, vol. 37, p. 283.
12. I. Cornelis, R. Oshima, H. C. Tong and C. M. Wayman: Direct Observations of Pretransformation Lattice Instabilities, *Scripta Met.*, 1974, vol. 8, p. 133.
13. R. F. Hehemann and G. D. Sandrock: Relations Between the Premartensitic Instability and the Martensite Structure in TiNi, *Scripta Met.*, 1971, vol. 5, p. 801.
14. L. Delaey, J. Van Paemel and T. Struyve: The Relations Between the Premartensitic Instability of the β -Phase and the Martensite Structures and the Shape Memory Effect in the Noble Metal Base Alloys, *Scripta Met.*, 1972, vol. 6, p. 507.
15. J. Perkins: Lattice Transformations Related to Unique Mechanical Effects, *Met. Trans.*, 1973, vol. 4, p. 2709.
16. J. Perkins: Strain Triggering of Shear Transformations by the Stress Field of Unstable Lattice Vibration Modes, *Scripta Met.*, 1974, vol. 8, p. 975.
17. P. Clapp: A localized Soft Mode Theory for Martensitic Transformations, *Phys. Stat. Sol. (b)*, 1973, vol. 57, p. 561.
18. D. deFontaine, N. E. Paton and J. C. Williams: The Omega Phase Transformation in Titanium Alloys as an Example of Displacement Controlled Reactions, *Acta Met.*, 1971, vol. 19, p. 1153.
19. G. B. Olson: A General Mechanism of Martensitic Transformation, Ph.D. Thesis, M.I.T., 1974.
20. T. Bell and W.S. Owen: The Thermodynamics of the Martensite Transformation in Iron-Carbon and Iron-Nitrogen, *Trans. A.I.M.E.*, 1967, vol. 239, p. 1940.

21. V. I. Goldanskii and R. H. Herber: Chemical Applications of Mossbauer Spectroscopy, Academic Press, Inc., New York, 1968.
22. International Tables for X-Ray Crystallography, p. 241, Kynock Press, Birmingham, England, 1965.
23. Y. Tanji: Debye Temperatures and Lattice Deviation in Fe-Ni (fcc) Alloys, J. Phys. Soc. Japan, 1971, vol. 30, p. 133.
24. S. Hanna and R. Preston: Mossbauer Cross Section of Fe⁵⁷ in Iron, Phys. Rev., 1965, vol. 139, 3A, p. 722.
25. N. DeCristofaro and R. Kaplow: Interstitial Atom Configurations in Iron-Carbon and Iron-Nitrogen Solid Solutions, Chapter II of this thesis.
26. A. Muir, K. Ando and H. Coogan: Mossbauer Effect Data Index 1958 - 1965, Interscience, New York, 1966.
27. S. R. Pati and M. Cohen: Nucleation of the Isothermal Martensitic Transformation, Acta Met., 1969, vol. 17, p. 189.

VI. SUMMARY

1. Mössbauer spectroscopy has revealed that carbon atoms in the retained austenite and virgin martensite structures are separated on the octahedral interstitial sublattice such that the presence of a carbon atom in an interstitial site effectively blocks the twelve neighboring octahedral interstitial sites from occupation by other carbon atoms. In contrast, nitrogen atoms in these structures are randomly arranged on the octahedral sites.

Both iron-carbon and iron-nitrogen virgin martensites age at room temperature by a clustering and ordering of interstitial atoms. The interstitial-atom rich regions in carbon-martensite are believed to be of Fe_4C stoichiometry where in nitrogen-martensite the Fe_{16}N_2 structure is formed.

The activation energy associated with the process of clustering and ordering of carbon atoms into Fe_4C regions and the simultaneous creation of carbon-depleted regions is 89,525 joules/mole. This indicates that the process is controlled by the rate of diffusion of carbon atoms through the regions of the martensite which are essentially free of carbon.

2. The hexagonal-close-packed ϵ -nitride may be completely retained at room temperature for nitrogen contents as low as 17 at. %

by rapid quenching from 700°C . The Curie temperature of this phase is a maximum of 294°C at approximately 24 at.%, and decreases sharply as the nitrogen content is either increased or decreased from this value.

Alloys in the range of 17 at.% nitrogen, which initially are paramagnetic at room temperature, are partially ferromagnetic at room temperature after quenching below their Curie points to -193°C . These phenomena, and the details of the accompanying structural changes, remain unexplained.

ϵ -nitride undergoes an ordering of nitrogen atoms on the interstitial sites at 25 at.% nitrogen with the degree of ordering being a function of temperature. However, a perfectly ordered Fe_3N structure, in which each iron atom has two nitrogen neighbors, is not achieved before dissociation occurs at temperatures below 550°C .

3. For an iron - 2.4 wt.% nitrogen alloy (8.9at.%), at temperatures below ambient and below the M_s , the recoilless fraction of the austenite decreases continuously with decreasing temperature. This behavior is associated with the localized lattice instabilities of the austenite related to its transformation to martensite. The magnitude of the effect indicates that although the excitations themselves may be localized, these instabilities are characteristic of the bulk material and cannot be explained in terms of the conventional theory of pre-existing martensitic embryos.

VII. SUGGESTIONS FOR FURTHER WORK

1. The basic understanding of the Mössbauer spectra and atomic arrangements of plain carbon and nitrogen steels should serve as an adequate foundation for the study of ternary alloys. Initially, the iron-carbon -nitrogen system merits investigation as this ternary has received little attention and these two interstitial alloying elements commonly co-exist in commercial steels. The interaction of carbon and nitrogen in the various carbide and nitride structures may assist in the understanding of the iron-interstitial atom bond and of the differences in the behavior of carbon and nitrogen in iron.

The more general category of ternaries involving an interstitial and a substitutional alloying element may now be approached in an analytical sense. Knowledge of the Mössbauer spectra associated with particular iron-interstitial atom configurations should permit evaluation of the substitutional-interstitial atom interactions. However, as ternary phase diagrams are often not available, the fundamental work associated with their construction is required to guide the research. (Some preliminary work on an Fe-Mn-N alloy is reported in Appendix F.)

Fabrication of thin foils (thickness = 0.001 inch) from the base alloys of interstitial-substitutional ternaries for transmission Mössbauer spectroscopy may often be difficult. In this context, a "back-reflection" spectrometer should be assembled for the ternary work. The "back-reflection" technique may also open new avenues of research in surface studies. (The basic components for use of this technique have already been obtained.)

2. Investigation of the hexagonal-close-packed ϵ -nitride remains far from being complete. Direct magnetic measurements of the Curie temperature of this phase as a function of nitrogen content should be made in the range of 17 to 25 at. % nitrogen. For ϵ -nitrides with sub-ambient Curie temperatures, more precise X-ray diffraction data may help to unravel the question of what structural changes accompany the non-reversible magnetic changes which occur when a sample is cooled to below its Curie temperature and then returned to room temperature. Neutron diffraction may also prove to be a helpful experimental tool in determining changes in the configuration of nitrogen atoms on interstitial sites, if any. This technique can also be employed in studying the ordering of Fe_3N alloys.

3. As demonstrated in Section V., Mössbauer spectroscopy should be a valuable tool in the study of premartensitic phenomena and the actual mechanism of the martensitic transformation. This may be extended to all martensitic systems containing iron. A more extensive examination of the temperature variation of the recoilless fraction of the parent phase, both above and below M_s , should be made for the bulk (in transmission mode) and of the surface (in back-reflection mode). Comparison of the two may add still further insights to the dynamic features of martensite formation.

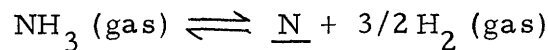
APPENDIX A: ALLOY PREPARATION

A.1 Iron-Carbon

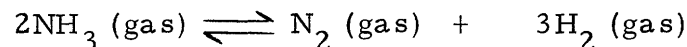
The preparation of a binary iron - 1.86 wt.% carbon alloy and its fabrication into thin flakes (thickness = 0.0005 inch) for transmission Mössbauer spectroscopy have been described by Choo.¹ Virtually fully-austenitic samples of this alloy could be produced by splat-quenching from the melt onto a chilled copper substrate.

A.2 Iron-Nitrogen

Iron-nitrogen specimens were prepared by nitriding pure iron foils (99.9%, thickness = 0.001 inch) in flowing ammonia-hydrogen gas mixtures. The chemical equilibrium involved is:



Hydrogen gas must be present in the nitriding atmosphere to control the following dissociation reaction:

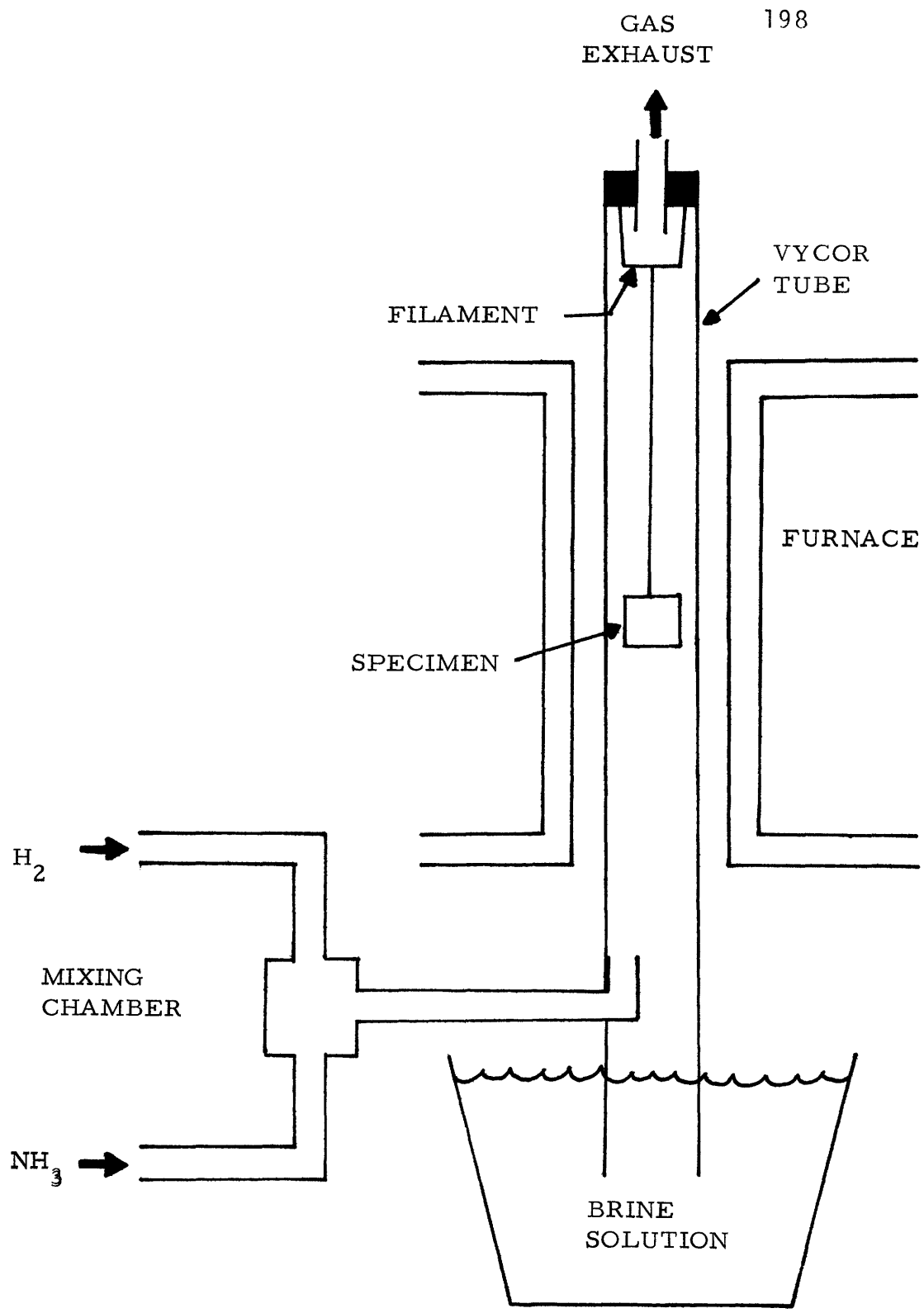


All samples were nitrided for at least one hour at temperatures between 650° and 700°C to permit the foil to reach equilibrium with the nitriding atmosphere. At a given temperature, the nitrogen content of the foil can be controlled by fixing the relative flow rates of the two gases.

The nitriding apparatus is illustrated in Figure (A. 1). The specimen holder and supporting filament were held in a vycor tube which ran through the furnace. Samples could be rapidly quenched directly from the nitriding atmosphere by melting the filament by Joule heating, which would allow the specimen to fall into the brine bath. In this manner, the austenitic phase could be completely retained at room temperature with nitrogen contents between 2.34 and 2.83 wt. % and the hexagonal-close-packed ϵ -nitride could be retained with nitrogen contents as low as 4.92 wt. % (17.1 at. %). At intermediate concentrations, mixtures of the two phases were obtained, as expected from recent versions of the high-temperature portion of the phase diagram.^{1,2}

1. V. G. Paranjpe, M. Cohen, M. B. Bever, and C. Floe: The Iron Nitrogen System, Trans. A.I.M.E., 1950, vol. 188, p. 261.
2. K. H. Jack: The Iron-Nitrogen System: The Crystal Structures of ϵ -Phase Iron Nitride, Acta Cryst., 1952, vol. 5, p. 404.

Figure A.1 The Nitriding Apparatus.



APPENDIX B: THE MOSSBAUER SPECTROMETER

The Mössbauer spectrometer (Figure B.1) consists of four basic interacting components:

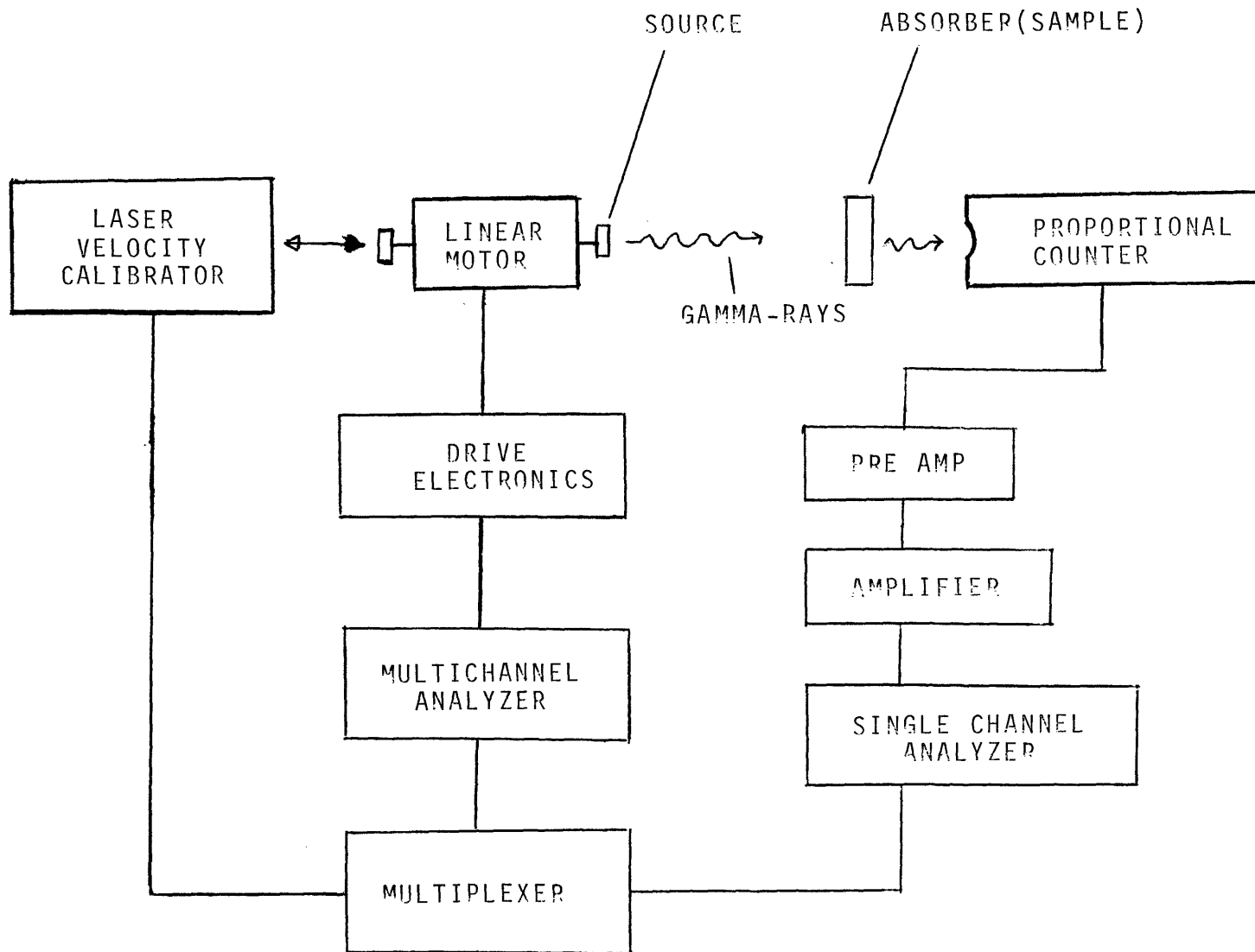
1. gamma-ray source
2. drive unit
3. absorber (the material being studied)
4. recording unit

All experiments were performed with a 25 mc gamma-ray source of radioactive Co^{57} diffused into a copper matrix (prepared by the New England Nuclear Corporation). The linewidth of the outer Mössbauer peaks of a 0.001 inch thick pure iron absorber was measured at 0.294 mm./sec., as compared to the theoretical ideal width for Fe^{57} emission and absorption of 0.194 mm./sec.¹

Sources of the additional broadening include:

1. the thickness of the absorber
2. divergence of the gamma-ray beam
3. finite time interval spent accumulating data in each channel
4. vibrations
5. Fe^{57} environment in the source

Figure B.1 The Mössbauer Spectrometer.



The drive unit consists of a linear motor (Austin Science Associates, ASA, K3), Mossbauer Drive Electronics (ASA, S3), and a Flyback Module (ASA, S4).² This unit provides the gamma-ray source with a constant acceleration motion. The velocity waveform is asymmetric triangular, i. e., a sawtooth. The velocity of the source is swept linearly from a negative maximum to an equal positive value through zero, providing the desired Doppler velocity spectrum (and corresponding energy variation) across the entire channel capacity of the multichannel analyzer (MCA). The velocity then quickly return to the negative maximum - the "flyback" step - with the MCA channel advance halted and the process is repeated.

The recording unit consists of a proportional counter (Reuter Stokes, RSG-61), a high-voltage supply (RIDL 40-9B), a preamplifier (Mech-Tronics, MT-404), an amplifier (Mech-Tronics, MT-500), and a 512 channel multichannel analyzer, (Northern Science NS-900), with a built-in single-channel analyzer. Radiation emitted by the source and transmitted through the absorber is detected by the proportional counter, which yields a charge pulse on receipt of a photon.

The pulses are sized according to the energy of the photon. After amplification, the single-channel analyzer is used to separate the pulses corresponding to the 14.4 Kev 'Mössbauer' gamma-ray from those of the higher and lower energy radiation also emitted in the decay of Co^{57} . The MCA, operating in multiscaling mode, receives the output of the single-channel analyzer. An internal clock activates each of the 512 channels in sequence and the counts as received are stored in the active channel. The velocity of the drive unit is coupled to the scan rate of the MCA such that each channel corresponds to a single, definite velocity.

The velocity calibration, i. e., the conversion from the multichannel analyzer channel number to the corresponding Doppler velocity of the source, was performed by two methods:

1. Measuring peak positions of a pure-iron absorber, and
2. using a laser absolute velocity calibrator (ASA, LC-9).

The velocity calibrator consists of a laser interferometer, a crystal oscillator and a Multiplexer (ASA, MP-9). The interferometer operates by splitting the laser beam and later recombining it. One component travels a fixed path length. The other reflects from a mirror attached to the armature of the Mössbauer linear motor and the resultant path

length includes the linear motion of the motor. The multiplexer interlaces velocity information from the interferometer with the Mossbauer spectrum in the multichannel analyzer memory at periodic intervals. The absolute velocity of the linear motor and, therefore, the gamma-ray source can then be calculated for the channels in which velocity information is stored.³

1. A. Muir, K. Ando and H. Coogan: Mossbauer Effect Data Index 1958 - 1965, Interscience, New York, 1966.
2. R. Collins: Mossbauer Equipment Catalogue, Austin Science Associates, Inc., Austin, Texas 78712.
3. J. Cosgrove, and R. Collins: Mossbauer Velocity Calibration via Interferometry, Nuc. Inst. Meth., 1971, vol. 95, p. 269.

APPENDIX C: ERROR ANALYSIS

C.1 Accuracy of Mössbauer DataC.1.1 Horizontal (Velocity) Scale

The benefits of the addition of a laser to the Mössbauer spectrometer for velocity calibration have been referred to in Chapter I. Essentially, the interferometer permits the accurate calibration of Doppler velocity across the entire spectrum. For most spectra recorded in this thesis, the standard deviation of the velocity is approximately 10% of a single channel width¹ (channel width = 0.031 mm./sec.). As this variance is minor compared to the statistical fluctuations in the radiation intensities (the error is less than the point size in the Mössbauer spectra of Figure (C.1)), it will be ignored.

C.1.2 Vertical (Intensity) Scale

In detecting photons emitted at random intervals of time during radioactive decay, the number of counts, N , recorded in a given time interval is subject to statistical fluctuations. When N is a large number, the standard deviation in the number of counts is²

$$s = \sqrt{N}$$

and the fractional standard deviation is:

$$S = 1 / \sqrt{N}$$

High precision measurements therefore require accumulation of a large

number of counts. The ^{57}Fe Mössbauer spectra reported in this thesis all represent $0.75 \times 10^6 < N < 1.25 \times 10^6$ counts per channel, making $S \sim 0.001$ (or 0.1%).

The quantity being measured in transmission Mössbauer spectroscopy is the magnitude of the absorption peak as a fraction, P , of the gamma-ray beam not absorbed. The fractional error E in the measurement of P may be represented in the form:

$$E = S/P$$

When P is approximately 0.2 at the absorption maximum, as in the spectrum of austenite, E is 0.5%. The relative error increases as you move away from the peak maximum. Small changes in P (e.g., of an absolute magnitude of 0.01) can be measured, but with a percent error of $\sim 10\%$, even with 10^6 radiation counts.

Additional systematic error may also occur in data acquisition, as discussed in Appendix A. Some, such as geometrical effects, were experimentally avoided. Others, which may exist but are neither known nor obvious in the data, are not treated here.

C.2 Analytical Fitting of the ^{57}Fe Mössbauer Spectra

A common method of determining the best fit between a set of experimental data points exhibiting a random distribution of

error and a mathematical model describing those points is least squares analysis. When the model is a linear one, the parameters of the model may be calculated directly. When the model is nonlinear, such an analysis needs to be accomplished by an iterative process.

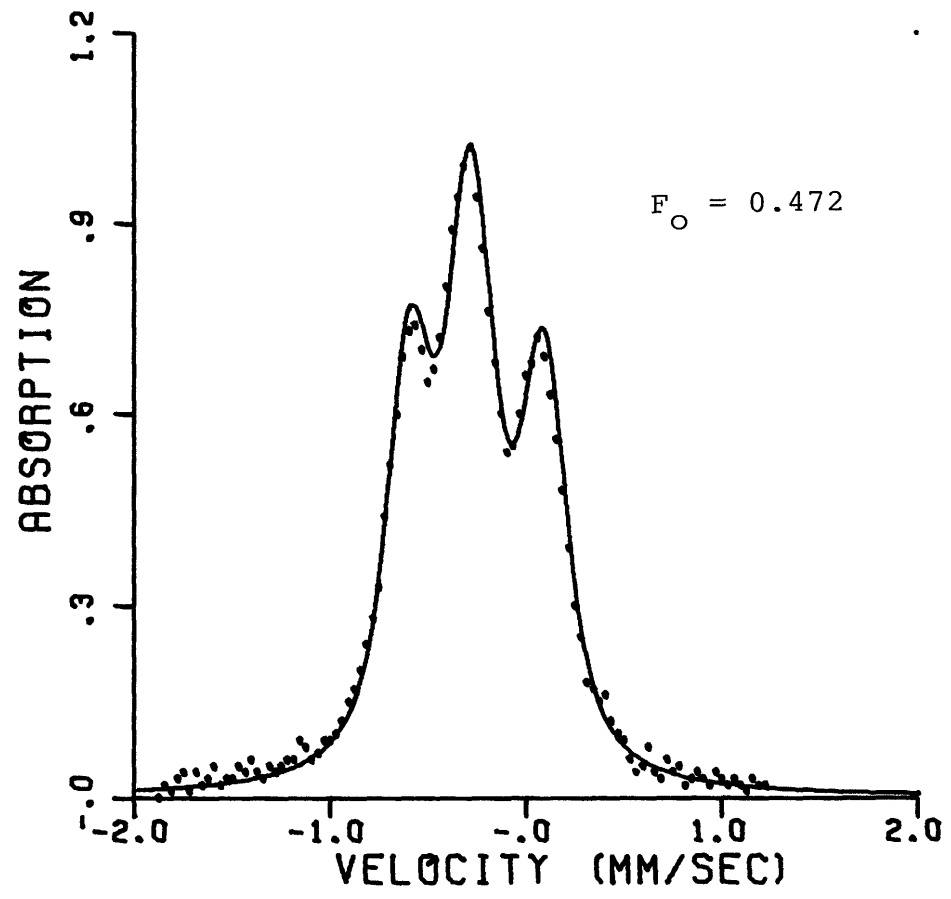
The mathematical Mössbauer model developed in Chapter II is a nonlinear model in that some of the unknown coefficients occur in exponents, and all are within convolutions. At the same time, the large number of unknown parameters makes a pre-programmed, automatic, iterative process cumbersome. The Mössbauer spectrum of a given phase is composed of n individual, superimposed spectra where n is the number of different iron atom environments in the structure. The number of unknown parameters include the fractional weights of each iron-atom type ($n-1$ total), the three hyperfine parameters (for ferromagnetic phases) determining the peak positions of each spectrum ($3n$ total), the intrinsic broadening parameters (due to minor internal diversities within each environment type) and an instrumental broadening parameter, which by comparison with an iron "standard" is a constant across the entire spectrum. Thus, there may be as many as $7n$ unknown parameters.

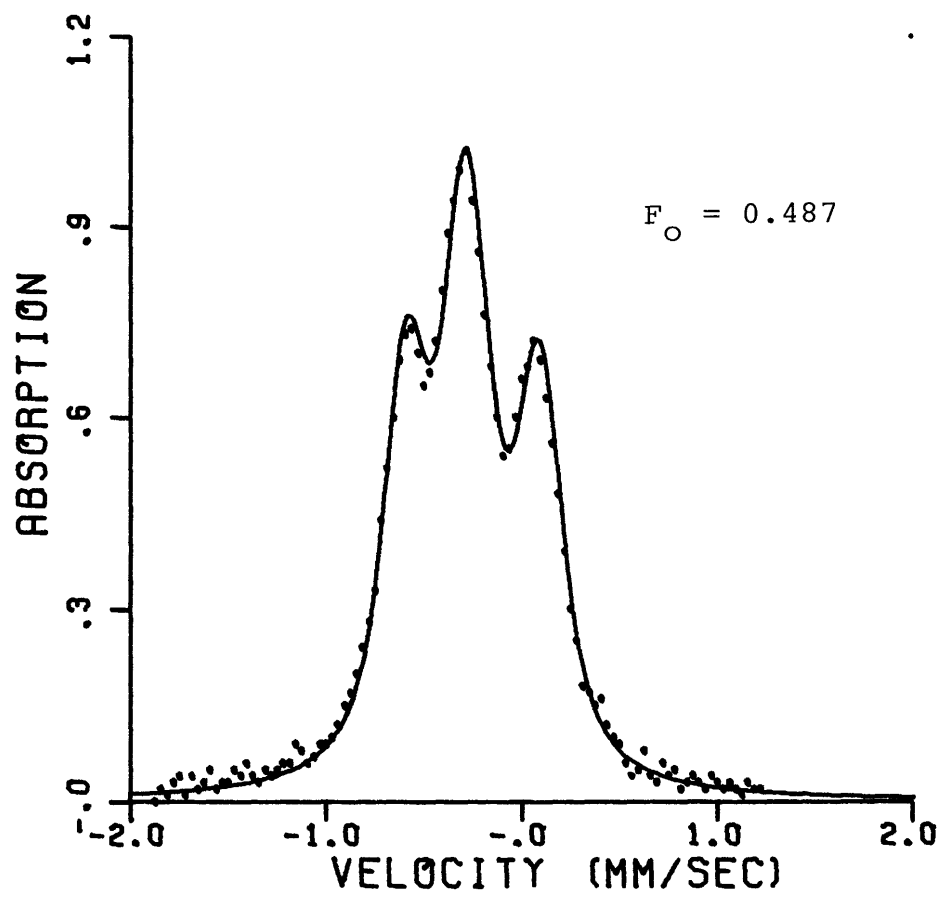
In the present work, an iterative process was used which involved: (a) human (experimenter) intervention in the variation

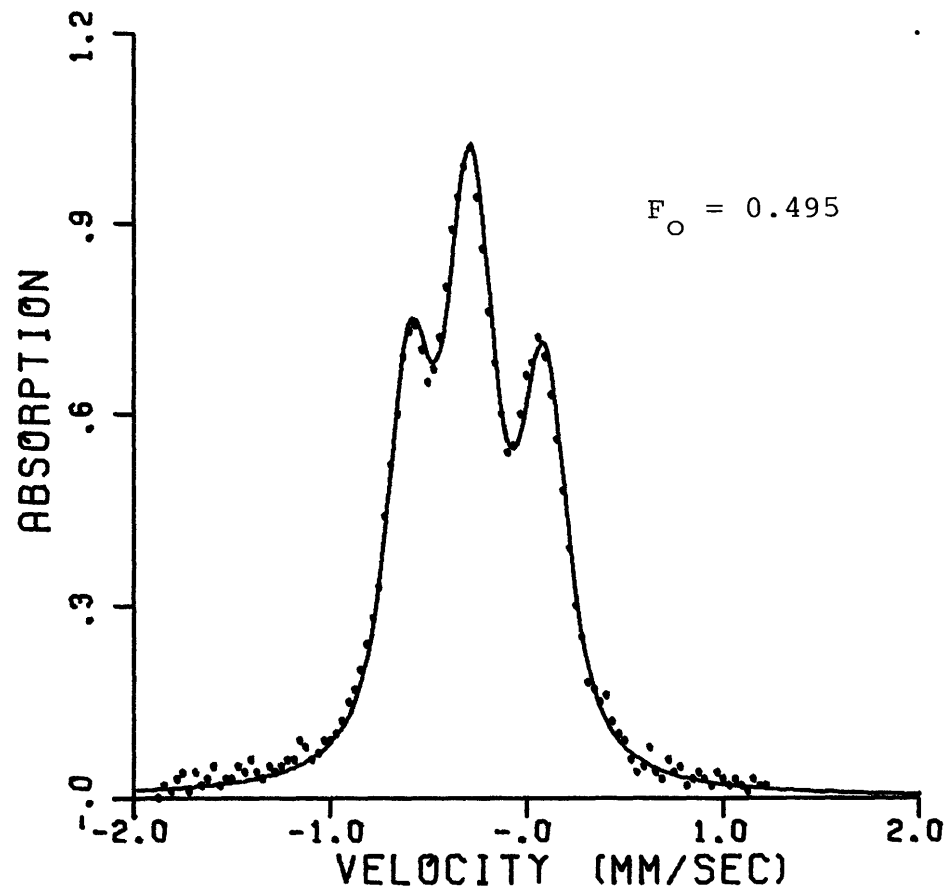
of the parameters, and (b) the determination of the quality of the fit "by eye". This method proved to be efficient in that the variation of the unknown parameters could be constrained to physically meaningful values. Also, human judgments, based on the overall (two dimensional) perception of "misfits" are difficult to automate as simple mathematical rules. "By eye" fitting has many of the attributes of a least squares analysis, as this technique operates with a tendency to fit by avoiding large deviations which would contribute the major amount to the sum of the squares.

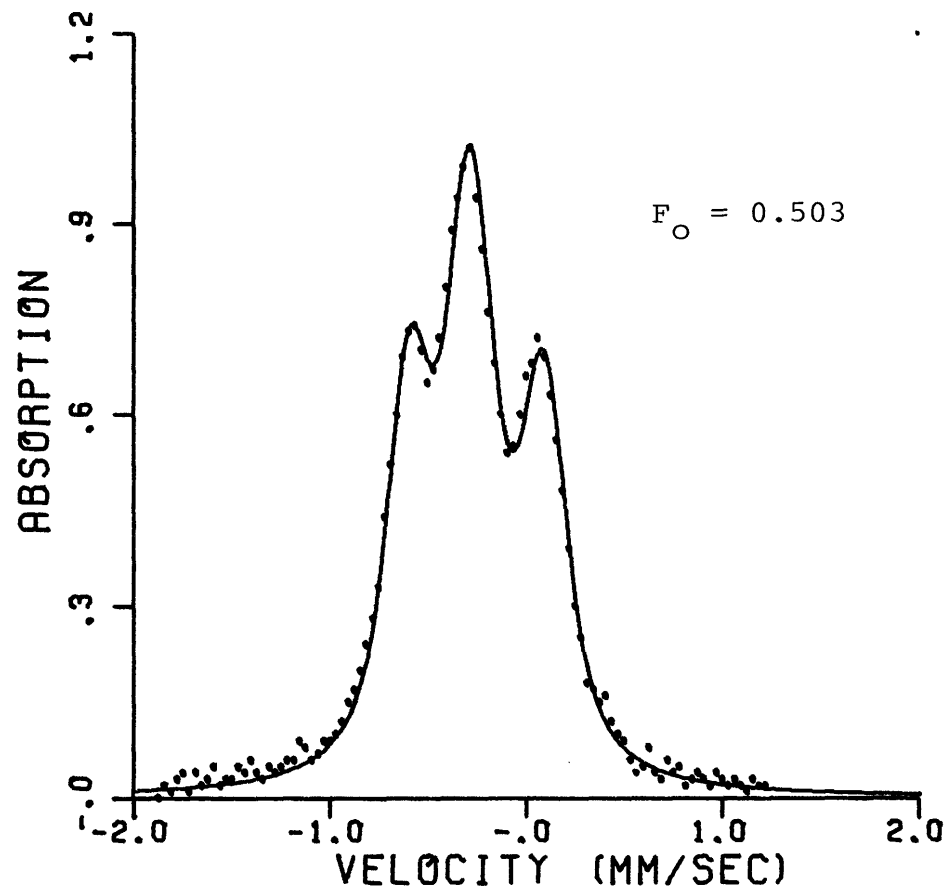
To assist in quantifying the sensitivity of these measures, the case of iron-carbon austenite will be reviewed to determine the sensitivity of the fit to a critical parameter, i. e., to the fractional weights of the two components, once a "best fit" had been determined, the weight of the components were stepped by approximately 10% of the difference between the best fit value and a limiting case, i. e., the value for a random distribution model. In this instance, the best fit value of the central peak weight (F_0) was 0.495 and the limiting case was that calculated for a random distribution of carbon atoms (0.577). The comparisons between model and experimental data for five values near 0.495 are illustrated in Figure (C.1). Values outside the range

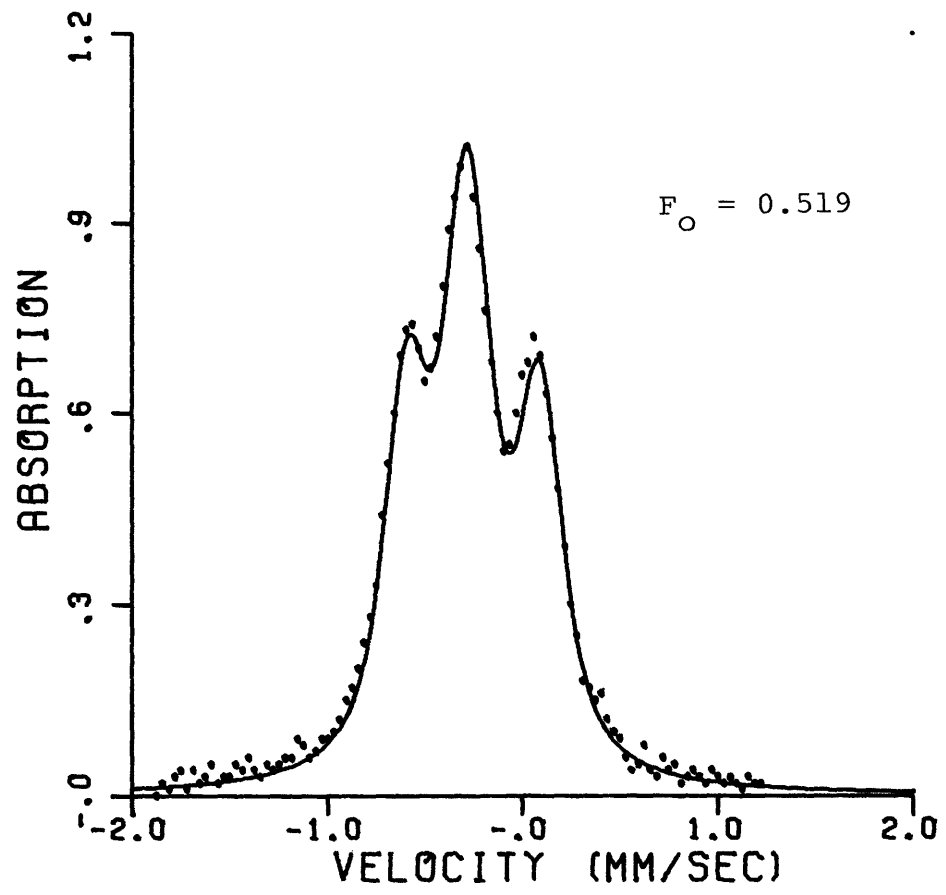
Figure C.1 Comparison Between Model and Experimental
Data for Five Values of F_o near 0.495.











of 0.487 to 0.503 produce clearly unacceptable fits and the uncertainty is, therefore, judged to be of the order of ± 0.008 (which is approximately 10% of the difference between 0.495 and the random distribution value).

C.3 Error in the Determination of the Activation Energy

The technique of choosing the best fit of a straight line of the form:

$$y = a + bx$$

where a is the intercept on the y - axis and b is the slope, to a set of experimental data points (x_n, y_n) is outlined by Beers.² s_y is the standard deviation of y about a line defined by a and b and is estimated as:

$$s_y = \sqrt{\frac{\sum (dy_n)^2}{k-2}}$$

where k is the number of observations and:

$$dy_n = y_n - (a + bx_n)$$

The standard deviations s_a and s_b are given as:

$$s_a = s_y \sqrt{\frac{\sum x_n^2}{k \sum x_n^2 - (\sum x_n)^2}}$$

$$s_b = s_y \sqrt{\frac{k}{k \sum x_n^2 - (\sum x_n)^2}}$$

This analysis of variance was applied to the determination of error in the calculation of the activation energy (Section III. 4), from the horizontal separation of two experimental lines. In this case, the fraction transformed was plotted along the y coordinate and the natural logarithm of the time along the x coordinate. The experimental slopes, intercepts and variances are given in Table (C.1). The horizontal displacement of each line associated with a variation of the y-intercept, s_a , was calculated using the formula:

$$\Delta x_a = s_a / b$$

To calculate the horizontal displacement caused by a variation of the slope, s_b , a reference point in the range where y varies linearly with x must be chosen. The value $y_R = 0.25$ was used as this is the center of the range of y values measured. The horizontal displacement caused by a pivoting of each line about y_R corresponding to a change in slope of s_b is

$$\Delta x_b = \frac{y - y_R}{b} - \frac{y - y_R}{b \pm s_b}$$

An upper bound Δx_b may be calculated using the extreme values within which data exists, $y = 0.14$ and $y = 0.35$. This contribution to the total error turns out to be small compared to the error due to the

TABLE C.1
Slopes, Intercepts and Variances

Analytical Form Assumed:

$$y=a+bx \quad (\text{fraction transformed} = a + b*\ln(\text{time}))$$

<u>Temperature</u>	<u>a</u>	<u>s_a</u>	<u>b</u>	<u>s_b</u>
295°K	-0.08887	0.00679	0.02536	0.000517
323°K	-0.00104	0.00737	0.0245	0.000755

variance in the intercepts.

The statistical estimation of the total error in the horizontal separation of the two lines, due to both slope and intercept uncertainty, was estimated as being:

$$\text{ERROR} = \sqrt{\Delta x_{a_{295}}^2 + \Delta x_{b_{295}}^2 + \Delta x_{a_{323}}^2 + \Delta x_{b_{323}}^2}$$

This corresponds to an estimated error of 12,200 joules per mole in the determination of the activation energy.

According to the kinetic expression used in Chapter III, the two lines should be parallel. The actual, experimental difference between the two slopes is 8.6×10^{-4} . From the standard deviations of each slope, the expected difference, represented as

$\sqrt{(S_b(295))^2 + S_b(323)^2}$ is 9.2×10^{-4} . The closeness of these two values indicates that the estimations of the individual errors are meaningful. However, since the activation energy quoted (89,525 joules per mole) was determined as the average within the experimentally accessible region, we judge the estimated error (12,200 joules per mole) to be a slight overestimate of the uncertainty.

References

1. J. C. Cosgrove and R. C. Collins: Mössbauer Velocity Calibration via Interferometry, *Nuc. Inst. Meth.*, 1971, vol. 95, p. 269.
2. Y. Beers: Theory of Error, Addison-Wesley, Reading, 1953.

APPENDIX D: COMPUTER PROGRAM

```

C*****      MAIN PROGRAM
      DIMENSION F(1025),G(1025),H(1025),V(1025),X(1025),FUNCT(1025),
      ISPECT(1025),P(1025),U(2),S(2),Z(1025),PTS(500),X2(500)
      REAL LAM
      CALL PLOTS (IDUM,IDUM,02)
      NCT=0
      NP=1024
      DO 5 I=1,NP
5 X(I)=I
C*****      NMS = NUMBER OF MOSSBAUER SPECTRA TO BE GENERATED
      READ(5,97) NMS
      DO 11 NW=1,NMS
C*****      SPT GENERATES THE MOSSBAUER ABSORPTION PROFILE
      CALL SPT(X,SPECT,NCT)
C*****      RCS=RESONANT CROSS SECTION X RECOILLESS FRACTION
C*****      T=THICKNESS OF ABSORBER IN 0.001 INCHES
      READ(5,98) RCS,T
C*****      F(I)=EXPONENTIALLY REDUCED LORENTZIAN SUM
      DO 6 I=1,NP
6 F(I)=1.0-EXP(-RCS*T*SPECT(I))
C*****      P(I)=SOURCE SPECTRUM (LORENTZIAN)
C*****      LAM=WIDTH OF LORENTZIAN MOSSBAUER EMISSION EVENT
      LAM=6.0474
      DO 7 I=1,512
7 P(I)=(LAM**2)/(4.*(I-1)**2+LAM**2)
      DO 8 I=513,1024
8 P(I)=(LAM**2)/(4.*(I-1025)**2+LAM**2)
C*****      H IS THE CONVOLUTION OF P AND F
      CALL CONV(F,P,H)
C*****      SET UP GAUSSIAN INST. BROAD.
C*****      G(I)=EXPERIMENTAL BROADENING FUNCTION (GAUSSIAN)
      READ (5,300) SIG
      D=1./(SIG*SQRT(2.*3.14159))
      TSIGS=SIG*SIG*2.
      DO 9 I=1,512
9 G(I)=D*EXP(-(I-1)**2/TSIGS)
      DO 10 I=513,1024
10 G(I)=D*EXP(-(I-1025)**2/TSIGS)
C*****      V IS THE CONVOLUTION OF H AND G
      CALL CONV(H,G,V)
      DO 204 I=1,NP
      FUNCT(I)=V(I)
204 CONTINUE
      D=1.0/FUNCT(282)
      DO 205 I=1,1000
      Z(I)=FUNCT(I)*D
205 CONTINUE

```

```
S(1)=0.0
S(2)=1000.
U(1)=0.0
J(2)=1.25
CALL PICTUR(10.,5.0,'CHANNEL',7,'INTENSITY',9,X,7,1000,0.0,1,
IS,U,-2,0.,0)
11 CONTINUE
95 FORMAT(F10.5)
96 FORMAT(F10.2)
97 FORMAT(I5)
300 FORMAT(F10.3)
98 FORMAT(2F10.5)
207 CALL ENDPLT(0,0,0,0,999)
CALL EXIT
STOP
END
```

```

      SUBROUTINE SPT(V,SPECT,CI)
C*****      SPT GENERATES THE MOSSBAUER ABSORPTION PROFILE
      DIMENSION V(1025),PEAKS(1025),VP(10),N(10),SPECT(1025),
      IG(1025),DIM(1025)
      REAL NJNT,MU,LAM
      NCT=NCT+1
      NP=1024
      DO 105 K=1,NP
      PEAKS(K)=0.0
      SPECT(K)=0.0
105 CONTINUE
C*****      CTR=CENTER OF THE SPECTRUM (VELOCITY=0.0)
      CTR=500.
C*****      LAM=WIDTH OF LORENTZIAN MOSSBAUER ABSORPTION EVENT
      LAM=6.0474
C*****      GGP AND GFX ARE THE GYROMAGNETIC RATIOS OF
C*****      THE GROUND AND EXCITED STATES
      GGP=0.1806
      GFX=-0.102
C*****      CL=SPEED OF LIGHT
C*****      E0=ENERGY OF THE GAMMA RAY (EV)
C*****      MU=NUCLEAR BOHR MAGNETON
      CL=3.E+11
      E0=14370.
      MU=3.15219E-12
      PI=3.14159
C*****      NSPCT=NUMBER OF IRON ATOM ENVIRONMENTS
      READ(5.97) NSPCT
      DO 201 NT=1,NSPCT
C*****      IP=NUMBER OF PEAKS      H=HYPERFINE MAGNETIC FIELD
C*****      EPS=QUADRUPOLE SPLITTING(CHANNELS) DEL=ISOMER SHIFT(CHANNE
C*****      WT=FACTIONAL WEIGHT OF ENVIRONMENT
      READ(5.99) IP,H,EPS,DEL,WT
      IF (IP.EQ.1) GO TO 250
      IF (IP.EQ.2) GO TO 230

```

```

C*****      FOR FERROMAGNETIC SPECTRA
C*****      W(I)=FRACTIONAL PEAK WEIGHTS  VP(I)=PEAK POSITIONS
C*****      Q IS THE CONVERSION FACTOR FROM MM/SEC TO CHANNEL
      W(1)=0.25
      W(2)=1.0/6.0
      W(3)=1.0/12.0
      W(4)=1.0/12.0
      W(5)=1.0/6.0
      W(6)=0.25
      VP(1)=DFL+EPS-CL*MI*(0.5*GGR-1.5*GEY)*H*Q/EO
      VP(2)=DFL-EPS-CL*MI*(0.5*GGR-0.5*GEY)*H*Q/EO
      VP(3)=DFL-EPS-CL*MI*(0.5*GGR+0.5*GEY)*H*Q/EO
      VP(4)=DFL-EPS+CL*MI*(0.5*GGR+0.5*GEY)*H*Q/EO
      VP(5)=DFL-EPS+CL*MI*(0.5*GGR-0.5*GEY)*H*Q/EO
      VP(6)=DFL+EPS+CL*MI*(0.5*GGR-1.5*GEY)*H*Q/EO
      WRITE(6,98) (VP(I),I=1,6)
C*****      SET UP MARTENSTIC BROADENING
C*****      ASIG=WIDTH OF GAUSSIAN BROADENING FUNCTION
      READ(5,300) ASIG
      DO 101 J=1,JP
C*****      PEAKS(I)=THEORETICAL MOSSBAUER ABSORPTION PROFILE
      DO 399 I=1,MP
      PEAKS(I)=WT*(J)*((LAM**2)/((4.0*(V(I)-VP(J))**2)+(LAM**2)))
      399 CONTINUE
      SIG=ASIG*ABS(VP(I)-QTB)/282.
      IF(SIG.LT.1.0) GO TO 403
C*****      G(I)=GAUSSIAN FUNCTION USED TO BROADEN PEAKS
C*****      ASIG=WIDTH OF GAUSSIAN      SIG=FUNCTION(ASIG)
      D=1./(SIG*SQRT(2.*3.14159))
      TSIGS=SIG*SIG*2.
      DO 400 I=1,512
      400 G(I)=D*EXP(-(I-1)**2/TSIGS)
      DO 401 I=513,MP
      401 G(I)=D*EXP(-(I-1025)**2/TSIGS)
C*****      DUM IS THE CONVOLUTION OF PEAKS AND G
      CALL CONV(PEAKS,G,DUM)
      DO 402 I=1,MP
      402 SPECT(I)=SPECT(I)+DUM(I)
      GO TO 405
      403 CONTINUE
      DO 404 I=1,MP
      404 SPECT(I)=SPECT(I)+PEAKS(I)
      405 CONTINUE
      101 CONTINUE
      GO TO 201
      230 CONTINUE

```



```

C*****      FOR QUADRUPOLE SPLIT DOUBLETS
      W(1)=0.5
      W(2)=0.5
      VP(1)=DEL+FPS+CTR
      VP(2)=DEL-FPS+CTR
      WRITE(6,98) (VP(I),I=1,TP)
      DO 231 J=1,TP
      DO 232 K=1,MP
      SPECT(K)=SPECT(K)+WT*W(I)*((LAM**2)/((4.0*(V(K)-VP(J))**2)+(LAM**2
1)))
232 CONTINUE
231 CONTINUE
      GO TO 201
250 CONTINUE
C*****      FOR SINGLE UNSPLIT PEAKS
      W(1)=1.0
      VP(1)=DEL+CTR
      WRITE(6,98) (VP(I),I=1,TP)
C*****      SPECT IS THE MOSSBAUER ABSORPTION PROFILE
      DO 251 J=1,TP
      DO 252 K=1,MP
      SPECT(K)=SPECT(K)+WT*W(I)*((LAM**2)/((4.0*(V(K)-VP(J))**2)+(LAM**2
1)))
252 CONTINUE
251 CONTINUE
201 CONTINUE
      97 FORMAT(I10)
      98 FORMAT (5X,6F12.5)
      99 FORMAT(I5,F10.2,2F10.6)
300 FORMAT(F10.3)
      RETURN
      END

```

```

      SUBROUTINE CONV(F,G,H)
C*****      CONV(F,G,H)  H IS THE CONVOLUTION OF F AND G
      DIMENSION F(1025),G(1025),H(1025)
      INTEGER*4 NN(1),NDIM,ISIGN,IFORM
      COMPLEX*8 DF(1025),DG(1025),FTH(1025)
      REAL*4 WORK
C      THIS SUBROUTINE PERFORMS THE CONVOLUTION OF F AND G
      ISIGN=-1
      NN(1)=1024
      NP=NN(1)
      NDIM=1
      IFORM=0
      WORK=0
      DO 9 I=1,NP
      DF(I)=CMPLX(F(I),0.0)
      DG(I)=CMPLX(G(I),0.0)
9 CONTINUE
C*****      FOURIER TRANSFORMS OF F AND G
      CALL FOURT(DF,NN,NDIM,ISIGN,IFORM,WORK)
      CALL FOURT(DG,NN,NDIM,ISIGN,IFORM,WORK)
      DO 9 I=1,NP
      FTH(I)=DF(I)*DG(I)
9 CONTINUE
      ISIGN=1
      IFORM=1
      CALL FOURT(FTH,NN,NDIM,ISIGN,IFORM,WORK)
      DO 7 I=1,NP
      H(I)=REAL(FTH(I))/NP
7 CONTINUE
      RETURN
      END

```

APPENDIX E: LOSS OF LATTICE RIGIDITY IN IRON-
NITROGEN AUSTENITE: N. DeCristofaro
and R. Kaplow, Scripta Met., 1975,
vol. 9, p. 781.

LOSS OF LATTICE RIGIDITY IN IRON-NITROGEN AUSTENITE

Nicholas De Cristofaro and Roy Kaplow
Department of Materials Science and Engineering
Massachusetts Institute of Technology
Cambridge, Massachusetts 02139

(Received May 9, 1975)

Introduction

The fact that increasing atomic vibrations may lead to structural instabilities in a crystalline lattice during heating has long been recognized. Lindemann, in 1910, sensing that melting is determined by the vibrational amplitudes of atoms, showed that an essentially constant relationship exists between the melting point of an element, its atomic weight, its lattice parameter, and its characteristic vibrational frequency (1). More recently, it has been shown that Lindemann's empirical relationship is determined by a detailed balance between the vibrational amplitude and the size of the "passageway" available for diffusion (2).

The potential instability of certain lattices with respect to interatomic displacements, on cooling, has also been recognized. In 1948, Zener (3) pointed out that the body-centered-cubic lattice is inherently unstable with respect to (110)[$\bar{1}\bar{1}$ 0] shear if only central interatomic forces are present. Without any detailed discussion of the nature of the interatomic bonding, or of the variation with temperature of the type of bonding, he relied on the entropy dependence of the free energy to argue that a real b.c.c. crystal is likely to become less stable as it is cooled. More recently, the concept that various crystal lattices become structurally unstable on cooling has assumed an important role in models for martensitic or displacive transformations. In that context, a number of experimental evidences have been published for the existence of pre-martensitic instabilities in the parent (austenite) phase (4, 5, 6, 7, 8, 9). It has also been argued that abnormal fluctuations continue to exist in the retained austenite below the temperature at which martensite formation starts, M_s (10). By analogy with fluctuations found to be associated with certain ferroelectric compound transitions (11), these instabilities are usually thought of as "soft" vibrational modes, but static displacement waves have also been cited (12).

Results

In the present paper we report the results of an iron-57 Mössbauer γ -ray spectroscopy (13) investigation of an iron-nitrogen alloy. The experiment demonstrates a lessening of lattice rigidity -- with respect to γ -ray absorption -- in the high-temperature phase at 183°K, which is below M_s (14). In this instance the high-temperature phase is face-centered-cubic (austenite), with nitrogen atoms in interstitial positions, and the martensitic phase is body-centered-tetragonal.

At 183°K the Mössbauer spectrum indicates about 40% martensite and the remainder austenite. Figure 1 shows: 1) the ferromagnetically-split spectra of martensite, nominally a single six-peak spectrum, but actually

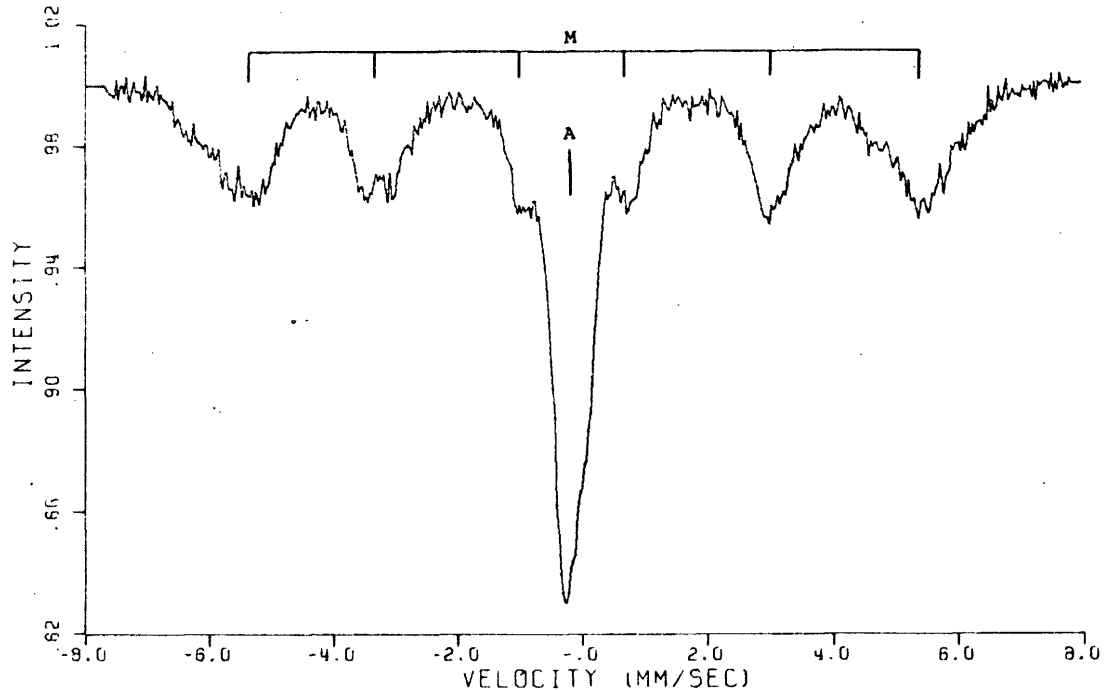


FIG. 1

The Mössbauer spectrum, taken at 183°K, indicates the presence of martensite, the "six" peaks labeled M, and austenite, the "single" peak labeled A.

comprised of contributions from a number of different iron atom environments, which depend on the atom's position with respect to the nitrogen interstitials; and 2) the spectrum of paramagnetic austenite, nominally a single peak at the center of the pattern, but actually comprised of three peaks from two distinguishable iron-atom environments (15).

The intensities of Mössbauer spectra are proportional to the so-called recoilless fraction (13):

$$f = \exp(-E_R/E^*) \quad (1)$$

where E_R is the recoil energy that would be transferred to a single free atom when its nucleus absorbed the γ -ray, and E^* is the effective, quantized, energy increment for available lattice excitations. For the vibrational excitations of an Einstein solid, for example, $E^* = K_B\theta_E$, the Einstein oscillator energy; for a Debye solid, the effective energy is $E^* = 2/3 K_B\theta_D$. The recoilless fraction can also be expressed in terms of the atomic displacements;

$$f = \exp(-\overline{u^2} k^2) \quad (2)$$

where $\overline{u^2}$ is the mean-square amplitude of displacement resolved along the γ -ray absorption direction, and k is the γ -ray wave number. Irrespective of the precise mechanism, a decrease in f can be tied to an increase in the

Correction to Scripta Met., 1975, Vol. 9

Loss of Lattice Rigidity in Iron-Nitrogen Austenite
by Nicholas DeCristofaro and Roy Kaplow, pp. 781-785

Page 782

The expression given for the oscillator energy of a Debye solid corresponds only to the low temperature limit of this parameter and it was intended to give the temperature variation as well. At temperatures greater than $\theta_D/2$, this term becomes approximately $E^* = K_B \theta_D^2 / 6T$. Paragraph 2 on page 782 should therefore be corrected to read:

The intensities of Mössbauer spectra are proportional to the so-called recoilless fraction (13):

$$f = \exp (-E_R/E^*) \quad (1)$$

where E_R is the recoil energy that would be transferred to a single free atom when its nucleus absorbed the γ -ray, and E^* is the effective, quantized energy increment for available lattice excitations. For the vibrational excitations of an Einstein solid, for example, $E^* = K_B \theta_E$, the Einstein oscillator energy; for a Debye solid, the effective energy is $E^* = 2/3 K_B \theta_D$ at low temperatures and $E^* = K_B \theta_D^2 / 6T$ at temperatures greater than $\theta_D/2$. The recoilless fraction can also be expressed in terms of the atomic displacements;

probability of creating lattice excitations, either static or dynamic, and therefore to a weakening of the resistance of the iron atoms to displacement by the γ -ray recoil.

For the present experiment, a sample was cycled from room temperature to 183°K and back to room temperature a total of five times. The total time at room temperature after the first quench was more than one week. This process served to ensure that the martensite formed was stabilized both in terms of its amount and in terms of room-temperature aging. The data given in Table I and described below relate to the last three sets of measurements: room temperature, 183°K, room temperature.

TABLE I
The Recoilless Fractions and Mean-Square Amplitudes of Displacement for Austenite and Martensite as Determined from Theory and Experiment

	293°K theory	183°K theory	183°K experiment (Austenite)	183°K experiment (Martensite)
f	0.7679	0.8334		
$\frac{f_{293}}{f_{183}}$		0.9214	1.087	0.923
$\bar{u}_x^2 (\text{Å}^2)$	0.00494	0.00341	0.0065	0.0034

The effective Debye temperatures for the iron atoms are not known precisely in either the martensite or austenite phases. The value of $\theta_D = 411^\circ\text{K}$, taken as an average and from interpolation and extrapolation of various data (16,17) seems appropriate for both phases, and is -- in any case -- accurate enough for our purposes. This value predicts that on the basis of ordinary vibrational behavior, the recoilless fraction should increase by approximately 8.5% for both phases when the sample is cooled from room temperature to 183°K. In fact, this is exactly the increase detected for the martensitic phase within statistical precision. The austenite, however, shows a decrease of 8% in f under the same conditions. On the return to room temperature, the intensities revert to their original values.

Discussion

From these results we can rule out the following potential uncertainties which might ordinarily beset such an experiment:

1. erroneously low intensities measured at low temperature (because the intensity of the spectrum of the martensite phase in the same sample increases);
2. additional irreversible conversion of austenite to martensite during the last cooling to 183°K (because the intensities revert to their original values when the sample is returned to room temperature);
3. reversible conversion of austenite to martensite (because the actual increase in the intensity of the martensite spectrum at 183°K is just what is expected from decreased thermal vibrations alone); and

4. instability in the detection electronics (because of the reproducibility of values on the specimen and on standard samples).

Thus, we believe the anomalous decrease in f for the austenitic phase on cooling from room temperature to 183°K to be a valid and quantitatively meaningful result.

In terms of atomic displacements, the difference between the thermally anticipated value and the measured f corresponds to $\Delta u^2 = + 0.00309 \text{ \AA}^2$. This is a large value, relatively speaking, roughly equal to the total expected value at 183°K, $u^2 \approx 0.00341 \text{ \AA}^2$.

For an f.c.c. phase, we do not expect an inherent instability like the classical b.c.c. phenomenon referred to by Zener. However, a lattice instability in the f.c.c. alloy may be associated with the size difference between atoms in the alloy. In the present case, that difference is so large that the nitrogen atoms are present interstitially and, moreover, are known to be highly mobile. It is interesting, therefore, to note that the measured anomalous Δu^2 is closely related to the iron-atom displacements caused by the neighboring nitrogen atoms (18). Considering the equilibrium Fe-N distances in the compound Fe₄N (19), we estimate that the displacement caused by the nitrogen atoms in octahedral interstitial sites in f.c.c. iron is $\delta = 0.111 \text{ \AA}$. Then, $\delta^2 = 0.0122$, and the component resolved along an arbitrary direction would be $\delta^2/3 = 0.00405 \text{ \AA}^2$. The alloy studied contained approximately 10.6 nitrogen atoms per 100 iron atoms; thus, approximately two-thirds of iron-atom positions were directly affected. This gives an estimate for the average of about 0.0026 \AA^2 , but we would expect the true average of static displacements to be somewhat larger because of effects on more distant neighbors. The measured value of Δu^2 , 0.0031 \AA^2 is thus very close to what would be expected if the anomalous γ -ray recoil effect was associated with nitrogen atom diffusive motions. If this view is a correct one, the magnitude of the effect measured by Fe⁵⁷ Mössbauer spectroscopy should decrease with decreasing nitrogen content, other factors being constant.

Summary

Mössbauer spectra were taken at room temperature and at 183°K of an iron-nitrogen sample containing about 40% of room temperature-aged martensite and the remainder austenite. The intensities of the martensite spectra are larger by about 8% at the lower temperature, as expected from thermal variation of the recoilless fraction. Conversely, the intensities of the austenite spectra are smaller at 183°K. This is associated with a lessening of lattice resistance to excitations caused by absorption of the γ -ray recoil energy. The abnormal decrease in lattice rigidity in the austenite at this temperature, which is below M_s , may be related to the transformation to martensite.

Acknowledgements

We gratefully acknowledge the support of this work at M.I.T. by the Office of Naval Research, under Contract # N00014-67-A-0204-0027. We also appreciate the thoughtful comments of Professor Morris Cohen.

References

1. F. A. Lindemann, *Phys. Zs.* 11, 609 (1910).
2. R. Kaplow, B. L. Averbach and S. L. Strong, *J. Phys. Chem. Solids* 25, 1195 (1964).
3. C. Zener, *Elasticity and Anelasticity of Metals*, p. 36, Univ. of Chicago Press (1948).
4. G. D. Sandrock, A. J. Perkins and R.F. Hehemann, *Met Trans.* 2, 2769 (1971).
5. J. Perkins, *Met. Trans.* 4, 2709 (1973).
6. L. Delaey, J. Van Paemel and T. Struyve, *Scripta Met.* 6, 507 (1972).
7. J. Perkins, *Scripta Met.* 8, 975 (1974).
8. Ye. Ye. Yurchikov and A. Z. Men'shikov, *Phys. Metal, Metallog.* 32, No. 1, 169 (1971).
9. B. S. Bokshtein, Yu. B. Voitkovskii, G. S. Nikol'skii and I. M. Razumovskii, *Sov. Phys. JETP* 37, 283 (1973).
10. I Cornelis, R. Oshima, H. C. Tong and C. M. Wayman, *Scripta Met.* 8, 133 (1974).
11. W. Cochran, *Advances in Physics* 9, 387 (1960).
12. D. de Fontaine, N. E. Paton, and J. C. Williams, *Acta Met.* 19, 1153 (1971).
13. H. Frauenfelder, *The Mössbauer Effect*, W. A. Benjamin Inc., Reading, Mass. (1962).
14. T. Bell and W. S. Owen, *Trans. AIME* 239, 1940 (1967).
15. P. M. Gielen and R. Kaplow, *Acta Met.* 15, 49 (1967).
16. *International Tables for X-Ray Crystallography*, Kynoch Press (1965).
17. Y. Tanji, *J. Phys. Soc. Japan* 30, 133 (1971).
18. K. H. Jack, *Proc. Roy. Soc.* 208A, 200 (1951).
19. D. H. Jack and K. H. Jack, *Mat. Sci. and Eng.* 11, 1 (1973).

APPENDIX F: IRON-MANGANESE-NITROGEN ALLOYS

An Iron - 12.2 wt. % manganese - 3.9 wt. % nitrogen foil (0.0013 inch thickness) of nearly 100% austenite was produced by rolling an iron-manganese base alloy to the proper thickness nitriding and rapid quenching to room temperature. The Mössbauer spectra of this sample is illustrated in Figure (F.1).

To test for pre-precipitation phenomena in the austenite, such as a partition of nitrogen atoms to interstitial sites surrounding manganese atoms, the sample was tempered for six hours at 100°C, 140°C, 180°C, 200°C and 220°C, with Mossbauer spectra recorded after each heat treatment. No change in the austenite spectrum occurred prior to treatment at 220°C, indicating that no substantial rearrangement of nitrogen atoms was taking place. The spectrum recorded after six hours at 220°C (Figure F.2) indicates that some decomposition of the austenite has occurred, to α -iron plus an as yet unspecified nitride.

The room-temperature, as-quenched Mössbauer spectrum of the Fe-Mn-N austenite may be analyzed by applying the technique described in Chapter II for the binary Fe-N and Fe-C systems. However, this technique must be modified to include the broadening resulting from the various Fe-Mn pairs existing in the austenite structure.

Figure F.1 The Mössbauer Spectrum of Fe - 12.2 wt.%Mn - 3.9 wt.%N Austenite.

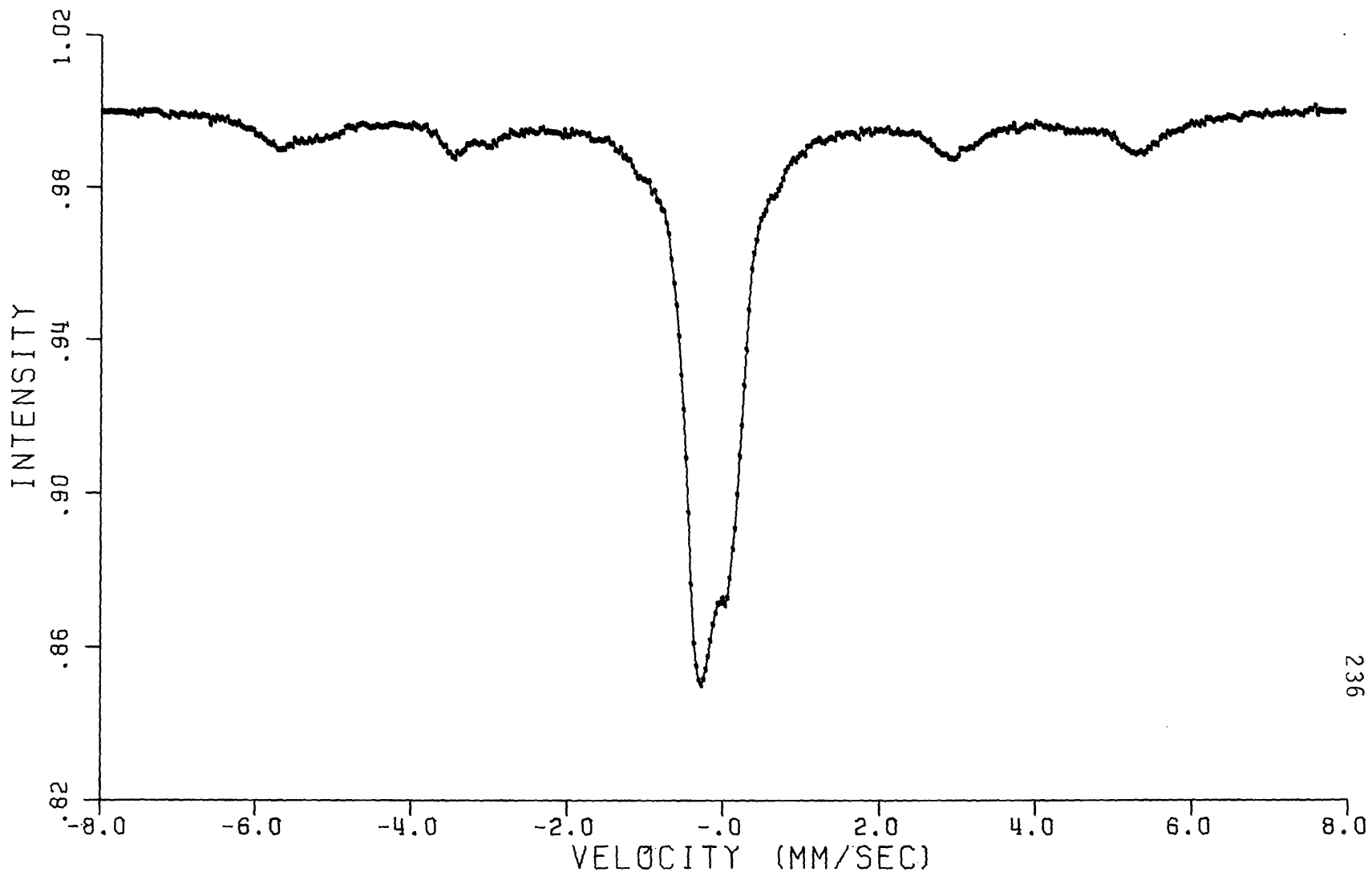
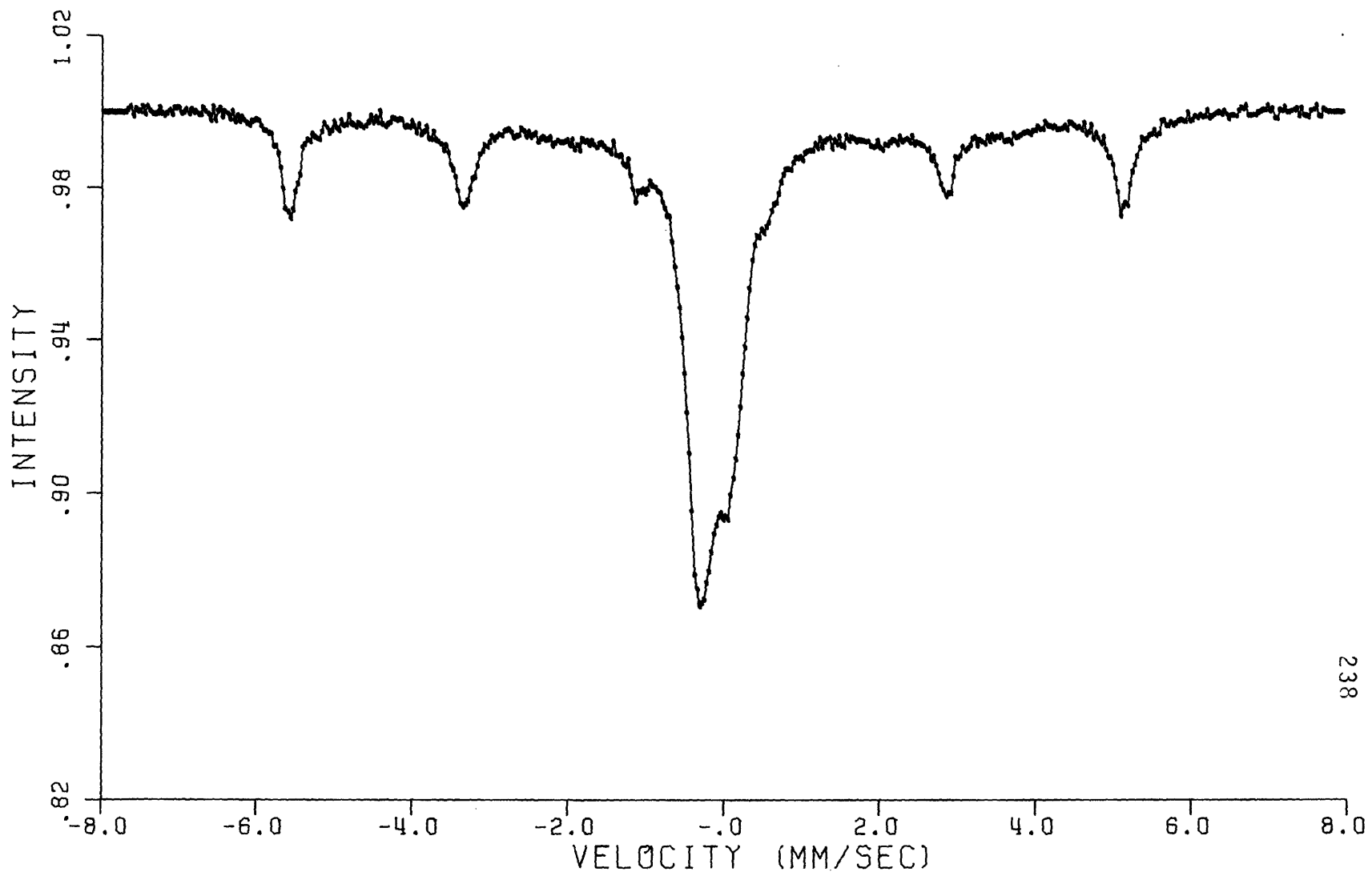


Figure F.2 The Mössbauer Spectrum of Fe - 12.2 wt.%Mn--
3.9 wt.%N Austenite after Tempering for Six Hours
at 220°C.



Biographical Note

Nicholas J. DeCristofaro was born on July 3, 1949, in Manhattan, New York. Raised primarily in Yonkers, New York, he graduated from Mt. St. Michael High School in June of 1967, entered M.I.T. the following fall, and received the degrees of B.S. and S.M. in Metallurgy in June of 1973. Continuing in a doctoral program in Materials Science, he has minored in managerial economics and finance.

While at M.I.T., he has been an active member of Theta Chi Fraternity and has been awarded the Materials Science Prize (1970) by the Boston Chapter A.I.M.E., and the John Wulff Award (1972-73) for contributions as a teaching assistant.

On October 20, 1973, he was married to Sandra Sanders at the M.I.T. Chapel.